



**NEURAL REPRESENTATION OF
DYNAMIC ECHO-ACOUSTIC SCENES
IN BATS**

Dissertation

Chair of Zoology

Department of Animal Sciences

School of Life Sciences Weihenstephan

Technical University of Munich

Wolfgang Greiter



Technische Universität München
Wissenschaftszentrum Weihenstephan
für Ernährung, Landnutzung und Umwelt

Neural representation of dynamic echo-acoustic scenes in bats

Wolfgang Greiter

Vollständiger Abdruck der von der Fakultät Wissenschaftszentrum Weihenstephan für Ernährung, Landnutzung und Umwelt der Technischen Universität München zur Erlangung des akademischen Grades eines Doktors der Naturwissenschaften (Dr. rer. nat.) genehmigten Dissertation.

Vorsitzender:

Prof. Dr. Michael Schemann

Prüfende der Dissertation:

1. Priv.-Doz. Dr. Uwe Firzlaff
2. apl. Prof. Dr. Lutz Wiegrebe
3. Prof. Dr. Harald Luksch

Die Dissertation wurde am 27.11.2017 bei der Technischen Universität München eingereicht und durch die Fakultät Wissenschaftszentrum Weihenstephan für Ernährung, Landnutzung und Umwelt am 06.03.2018 angenommen.

CONTENT

| | |
|--|-----------|
| Content | 1 |
| Publications | 3 |
| Zusammenfassung | 4 |
| Summary | 6 |
| Introduction | 8 |
| Hearing and echolocation in bats | 8 |
| Neuronal basis of sound processing in bats..... | 9 |
| Neuronal processing of complex dynamic acoustic scenes | 11 |
| Influence of ear movements on spatial receptive fields in the superior colliculus | 13 |
| Echo-acoustic flow shapes object representation in spatially complex acoustic scenes | 14 |
| Three-dimensional receptive fields in the auditory cortex..... | 16 |
| Methods | 19 |
| Experimental animals: <i>Phyllostomus discolor</i> | 19 |
| Initial surgery..... | 19 |
| General experimental procedure..... | 20 |
| Influence of ear movements on spatial receptive fields in the superior colliculus | 22 |
| Spatial tuning in the superior colliculus | 22 |
| Influence of ear movements on spatial tuning | 22 |
| Frequency tuning in the superior colliculus | 23 |
| Echo-acoustic flow shapes object representation in spatially complex acoustic scenes | 24 |
| Characterization of basic delay tuning properties | 24 |
| Stimulus generation for naturalistic flight sequences..... | 25 |
| Data analysis for naturalistic flight sequences | 28 |
| Three-dimensional receptive fields in the auditory cortex..... | 30 |
| Characterization of basic delay tuning properties | 30 |
| Characterization of three-dimensional tuning..... | 30 |
| Influence of ear movements on spatial receptive fields in the superior colliculus | 33 |
| Results | 33 |
| Spatial tuning in the superior colliculus | 33 |
| Influence of ear movements on spatial receptive fields | 35 |
| Frequency tuning in the superior colliculus | 40 |
| Discussion..... | 41 |

| | |
|---|-----------|
| Topography and frequency tuning in the superior colliculus | 43 |
| Conclusion | 43 |
| Echo-acoustic flow shapes object representation in spatially complex acoustic scenes | 44 |
| Results | 44 |
| Delay Response Fields | 44 |
| Object focusing in naturalistic flight sequences | 46 |
| Cortical delay tuning in naturalistic flight sequences | 51 |
| Discussion..... | 55 |
| Basic delay tuning properties | 55 |
| Cortical object representation in dynamic flight sequences | 56 |
| Impact of pulse emission pattern on object representation and delay tuning | 58 |
| Auditory scene analysis in complex natural environment..... | 59 |
| Conclusion | 59 |
| Three-dimensional receptive fields in the auditory cortex | 60 |
| Results | 60 |
| Basic delay tuning properties | 60 |
| Spatial selectivity of neurons at best delay | 61 |
| Influence of call/echo level on spatial tuning..... | 67 |
| Three dimensional response properties..... | 69 |
| Discussion..... | 72 |
| Delay tuning and spatial selectivity | 72 |
| Systematic representation of target elevation..... | 73 |
| Three-dimensional representation of space | 76 |
| Conclusion | 77 |
| General discussion | 78 |
| Abbreviations..... | 80 |
| References | 81 |
| List of figures..... | 89 |
| Curriculum vitae..... | 90 |
| Acknowledgements | 91 |

PUBLICATIONS

The following research articles are part of this thesis:

Published as first author:

- **Greiter, Wolfgang; Firzlaff, Uwe (2017):**
Echo-acoustic flow shapes object representation in spatially complex acoustic scenes.
In Journal of Neurophysiology 117: 2113–2124, 2017. DOI: 10.1152/jn.00860.2016
- **Greiter, Wolfgang; Firzlaff, Uwe (2017):**
*Representation of three-dimensional space in the auditory cortex of the echolocating bat *P. discolor*.*
In PLoS ONE 12: e0182461, 2017. DOI: 10.1371/journal.pone.0182461

For both projects, Uwe Firzlaff and I designed and implemented the experiments. I performed the experiments and analyzed the data. I wrote both publications with assistance and corrections from Uwe Firzlaff.

Published as coauthor:

- **Hoffmann, Susanne; Vega-Zuniga, Tomas; Greiter, Wolfgang; Krabichler, Quirin; Bley, Alexandra; Matthes, Mariana; Zimmer, Christiane; Firzlaff Uwe; Luksch, Harald (2016):**
*Congruent representation of visual and acoustic space in the superior colliculus of the echolocating bat *Phyllostomus discolor*.*
In European Journal of Neuroscience, 2016. DOI: 10.1111/ejn.13394

I contributed to the publication by providing part of the data on spatial tuning using virtual echoes as stimuli as well as the data on frequency tuning in the SC.

- **Kugler, Kathrin; Greiter, Wolfgang; Luksch, Harald; Firzlaff, Uwe; Wiegrebe, Lutz (2016):**
Echo-acoustic flow affects flight in bats.
In Journal of Experimental Biology, 2016. DOI: 10.1242/jeb.139345

Kathrin Kugler and I designed and built the bat flight channel used in the experiments. I further assisted in the interpretation of the results and commented on the manuscript.

ZUSAMMENFASSUNG

Fledermäuse verwenden Echoortung zur Navigation in Dunkelheit. Dazu besitzen sie ein hoch spezialisiertes auditorisches System. Dieses ermöglicht ihnen einerseits die präzise Lokalisation von Schallquellen und andererseits die Bestimmung der Entfernung zu Objekten mit Hilfe der Zeitdifferenzen zwischen der Emission der eigenen Ortungslaute und dem Empfang der reflektierten Echos (Echo Delay). Die neuronale Verarbeitung der Echoortung bei Fledermäusen, insbesondere die Verarbeitung von spezifischen akustischen Parametern (z.B. Frequenz, Echo Delay), wurde in den letzten Jahrzehnten intensiv erforscht. Die meisten dieser Studien bedienten sich dabei jedoch eher einfachen akustischen Stimuli (z.B. Reintöne, simulierte Echos von statischen Objekten) um eine klare und zielgerichtete Auswertung der neuronalen Antworten zu ermöglichen. Diese Stimuli sind jedoch weit von der komplexen, dynamischen akustischen Umgebung entfernt mit der eine Fledermaus in natürlicher Umgebung konfrontiert wird.

In meinem Projekt verwendete ich typische Echoortungslaute sowie simulierte Echos einer virtuellen akustischen Umgebung um die neuronalen Antworten auf komplexere oder dynamische akustische Szenen bei der Fledermaus *Phyllostomus discolor* zu untersuchen. Alle akustischen Stimuli wurden den anästhesierten Tieren über speziell gefertigte Ohrhörer präsentiert. Die neuronalen Antworten auf die präsentierten Stimuli wurden mit Hilfe von elektrophysiologischen Methoden untersucht.

Im ersten Teil des Projekts untersuchte ich die neuronale Raumrepräsentation in den Colliculus superiores sowie den Einfluss von Ohrbewegungen auf diese Repräsentation. Die Struktur der Ohrmuscheln erzeugt zentrale Muster für die Lokalisation von Schallquellen. Eine Bewegung der Ohrmuscheln bei der Ortung führt daher zu deutlichen Änderungen der akustischen Wahrnehmung die vom Gehirn entsprechend kompensiert werden müssen um eine präzise Schalllokalisierung zu ermöglichen. Meine Ergebnisse zeigen Hinweise auf eine geordnete Raumkarte in den Colliculus superiores, jedoch keinen Einfluss von Ohrbewegungen auf diese Karte.

Im zweiten Teil meiner Arbeit untersuchte ich die kortikale Repräsentation von zwei virtuellen Objekten in einer dynamischen Umgebung, indem ich eine Serie von Echoortungslauten und entsprechende Objektechos präsentierte, die einen Vorbeiflug an zwei Objekten simulierten. Meine Ergebnisse zeigen, dass Neurone im auditorischen Kortex in einem komplexen Strom von Echos zweier Objekte auf die Echos eines bestimmten Objekts fokussieren können. Die

einzelnen Objekte werden dabei in der Reihenfolge des Vorbeiflugs prozessiert. Meine Ergebnisse zeigen außerdem einen deutlichen Einfluss der dynamischen Stimulation auf die kortikale Verarbeitung von Entfernungen.

Fledermäuse bewegen sich in einer dreidimensionalen Umgebung. Die neuronale Verarbeitung des dreidimensionalen Raums war das Thema im letzten Teil meines Projekts. Zahlreiche Studien zeigen Neurone die spezifisch auf bestimmte Echo Delays antworten und eine geordnete Entfernungskarte bilden. Andere Zellen verarbeiten direktionale Informationen. Es war jedoch bislang unklar ob Neurone auch 3-D-Informationen verarbeiten können. Um dies näher zu untersuchen verwendete ich eine Kombination von typischen Echoortungsrufen und virtuellen Echos aus dem dreidimensionalen Raum und untersuchte die damit hervorgerufenen neuronalen Antworten im auditorischen Kortex der Fledermäuse. Die Ergebnisse zeigen, dass diese kortikalen Neurone auf Echos von bestimmten Positionen im dreidimensionalen Raum spezifisch antworten können.

Dieses Projekt gibt neue Einblicke in die neuronale Verarbeitung von komplexen und dynamischen echo-akustischen Szenen bei Fledermäusen und zeigt den flexiblen und anpassungsfähigen Charakter von neuronalen Karten.

SUMMARY

Microchiropteran bats use echolocation for navigation in darkness. For this, they have evolved a highly specialized auditory system, which not only enables them to precisely localize sound sources, but also to estimate the distance to objects from the echo delay between emission of their own sonar calls and the reception of reflected echoes. The neuronal basis of echolocation in bats was intensively studied over the past decades by investigating the neuronal processing of specific acoustic parameters (e.g. frequency, echo delay). However, most of these studies used rather simplified acoustic stimuli (e.g. pure tones, simulated echoes from static objects) to enable a straightforward analysis of the elicited neuronal responses. This is, however, far from the complex dynamic acoustic situation a bat has to face in a natural environment.

In my project, I used typical echolocation pulses and simulated echoes from a virtual acoustic environment to investigate the neuronal responses to more complex or dynamic acoustic scenes in the bat *Phyllostomus discolor*. For this, all acoustic stimuli were presented *via* custom-made ear-phones to the anesthetized animals. An electrophysiological approach was used to determine the neuronal responses to the presented stimuli.

In the first part of the project, I investigated the neuronal representation of space in the superior colliculus and the influence of ear movements on this representation. The structure of the outer ear (pinna) generates essential cues for the localization of sound sources. Because of this, a movement of the pinna during sound localization causes drastic changes to the auditory input and consequently the brain has to compensate this movement to allow precise localization. I found evidence for an orderly representation of space in the superior colliculus, but no influence of ear movements on this space representation.

In the second part, I investigated the cortical representation of two virtual objects in a dynamic situation by presenting a series of echolocation pulses with object echoes simulating a typical fly-by situation. My results demonstrate that neurons in the auditory cortex (AC) can lock on echoes from a specific object in a complex stream of echoes originating from two objects. The objects were processed sequentially in the order in which they were approached. Furthermore, I found a significant influence of the dynamic simulation on the target range representation in the AC.

Bats move in three-dimensional space. The neuronal representation of 3-D-space was the topic of the last part. Several studies could show neurons responding specifically to echo delay and forming an organized target distance map. Other neurons process directional information.

However, it was up to now unclear if neurons can also process 3-D-information of space. I used typical echolocation pulses combined with virtual echoes from 3-D-space and investigated the evoked neuronal responses in the AC of the bats. The results demonstrate that AC neurons can respond selectively to specific positions in 3-D-space.

This project provides new insights into the neuronal processing of complex, dynamic echo-acoustic scenes in bats and shows the flexible and adaptable character of computational neuronal maps.

INTRODUCTION

Hearing and echolocation in bats

Bats are special. They are the only mammals that can fly. And they are, together with toothed whales and some shrews, the only mammals that can use echolocation for orientation when no visual cues are available (Fenton et al., 2016; Johnson et al., 2004; Siemers et al., 2009). For this, they have evolved a highly specialized auditory system.

The bats' echolocation system consists of two main parts: the pulse emission system and the hearing system. Both systems are highly directional. The high frequency sonar calls, usually between 10 – 200 kHz (Jones and Holderied, 2007), are emitted through mouth or nostrils and can be tightly controlled with respect to intensity, duration, timing, frequency content and directional aim (Jakobsen et al., 2015; Linnenschmidt and Wiegrebe, 2016). Sonar emissions usually consist of constant frequency (CF) or frequency modulated (FM) calls. While CF calls are especially suited to detect Doppler shifts caused by movement or fluttering from flying insects, FM calls are more suited for 3-D target localization (Moss and Schnitzler, 1995).

The bat's hearing system is, in principle, the same as in other mammals with some important specializations: the hearing range of bats extends from around 1 kHz to well above 100 kHz, with an especially high sensitivity and high resolution at the species specific call frequencies in CF-bats (Moss and Surlykke, 2010). Furthermore, bats have large and movable ears that can be targeted in specific directions to increase binaural localization cues and to facilitate vertical localization (Mogdans et al., 1988). Like other mammals, bats can use binaural cues like interaural level differences (ILDs) and possibly to some extent also interaural time differences (ITDs, Grothe and Park, 1998) to localize sound in the horizontal plane (azimuth position). Furthermore, the head shape and the large pinna generate spectral cues that are most important to localize sound in the vertical plane (elevation) but also in azimuth (Firzlaff and Schuller, 2003; Mey et al., 2008). The spectral cues due to the pinna and head shape, as well as the ILDs and ITDs, can be measured and are expressed in the so called head-related transfer function (HRTF, Young et al., 1996). Unlike most other mammals, however, echolocating bats can further use the time delay between the emission of a sonar call and the reception of its reflected echoes to measure their distance from objects or prey. For this, the auditory system of bats can process auditory information with extremely high temporal precision. This is most important for the bats ability to estimate target distance from the echo delay between pulse

emission and echo perception. This remarkable feature allows bats to estimate time differences down to about 25 μ s, corresponding to a change in distance of about 4 mm (Goerlitz et al., 2010; Simmons et al., 1990).

Neuronal basis of sound processing in bats

The bat's ascending auditory pathway corresponds mainly to that of other mammals but has some important specializations:

Sound waves are converted into receptor potentials in the inner ear. Specific frequencies in an incoming sound wave activate neurons at specific positions of the basilar membrane in the cochlea. High frequencies are represented close to the base of the cochlea and systematically decrease along the basilar membrane (Neuweiler, 2000). While this is a general principle for all mammals, bats have, compared to other mammals, an especially long basilar membrane and a

higher density of neurons allowing a high frequency range (Bruns et al., 1989). Furthermore, CF bats often have an acoustic fovea at the species specific call frequencies which allow them to detect even the slightest frequency differences caused by Doppler shifts. After the conversion of the sound waves into receptor potentials in the cochlea, the acoustic information is relayed *via* the auditory nerve fibers to the cochlear nucleus. As in other mammals, the different nuclei in the ascending auditory pathway (i.e. cochlear nucleus, trapezoid body, lateral and medial superior olivary nucleus) are organized tonotopically (or "cochleotopically" = based on the frequency distribution in the cochlea). Up to the inferior colliculus (IC) of the midbrain, as well as in the medial geniculate body and parts of the auditory cortex (AC), different laminae or different areas process different frequency

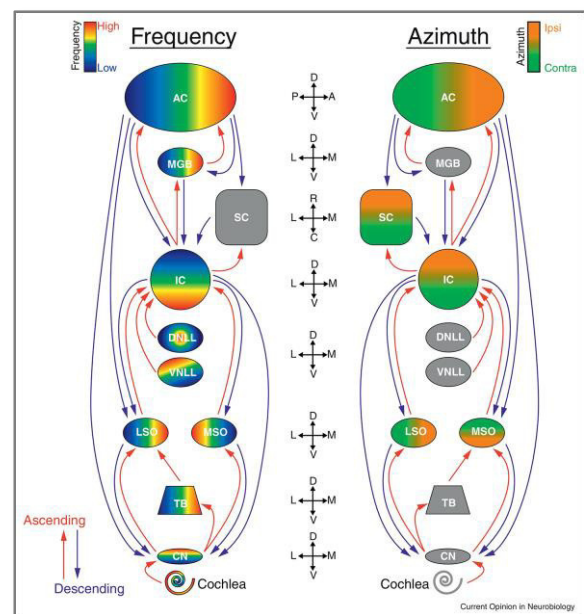


Figure 1: Frequency tuning and spatial tuning in the ascending auditory pathway

Left: tonotopic arrangement of neurons in the ascending auditory pathway. Blue indicates low frequencies, red indicates high frequencies. Right: spatial topography of neurons in different regions of the auditory pathway. Green indicates contralateral tuning, orange ipsilateral tuning. Gray indicates no tonotopic or topographic distribution of the neurons. Anatomical axes are shown in the middle. AC, auditory cortex; MGB, medial geniculate; SC, superior colliculus; IC, inferior colliculus; DNLL/VNLL, dorsal/ventral nucleus of the lateral lemniscus; LSO/MSO, lateral/medial superior olivary nucleus; TB, trapezoid body; CN, cochlear nucleus (*Pteronotus parnellii*). (Figure reprinted from Wohlgenuth et al., 2016b, with permission from Elsevier.)

bands (Wohlgemuth et al., 2016b, see Figure 1 left side).

As mentioned before, spatial information is derived from monaural (spectral) and binaural (ITD, ILD) cues. The monaural and binaural pathways process sound information in parallel in the lower auditory nuclei and converge in the inferior colliculus. Both the inferior and the superior colliculus in the midbrain are considerably larger than in other mammals. From the inferior colliculus, information is further transmitted *via* the medial geniculate body to the auditory cortex. Further auditory interconnections exist between the IC and the superior colliculus (SC) as well as between the AC and the SC (Neuweiler, 2000; Wohlgemuth et al., 2016b).

Beside this processing of spatial and frequency information, which is comparable to that of other mammals, bats further have neurons that process distance information encoded in the echo delay between sonar call emission and echo perception. Neurons that selectively encode specific echo delays emerge in the ascending auditory pathway of bats from the midbrain on (O'Neill and Suga, 1982; Olsen and Suga, 1991; Portfors and Wenstrup, 1999; Valentine and Moss, 1997). In the auditory cortex, these neurons have been shown to form chronotopically organized computational maps of target distance (Hagemann et al., 2010; Schuller et al., 1991; Suga and O'Neill, 1979). Dear et al. (1993b) proposed that a concurrent representation of multiple echo delays in these maps acts as the neuronal basis for a complex acoustic scene representation.

This work is mainly focused on two regions of the auditory pathway that are essential to the processing of spatial information: the superior colliculus and the auditory cortex.

The superior colliculus is known to play an important role in orienting responses and contains visual sensory maps in the upper layers as well as somatosensory maps in the intermediate layers. Auditory maps of space in the intermediate and deeper layers of the SC were further found in several mammals (e.g. guinea pigs: Palmer and King, 1982; cats: Middlebrooks and Knudsen, 1984; ferrets: King and Hutchings, 1987) and suggested for bats (Kothari et al., 2016). Moreover, studies also found neurons that process distance or echo delay information in the SC of bats (Valentine and Moss, 1997).

The auditory cortex plays a major role in the localization and evaluation of sounds in mammals (Derey et al., 2015; Jenkins and Merzenich, 1984; Middlebrooks et al., 1998). In bats, the auditory cortex was intensively studied with respect to frequency tuning, spatial tuning (Razak,

2011), echo delay tuning (Hagemann et al., 2010) as well as processing of complex sounds (Bartenstein et al., 2014; Beetz et al., 2016a).

Neuronal processing of complex dynamic acoustic scenes

The neuronal processing of the complex sounds present in a natural environment is still only poorly understood. A bat moving and navigating in a natural environment has many important challenges. In the following, some of these will be addressed:

First of all, the bats' echolocation system is highly directional. The echolocation sounds are emitted to a narrow cone in front of the bat where objects are insonified. Bats can widen or sharpen their sonar beam situation specific (e.g. to enhance detection of moving prey or to reduce clutter echoes, Linnenschmidt and Wiegrebe, 2016; Surlykke et al., 2009). In addition to the directionality of the pulse emission system, the bats hearing system has a highly directional character, which is mainly determined by the shape and structure of the pinna (Firzlaff and Schuller, 2004; Mey et al., 2008). This directionality of the sonar system allows on the one hand precise target localization but at the same time restricts the bats sonar perception to mainly the frontal hemisphere. Movement of the bat's ears, as often seen in cats, can help to localize sound sources but has at the same time, due to the high directionality of the ears, a severe influence on the bat's perception. At the moment, it is an unsolved scientific question how changes of the sound perception due to ear movements are compensated in the neuronal auditory system.

Movement of an animal (e.g. flying bat) or objects relative to the animal (e.g. flying prey) is a further challenge for the auditory system. In the visual system, objects are represented by a persistent image on the receptor surface of the retina. If an object (e.g. flying prey) moves in relation to the animal, the image on the retina will continuously move on the receptor surface. This apparent motion of the visual scene is called optic flow (Gibson, 1954). The optic flow can be used to estimate the direction of self-motion and help to detect the movement of other objects (Lappe et al., 1999; Warren and Rushton, 2009). In contrast to this, in the auditory system movements of sound sources will not cause a shift of activity on the cochlea but can only be extracted from continuous changes of interaural level and time differences as well as spectral changes. Neurons in the ascending auditory pathway can then compute the movements of sound sources. Similar to the visual system, self-motion induced echo-acoustic flow information can help to estimate direction and distance to passing objects in a complex acoustic environment (Bartenstein et al., 2014; Kugler et al., 2016).

For echolocating bats, however, this becomes even more complex as they do not receive a continuous stimulus like in the visual system or during passive hearing. Due to the stroboscopic nature of the bat's echolocation pulses, they receive a series of acoustic snapshots of their environment. The auditory system then has to group this series or stream of incoming snapshots together to form a continuous sensation of static or moving objects. Auditory streaming as well as auditory stream segregation was of course intensively studied in the past in many animals, including bats (Kanwal et al., 2003; Micheyl et al., 2005; Noorden, 1975). But most of these studies used rather simplified, artificial stimuli such as alternating pure tones (Kanwal et al., 2003), which have almost no resemblance to the complex, dynamic pattern of echoes a bat receives during echolocation in a complex natural environment (e.g. flight along bushes, trees).

In this work, I wanted to focus on the neuronal representation of complex, dynamic echo-acoustic scenes and especially investigate the challenges mentioned above:

- Which influence has movement of the bat's ears on the neuronal representation of space in the midbrain (i.e. superior colliculus)?
- Is echo-acoustic flow information important for the neuronal representation of complex echo-acoustic scenes?
- Echolocating bats move in three-dimensional space: How can neurons encode this three-dimensional space?

For my experiments, I used a typical echolocation call of *P. discolor* as basis for the generation of the acoustic stimuli. For the generation of naturalistic virtual echoes from specific spatial positions, this call was convolved with a left and right pair of the HRTF (Firzlaff and Schuller, 2003). The resulting virtual echoes included all relevant spatial localization cues (i.e. ILD, ITD, frequency content). The final stimuli were presented binaurally *via* custom-made ear-phones (see methods section for details). With this method, all important parameters for the different projects (e.g. independent control of call and echo level, echo delay, stimulus repetition rate, echoes from multiple objects) could be tightly controlled to enable a naturalistic acoustic stimulation and following clear analysis of the evoked neuronal responses.

Influence of ear movements on spatial receptive fields in the superior colliculus

As mentioned above, animals with moveable pinna can use these movements to target sound sources to optimize listening conditions while localizing prey or to increase binaural cues for target localization. Because of this, ear movements were investigated in cats and other mammals in detail during the last decades (Populin and Yin, 1998). Animals that hunt in dim light conditions or during complete darkness are especially dependent on precise sound localization capabilities. Therefore, bats as nocturnal hunters that rely on echolocation for navigation and hunting are a most interesting model system to investigate ear movements and their influence on sound localization. The function of ear movements during active echolocation and passive sound localization was investigated in several studies (Kugler and Wiegrebe, 2017; Mogdans et al., 1988). It was suggested that these movements not only help to localize targets, but might also be suited to amplify echoes of interest while reducing clutter echoes (Holland and Waters, 2005).

It is important to note, however, that the pinna structure, together with the shape of the head, causes the characteristic spectral patterns that are the basis of monaural sound localization cues (Firzlaff and Schuller, 2003; Mey et al., 2008; Schnyder et al., 2014). Because of this, tilting or rotation of the pinna, in addition to potential head movements, introduces drastic changes on the sensory perception (Young et al., 1996). Therefore, animals have to take these movements or their current pinna position into account when they want to precisely localize sound sources. The neuronal system has to compensate changes related to ear movements (e.g. spectral changes due to the HRTF) to stabilize the spatial information.

The superior colliculus of the midbrain might be possible center for this integration of auditory spatial information and information about the pinna position. As mentioned before, visual sensory maps, somatosensory maps and also auditory maps were found in the different layers of the SC. Due to this proximity of different modalities in the different layers of the SC, a multisensory integration is likely and was already investigated in different mammals (King and Palmer, 1985; Knudsen, 1982; Meredith et al., 1992). Several studies found that the superior colliculus plays an important role in the control of visual fixation and saccadic eye movements (Lee et al., 1988; Munoz and Wurtz, 1992). Furthermore, it was shown that auditory spatial receptive fields shifted with changes in eye position (Jay and Sparks, 1984) and there is

evidence for a influence of the ear position on the spatial tuning of auditory neurons in cats (Middlebrooks and Knudsen, 1987). However, a clear investigation of the influence of ear movements on the spatial tuning of SC neurons in bats is still missing.

In this study, I tested the hypothesis that ear movements cause a shift of the spatial receptive fields of direction sensitive neurons in the SC of *P. discolor*. I simulated ear movements by electrically stimulating the ear muscles of the ear contralateral to the recording site in the SC while testing the spatial response profiles of SC neurons with virtual acoustic stimuli. By using an acoustic stimulation *via* ear-phones placed at the outer ear canal (see methods), the acoustic stimulus was kept constant while on the same time a proprioceptive input simulating a movement of the pinna was generated. In addition to the investigation of this specific hypothesis, I tested the general spatial and frequency response characteristics of the SC neurons.

Echo-acoustic flow shapes object representation in spatially complex acoustic scenes

The following part of the introduction corresponds to the publication:

*“Echo-acoustic flow shapes object representation in spatially complex acoustic scenes”
(Greiter and Firzlaff, 2017a)*

The article is published in the Journal of Neurophysiology which permits authors the reproduction of published articles for dissertations without charge or further license.

Segregating signals from specific objects in a complex environment is a ubiquitous challenge for sensory systems (Lamme, 1995; Pawluk et al.; Roelfsema et al., 1998; Rokni et al., 2014). In the auditory world, auditory scene analysis deals with the organization of complex sounds in perceptually meaningful elements (Bregman, 1990). Perceptual organization of sounds into auditory streams has been studied in many different species, including humans (Fay, 1998; Izumi, 2002; MacDougall-Shackleton et al., 1998; Micheyl et al., 2005; Noorden, 1975; Schul and Sheridan, 2006). Most neurophysiological studies investigated auditory stream segregation using fairly simplified acoustic stimuli such as alternating pure tones (Fishman et al., 2001; Kanwal et al., 2003; Micheyl et al., 2005); therefore, the neural basis of perceptual organization of more complex sounds in a natural environment is still not well understood.

For bats evaluating and sorting of complex sounds is most important as they use echolocation for navigation in darkness. This might be a comparable easy task when single bats hunt isolated insects in empty air space. But the sorting and correct identification of objects gets extremely complicated when bats have to identify possible prey in dense foliage or with huge numbers of surrounding conspecifics.

As mentioned before, combination sensitive neurons in the auditory cortex form a chronotopically organized computational map of target distance. Objects at different distances evoke neuronal responses at different positions in this neuronal map. However, it remained so far unknown, how multiple targets in a complex, cluttered and dynamic environment are represented and segregated in this neuronal map. Dear et al. (1993b) proposed that a concurrent representation of multiple echo delays in this map acts as the neuronal basis for a complex acoustic scene representation. Other studies in bats propose an organization of dynamic auditory stimuli into auditory streams. In a natural situation, during flight, a bat receives a sustained echo stream that provides continuously changing acoustic information (echo-acoustic flow) about the surrounding objects in a complex acoustic environment (Moss and Surlykke, 2010). Echo-acoustic flow contains not only information about echo delay but also about the geometric relationship between objects and their motion relative to the bat (McKerrow, 2008).

Recent studies simulating a flight using naturalistic pulse/echo sequences have shown that echo-acoustic flow fields significantly increase the selectivity of echo-delay-tuned neurons in the AC and modify the cortical target range representation (Bartenstein et al., 2014; Beetz et al., 2016b). However, receptive fields of adjacent echo-delay-tuned neurons largely overlap and the cortical target distance map is more blurry than precise (Hechavarría et al., 2013b; O'Neill and Suga, 1982; Schuller et al., 1991). Furthermore, in a dynamic and cluttered environment, bats have to deal with complex interfering patterns of incoming echo streams from multiple objects (Moss et al., 2006; Moss and Surlykke, 2001). Moss and Surlykke (2010) proposed that the bat's perceptual system might organize complex echo-acoustic information into auditory streams, allowing it to track specific auditory objects during flight. The temporal pattern of sonar emissions, such as grouping into so-called "strobe groups" (sequences of clustered pulses, containing two or more pulses at high repetition rate; Moss et al., 2006), might further facilitate echo stream segregation in cluttered environments (e.g. Kothari et al., 2014, Wheeler et al., 2016).

This project aims to investigate the cortical representation of echo streams from multiple objects during a simulated naturalistic pulse/echo sequence and the impact of dynamic stimulation on the cortical target range map. Our hypothesis was that neurons in the auditory cortex of anesthetized bats can lock onto echoes from specific objects in a complex echo-acoustic pattern while the representation of surrounding objects is suppressed.

For this, we used a typical echolocation call of *P. discolor* to generate naturalistic pulse/echo sequences simulating a bat's flight while passing two virtual objects positioned lateral to its flight path. The sequences were presented to the anesthetized bat *via* ear-phones. We recorded the resulting neuronal responses evoked in the posterior dorsal auditory cortex during this presentation. Specifically, we were interested if neurons in the AC were able to track specifically one out of two objects that were presented in a complex sequence. We also varied the temporal pattern of sonar emissions during the simulated pulse/echo sequences to test their influence on the cortical target representation.

Three-dimensional receptive fields in the auditory cortex

The following part of the introduction corresponds to the publication:

*“Representation of three-dimensional space in the auditory cortex of the echolocating bat *P. discolor*” (Greiter and Firzlaff, 2017b)*

The article is published in PLOS one under the terms of the Creative Commons Attribution license which permits free reproduction of published articles.

In contrast to the current knowledge about the coding of target distance in the auditory cortex, the knowledge about spatial tuning in the auditory cortex of bats is rather limited. While different studies showed a topographic arrangement of neurons, at least for sound azimuth, in the superior colliculus (Hoffmann et al., 2016; Oshimozawa et al., 1984), no such topographic arrangement of neurons could be found for cortical neurons so far. The neurons in the primary fields of the auditory cortex are typically arranged tonotopically and can further encode interaural level differences (Esser and Eiermann, 1999; Hoffmann et al., 2008; Razak and Fuzessery, 2002). Spatial positions in azimuth and elevation seem to be encoded by the extent of the activated cortex resulting from the overlap of binaural and tonotopic maps (Razak, 2012; Razak et al., 2015).

The non-primary fields of the AC in bats were mainly investigated with respect to echo delay coding, but not to spatial tuning. The neurons in the non-primary fields show usually no tonotopic arrangement but respond to high frequency sounds in the echolocation range (Hoffmann et al., 2008) and might therefore be most important during active echolocation. As they do encode echo delay and thereby form a map of target distance, these neurons might be especially suited to further encode spatial information to form a three-dimensional representation of space. However, only few studies tried to investigate the directional sensitivity of combination-sensitive (= delay tuned) cortical neurons so far. It remains a matter of debate if these combination-sensitive neurons can process directional information and encode three-dimensional acoustic space.

Suga et al. (1990) investigated the spatial selectivity of cortical combination-sensitive neurons in the bat *Pteronotus parnellii* by presenting pairs of short frequency modulated pulses (FM pulses). They found that these combination-sensitive neurons were extremely broadly tuned to auditory space in azimuth and elevation (at 10 dB above threshold: width about 70° in azimuth and elevation, at 30 dB above threshold: outside measurable range in their study) and responded most strongly to sounds delivered from directly in front of the bat. They suggested that combination-sensitive neurons are not suited to process directional information but that this information is processed in parallel by a separate population of neurons in the cortex. However, it remained unclear where this directional information could be processed in the cortex and how bats are able to combine the directional information of objects in space with the information about the distance to these object.

In contrast to this study on cortical neurons, combination-sensitive neurons in the superior colliculus exhibited a higher spatial selectivity in azimuth to presented pairs of FM pulses and it was proposed that these 3D neurons might play a role in combining azimuthal, elevational and distance cues to guide perceptually driven orientation and vocalization responses (Valentine and Moss, 1997). However, the selectivity of these neurons to different positions in elevation was not systematically investigated in this study.

Hoffmann et al. (Hoffmann et al., 2013; Hoffmann et al., 2015) investigated the spatiotemporal response characteristics of cortical neurons by presenting sequences of echoes in virtual acoustic space and evaluated them using a reverse-correlation technique. They found that neurons with complex temporal response patterns, possibly corresponding to combination-sensitive neurons, exhibited a clear spatial selectivity in azimuth and elevation.

However, all studies mentioned above used rather artificial stimuli to investigate the temporal and spatial selectivity of neurons by presenting pairs or sequences of sounds from stationary loudspeakers or earphones without considering for example sonar emission characteristics. The bats' sonar system, however, is highly directional. Recent studies showed that *P. discolor* as well as other bats have a highly dynamical biosonar and are constantly controlling their biosonar field of view by adjusting their emitter aperture (Kounitsky et al., 2015; Linnenschmidt and Wiegrebe, 2016). The sonar beam aim and directionality serves to filter and separate target and clutter echoes. Therefore, it is crucial to include call emission characteristics; distance and frequency dependent sound damping as well as the ear directionality in such an investigation. We aimed this project to fill the gap of knowledge on the three-dimensional representation of auditory space in the auditory cortex. We specifically designed this study to use stimuli corresponding to a more natural situation than the studies mentioned above by including pulse emission characteristics of *P. discolor*, and distance and frequency dependent sound damping as well as all relevant spatial cues such as interaural time and level differences and spectral differences due to the head related transfer function (HRTF).

Our hypothesis was that combination sensitive neurons encoding target distance in the auditory cortex of *Phyllostomus discolor* can also process directional information. To test this hypothesis, we presented combinations of typical echolocation pulses of *P. discolor* and virtual echoes from different simulated positions in 3D-space and measured the evoked neuronal responses of combination sensitive neurons in the posterior dorsal field (PDF) of the AC in anesthetized bats.

METHODS

Experimental animals: *Phyllostomus discolor*

The Pale Spear-nosed Bat (*Phyllostomus discolor*) is a medium-sized neotropical bat (mean wingspan 42 cm, body weight 30-45 g) that occurs commonly and widespread from southern Mexico to Paraguay and southern Brazil (Barquez et al., 2015; Wilson and Reeder, 2005). *P. discolor* is omnivorous and the diet consists mainly of a mixture of fruits, nectar, pollen and insects (Kwieceński, 2006). The species uses short multi-harmonic, frequency modulated (FM) echolocation calls with a rather low sound pressure level of about 80 dB, a pulse duration of about 0.3-2.5 ms and a frequency range of about 40-100 kHz with a spectral centroid about 67 kHz (Linnenschmidt and Wiegrebe, 2016; Rother and Schmidt, 1982).

All animals used for the experiments originated from a breeding colony situated in the Department Biology II of the Ludwig-Maximilian University of Munich. The animals were kept separated from other bats under semi-natural conditions (reversed 12 day/12 h night cycle, 65%-70% relative humidity, 28 °C) with free access to food and water.

Initial surgery

All experiments complied with the principles of laboratory animal care and were conducted under the regulations set out by the current version of the German Law on Animal Protection (approval 55.2-1-54-2532-147-13 Regierung von Oberbayern). The initial surgery and all following electrophysiological experiments were performed under general anesthesia using a subcutaneously injected mixture of medetomidine (Dorbene[®], Zoetis, Berlin, Germany), midazolam (Dormicum[®], Hoffmann-La Roche, Mannheim, Germany) and fentanyl (Fentadon[®], Albrecht, Aulendorf, Germany) at a dosage of 0.4, 4.0 and 0.04 µg/g body weight, respectively. Anesthesia was maintained for up to 5 hours through additional injections containing two-thirds of the initial dose every 1.5 h. After completion of the surgery or the experiments at each day, anesthesia was antagonized using a mixture of atipamezole (Alzane[®], Novartis, Nürnberg, Germany), flumazenil (Flumazenil, Hexal, Holzkirchen, Germany) and naloxone (Naloxon-ratiopharm[®], Ratiopharm, Ulm, Germany), which was injected subcutaneously (2.5, 0.5 and 1.2 µg/g body weight, respectively).

In the initial surgery, the skin overlying the skull was opened along the midline and the skull surface was freed from the tissue. A small metal tube was then fixed to the skull using a microglass composite in order to immobilize the animal in a stereotaxic device during the experiments. The stereotaxic device allowed an accurate measurement of the positions of recordings and tracer injections in the brain of the animals during the experiments and a reliable comparison of coordinates among different experimental animals. Details of the stereotaxic device and the method to reconstruct the coordinates are described in detail by Schuller et al. (1986). In brief, the animal was fixed with the mounted rod to the stereotaxic device. The alignment of the animal's skull was then measured by scanning characteristic profile lines on the skull's surface in rostro-caudal and medio-lateral direction. The measured skull profile was then compared to a standardized brain atlas of *P. discolor* (A. Nixdorf, T. Fenzl, B. Schwellnus, unpublished data). This method allowed calculating the coordinates of all recorded positions in relation to the standardized brain atlas (Hoffmann et al., 2008). After surgery and measurement of the skull profile lines, the bat was treated with an analgesic (0.2 µg/g body weight; Meloxicam, Metacam, Boehringer-Ingelheim, Ingelheim am Rhein, Germany) to alleviate postoperative pain and antibiotics (0.5 µg/g body weight; enrofloxacin, Batril®, Bayer, Leverkusen, Germany). Both Metacam and Baytril were further administered on the next three post-operative days.

General experimental procedure

After initial surgery, experiments on the anesthetized animals were conducted in a sound-attenuated and heated (~35 °C) chamber. Recording sessions took place three days a week, with at least one day off between consecutive experiments, for up to eight weeks. The responses recorded from neurons under general anesthesia reflect the behavioral experiments of *P. discolor* well (Firzlaff et al., 2006). All extracellular recordings were made with parylene-coated tungsten microelectrodes (5 MΩ impedance, Alpha Omega, Ubstadt-Weiher, Germany). Electrode penetrations in the AC or SC in both hemispheres were run perpendicularly or obliquely to the brain surface with different medio-lateral and rostro-caudal angles. The electrode signal was recorded using an analog-to-digital converter (RA16 + RX5-2, Tucker-Davis Technologies (TDT), Alachua, USA, sampling rate: 25 kHz, band-pass filter: 400-3000 Hz) and the software package Brainware (TDT). The action potentials were threshold discriminated and saved for later offline analysis. As far as possible, single neurons were analyzed. However, it

was not always possible to clearly discriminate the activity of single units and some recordings reflect the collective activity of one to three neurons at the same recording site. Because of this, the term “unit” will be used in the following text to describe the collective activity of one to three neurons at a recording site.

All acoustic stimuli were created with MATLAB®, digital-to-analog converted (RX6, TDT, sampling rate 260 kHz, attenuator: PA5, TDT) and presented *via* custom-made transducer ear-phones (flat frequency response of ± 10 dB between 10 kHz and 120 kHz, Schuller, 1997). The ear-phones were calibrated using a Brüel & Kjaer reference microphone (type 4939) and a Brüel & Kjaer Measuring Amplifier (type 2610). In order to search for acoustically driven neural activity in the SC or AC, typical echolocation calls of *P. discolor* were used. For the projects focusing on the SC, this call was convolved with the left and right pair of the head-related transfer function (Firzlaff and Schuller, 2003; Mey et al., 2008) and presented binaurally with a repetition rate of about 4 Hz. For the projects focusing on combination-sensitive neurons in the AC, pairs of typical echolocation calls (representing a “pulse” and a virtual “echo”) were used. The delay and amplitude ration between the “pulse” and the “echo” could be varied. The pairs of stimuli were presented diotically (without any monaural or binaural spatial information) with a repetition rate of about 2 Hz. A detailed description of the acoustic stimuli used for the recordings is given separately for each project.

After completion of all electrophysiological experiments, a neuronal marker (BDA 3000, 1 mg/20 μ l phosphate buffer, Sigma-Aldrich, Munich, Germany) was pressure-injected (Nanoliter 2000 injector, World Precision Instruments, Sarasota, USA) into the brain at 2-3 different positions in the region of recording in order to reconstruct the position of the recording sites in standardized stereotaxic coordinates of a brain atlas of *P. discolor* (A. Nixdorf, T. Fenzl, B. Schweltnus, unpublished). The stereotaxic coordinates of these marker injections were documented and later compared to the positions of the marker in the stained tissue sections (Avidin-Biotin Complex (ABC) / Diaminobenzidine (DAB) staining procedure), which then served as references to the documented recording positions (Schuller et al., 1986). After the injection of the neuronal marker, the animals were euthanized by an intraperitoneally applied lethal dose of pentobarbital (0.16 mg/g bodyweight) and subsequently perfused transcardially.

Influence of ear movements on spatial receptive fields in the superior colliculus

Spatial tuning in the superior colliculus

The acoustic stimuli for the measurement of spatial receptive fields in the SC were generated by using a naturalistic echolocation call (pulse) of *P. discolor*. This call was convolved with the left and right ear pair of the head-related transfer function (Firzlaff and Schuller, 2003; Mey et al., 2008) and presented binaurally *via* ear-phones. The resulting stimuli mimicked a natural “echo” with all relevant spatial cues such as interaural level differences and spectral composition of echoes originating from different spatial directions. For this project, the “echoes” were simulated without a preceding echolocation pulse. The stimuli were presented with a level of 70-85 dB SPL, corresponding to typical level of call emission in *P. discolor* (Linnenschmidt and Wiegrebe, 2016; Rother and Schmidt, 1982).

The resulting neuronal activity was measured within a time window of 20-50 ms, starting directly after the echo presentation. Each spatial position was tested 10 times (10 repetitions). The order of the tested simulated spatial directions of the “echoes” was randomized. The mean number of action potentials (spikes) per stimulus presentation for each spatial position was calculated and the responses from neighboring spatial positions were smoothed using a 2D-moving average method (MATLAB®). Spatial receptive fields (SRF) were then visualized as filled contour plots. Spatial receptive fields included all responses that elicited at least 50% of the maximum response of all tested positions. The centroid (center of gravity) and the area of each SRF were calculated using MATLAB® functions (centroid function: written by Kirill Pankratov (1995), SRF area: built-in MATLAB® function “polyarea”).

Influence of ear movements on spatial tuning

I tested the influence of ear movements on the spatial receptive fields by inducing a proprioceptive sensory input corresponding to a specific movement or turning of the ears. For this, I electrically stimulated different ear muscles at the base of the pinna (i.e. adductor muscle: *M. adductor auricularis superior*, elevator muscle: *M. cervicoauricularis superficialis major/minor* and drawback muscle of the pinna: *M. cervicoauricularis profundus major/minor*, for anatomical details see Schneider and Möhres, 1960). However, due to technical issues only recordings with stimulations of the adductor and the elevator muscle could be analyzed and are

shown in the following results section. The electric stimuli for the ear stimulation were generated using an optically isolated, constant current stimulation unit (PSIU6 Photoelectric Isolation Unit, Grass, West Warwick, USA) and controlled *via* a RP2 (TDT). For each experiment, small metal insect pins were attached at the base of the pinna at a specific muscle and connected to the stimulation unit. The electric current for the stimulation was gradually increased until each stimulation pulse (duration 1 ms, monopolar, <10 mA) caused a visible twitch of the stimulated ear muscle. During the recordings, the electric stimulation pulse preceded the acoustic stimulation by 30 ms. Each spatial position was tested either with electrical ear stimulation (“stimulation”) or without stimulation (“control”). Control conditions and stimulation conditions were randomly interspersed. As the ear-phones for the acoustic stimulation were placed directly at the opening of the ear canal, the induced movements of the pinna did not influence the acoustic stimulation. Therefore, a simulated movement of the pinna (electric stimulation) was always coupled with constant acoustic spatial information.

The results were statistically analyzed using a Wilcoxon-Mann-Whitney test to check for differences between stimulation and control recordings. Correlation analysis was done using a Spearman’s rank correlation analysis. After an initial test using an Anderson-Darling test for normal distribution, all parameters were considered as not normally distributed (all statistical tests: MATLAB® Statistics Toolbox).

Frequency tuning in the superior colliculus

The frequency tuning in the SC was determined by presenting pure tones with different frequencies and sound pressure levels, durations of 20 ms and a repetition rate of about 3 Hz. For each recording, an individual center frequency and frequency range could be chosen. Usually, the center frequency was 50 kHz with a frequency range of 2 octaves (25-100 kHz) and 8 steps per octave. The tested sound pressure levels ranged at least from 40 dB to 80 dB in steps of 5-10 dB. For each unit, the lowest sound pressure level eliciting a neuronal response was determined. Each stimulus was presented with 10 repetitions in randomized order. The stimuli were generated with MATLAB® and presented monaurally to the contralateral ear *via* ear-phones. The resulting neuronal activity was measured within a time window of 20-50 ms, starting directly after the stimulus presentation. The tuning curves were visualized as filled contour plots. The response threshold was 50% of the maximum response. The frequency where the pure tones with the lowest sound pressure level cause a neuronal response (lowest

tip of the tuning curve) were defined as characteristic frequency (CF) of a unit. For the statistical analysis, a Spearman's rank correlation analysis was performed.

Echo-acoustic flow shapes object representation in spatially complex acoustic scenes

The text and the figures of following section correspond to the publication:

*"Echo-acoustic flow shapes object representation in spatially complex acoustic scenes"
(Greiter and Firzlaff, 2017a)*

The article is published in the Journal of Neurophysiology which permits authors the reproduction of published articles for dissertations without charge or further license.

Characterization of basic delay tuning properties

In order to measure the basic echo delay tuning properties, the following procedure was used: a pre-recorded typical echolocation pulse of *P. discolor* was presented with a constant level of 70 – 85 dB SPL. An "echo" was simulated by presenting the same pulse while randomly changing the delays from 1 to 29 ms and the amplitudes from -40 to 0 dB relative to the level of the "pulse". The resulting neuronal activity was measured within a time window of 20-50 ms, starting directly after the echo presentation. Units' responses were classified as "facilitated" if their response to at least one of the presented pulse/echo pairs was at least 30% stronger than the sum of the responses for only pulses or only echoes. Only facilitated units were further analyzed with regard to the basic delay tuning characteristics to ensure that responses were specific to pairs of pulses and echoes.

Delay response fields (DRFs) for facilitated units were visualized as filled contour plots, and threshold curves were calculated using a threshold of 50% of the maximum response for each unit. The DRF of each unit was further characterized by measuring the delay at the maximum response (best delay, BD) and the delay at the lowest tip of the threshold curve (characteristic delay, CD), corresponding to Hechavarría et al. (2013b). The BD and CD were used, together with the units' positions in the AC projected onto the cortical surface, to calculate cortical delay tuning maps. Furthermore, the distributions of the BD and CD on the cortical surface were statistically analyzed using Spearman's rank correlation analysis (MATLAB® Statistics Toolbox).

Stimulus generation for naturalistic flight sequences

Naturalistic flight sequences were generated in the manner described by Bartenstein et al. (2014). In detail, flight trajectories were calculated for a bat flying laterally toward two objects (target 1 and target 2) over a flight distance of 4.0 m. The objects were positioned at distances of 3.5 and 4.0 m (in the direction of the heading, which we will call the heading distance) with lateral distances to the bat's flight path of 0.6 and 0.2 m for target 1 and target 2, respectively (Figure 2 A). Both objects were positioned at the same height as the bat's flight path. The obstacles were assumed to be perfect reflectors.

To investigate the influence of naturalistic echolocation behavior, we used three different temporal echolocation pulse patterns (Figure 2 B,C,D):

- a. constant pulse rate of 12 Hz;
- b. linearly increasing pulse rate from 12 Hz up to 36 Hz and
- c. simulation of typical strobe groups (Rother and Schmidt, 1982) with a group frequency of 12 Hz and an increasing number of pulses in each group (1-3 calls per group).

The positions of the pulse emission and echo reception for both objects along the flight path were determined. The simulated flight speed was 3 m/s, which is in the range typically reported for phyllostomid bat species (Kugler et al., 2016; Morrison, 1980).

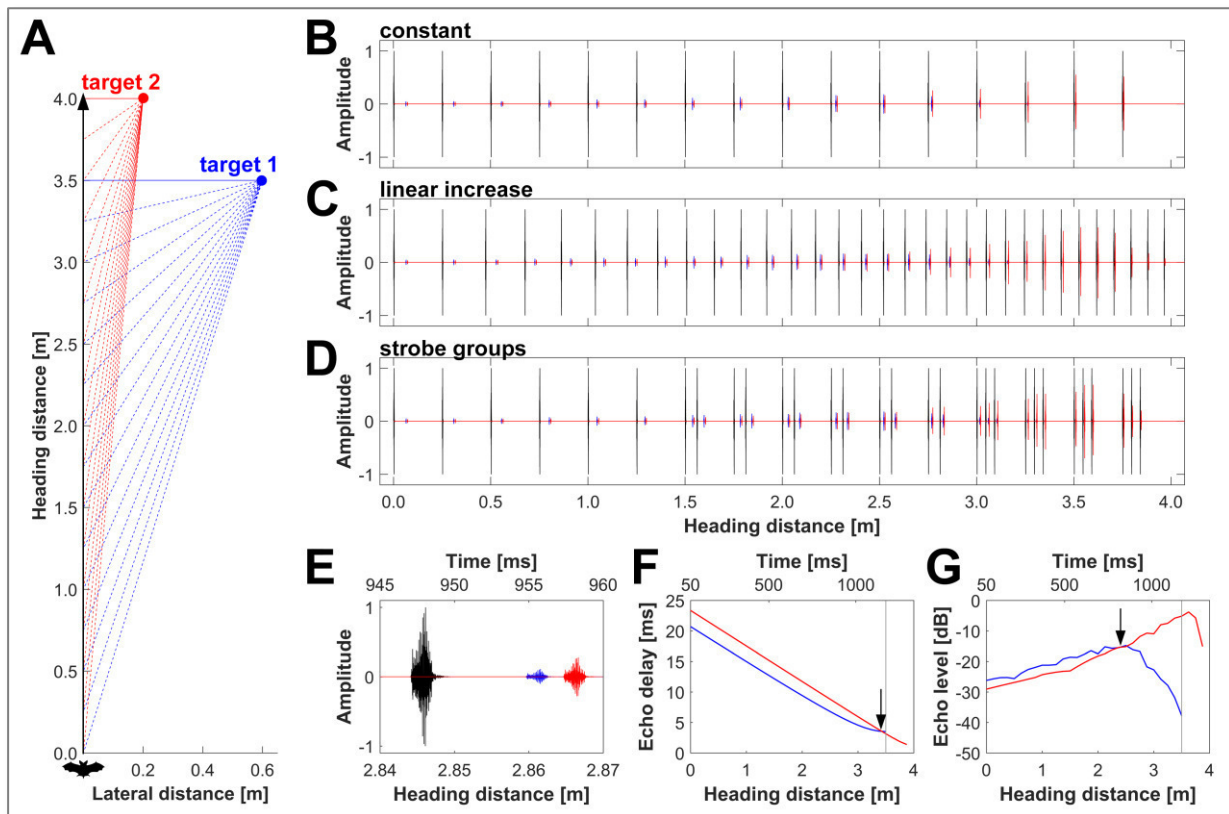


Figure 2: Generation of naturalistic pulse/echo sequences

(A) Spatial layout of the virtual flight sequence with two targets positioned at heading distances of 3.5 m and 4.0 m and at lateral distances of 0.6 m and 0.2 m, respectively. Blue (target 1) and red (target 2) lines indicate the reflected echoes from the objects during the flight sequence. (B-D) Sequences of pulses and echoes from both targets are shown for a constant pulse rate (B), a linearly increasing pulse rate (C) and strobe groups (D). (E) Details of a pulse/echo sequence showing a single echolocation pulse and corresponding echoes from target 1 and target 2. (F,G) Progression of echo delay (F) and echo level (G) for target 1 and target 2 along the flight path with corresponding timescale. The acoustic stimulation is preceded by a 50 ms silent period in order to determine the level of spontaneous activity and followed by another 200 ms silent period. The vertical grey lines mark the position where the bat passes target 1. (F) The echo delay of target 2 exceeds the echo delay of target 1 until 3.43 m heading distance (black arrow, 7 cm before passing target 1). (G) The echo levels for target 1 and target 2 increase when the bat approaches the targets. After about 2.4 m heading distance, the angle to target 1 increases considerably and consequently the target 1 echo level drops rapidly as target 1 leaves the beam of sonar emission.

(Figure adapted from Greiter and Firzlaff, 2017a. Adapted with permission.)

We generated pulse/echo sequences by using an echolocation pulse of *P. discolor* containing no directionality (see Bartenstein et al., 2014). The pulse was convolved with the left and right ear pair of the head-related transfer function (Firzlaff and Schuller, 2003; Mey et al., 2008) and the transfer function of pulse emission of *P. discolor* (Vanderelst et al., 2010) corresponding to the angular direction of the echo reflection for each position and object along the flight path. Geometric and atmospheric attenuation was calculated in MATLAB®. In detail, a vector of discrete frequency steps was generated ranging from 0 to 130 kHz in 10 kHz steps. A second vector contained the distance specific attenuations for each frequency step (derived from Stilz and Schnitzler, 2012), expressed in linear amplitude. In a next step, an impulse response was generated from both vectors using the MATLAB® `fir2` function (signal processing toolbox). This

impulse response was then convolved with the echoes to provide for frequency and distance specific atmospheric as well as geometric attenuation. Note, that atmospheric attenuation is the main determinant for echo attenuation at longer distances, while at shorter distance geometric attenuation is mostly determining echo attenuation. The resulting artificial echoes included all relevant spatial cues, such as ITDs, frequency-dependent ILDs and spectral profiles as well as distance and frequency dependent sound damping. We did not simulate the Doppler-shifts caused by the bat's movement as these effects are negligible in FM bats. To simulate the bat's echolocation pulses, non-directional pulses were attenuated by 26 dB so as to mimic the typical level of self-stimulation by vocalization (Pietsch and Schuller, 1987). Pulses and echoes for both objects were then combined, including the respective echo delays representing the distance to each object at each position during the flight sequence. The final sequences of pulses and echoes were generated with a constant pulse rate, a linearly increasing pulse rate, and simulated strobe groups. The complete pulse/echo sequences were calculated using MATLAB® functions custom build in our lab, DA converted (RX6, TDT) and presented *via* ear-phones (Schuller, 1997). In the final sequences, all echo-acoustically important parameters such as echo delay, echo amplitude, echo reflection angle and echo spectral content were changed dynamically as a function of flight time (i.e. the position of the bat along the flight path). The pulses were presented at 70-85 dB SPL, and the pulse level was constant within the sequence. We adapted the presented pulse sound pressure level to achieve stable neuronal responses to the presented sequences. Information for this was gained from the DRFs recorded for each cell. The echo delays decreased within the sequence from 20.7 to 3.5 ms and 23.4 to 1.2 ms for target 1 and target 2, respectively. The echo amplitudes increased from -34.4 to -15.7 dB and from -29.1 to -3.4 dB relative to the pulse level for target 1 and target 2, respectively (Figure 2 E,F,G). Pulses within the sequences never overlapped with preceding echoes (no pulse/echo ambiguity). We used exclusively the described spatial layout to keep the differences between the targets with respect to echo delay and echo level in a limited range. This was done to ensure that as many neurons as possible would respond to the presentation of echoes from both targets when presented alone in a sequence, a prerequisite of our experiment. Sequences were presented binaurally, with both objects positioned contralaterally to the recording site. Each stimulus sequence was preceded by a 50 ms silent period to determine the level of spontaneous activity and it had a duration of about 1.4 s. Sequences were presented every 3 s.

To measure the responses for each individual target, pulse/echo sequences were generated (1.) for both targets together; (2.) for target 1 only; (3.) for target 2 only. Additional sequences were presented for every unit and pulse emission pattern, containing only pulses (4.) or only echoes (5.), to ensure that the units responded only to pairs of pulses and echoes specifically. Consecutive presentations of pulse/echo sequences were separated by at least 30 s to prevent interactions due to the order of presentation.

Data analysis for naturalistic flight sequences

The spike responses evoked by the simulated flight sequences were arranged both as peristimulus time histograms (PSTHs, 2 ms bin width) and as raster plots. To determine the responses to each pulse/echo pair within a sequence, manually fixed response windows were set after each pulse/echo pair. Response windows started at the time of the first object echo and ended after the neuronal activity decreased below the level of the spontaneous activity, but not later than the time of the first echo of the subsequent pulse. To ensure that the response windows could not overlap between two successive pulse/echo pairs, the response window length never exceeded that of the minimal inter-pulse interval for each simulated pulse rate. The minimal inter-pulse interval was 83 ms for the constant pulse rate, 27 ms for the linearly increasing pulse rate and 15 ms for the simulated strobe groups. The length of the response window was equal for all pulse/echo pairs within a sequence and for all records of a unit for each simulated pulse rate. For every presented sequence (both targets, only target 1, only target 2, only pulses, only echoes), spikes occurring in each response window were summed so as to get the response rate of a unit for every pulse/echo pair within the sequence. Units' responses were classified as "facilitated" if their response in a pulse/echo-sequence was at least 30% stronger than the sum of responses from only pulses and only echoes. To determine the specific response of a facilitated unit to each object, the pulse/echo pair evoking the maximum response rate within sequences presenting only target 1 or target 2 was identified (maximum response position). The echo delay of the corresponding pulse/echo pair was considered to be the "specific delay" of the unit for the simulated object and pulse rate. Only units that showed a distinct and facilitated response to both individual targets ("specific response") were further analyzed regarding the cortical echo delay tuning and object representation. Cortical echo delay tuning maps were calculated for each target and pulse rate based on the specific delays and stereotaxic coordinates of all of the facilitated and specific units. The distributions of the specific delays for both targets at all different pulse rates were

statistically analyzed using a Kruskal-Wallis test, followed by a pair wise Wilcoxon-Mann-Whitney test (MATLAB® Statistics Toolbox).

To investigate, whether the neurons responded equally to the targets when they were presented alone in a sequence as compared to both targets being presented together in a complex sequence, we examined the response rate at the maximum response position for each object and compared the values between the individual presentations of the targets and the combined presentation (at the respective pulse/echo pairs within the sequence). It was essential for this comparison that the responses of both individual targets could be identified in the complex sequence. Therefore, units that responded to both targets on the same pulse/echo pair within the sequence (i.e. an overlap of the maximum responses) were excluded from further analysis (n=3).

The response of a unit in the combined presentation to the respective object was classified as an “equal” response if the spike rate was at least 50% of the original response in the individual presentation. The unit’s response was classified as “decreased” if the spike rate was less than 50% of the original spike rate. By using such strict criteria, we ensured that the number of neurons focusing on specific targets was not overestimated. Units’ responses were then further categorized as “no focus” if they responded equally to both targets, as “focus on target 1” if only the response to target 2 decreased and as “focus on target 2” if only the response to target 1 decreased. In some rare cases, the unit’s response decreased for both targets.

Three-dimensional receptive fields in the auditory cortex

The text and the figures of following section correspond to the publication:

*“Representation of three-dimensional space in the auditory cortex of the echolocating bat *P. discolor*” (Greiter and Firzlaff, 2017b)*

The article is published in PLOS one under the terms of the Creative Commons Attribution license which permits free reproduction of published articles.

Characterization of basic delay tuning properties

The basic delay tuning properties of the cortical neurons were determined with DRFs in the same way as described above. “Pulses” were presented at a constant level of 80-85 dB SPL. Echoes were presented without any spatial cues (no interaural level differences or spectral differences) with randomly changing echo delays (1 to 29 ms, step size 3 ms), and echo amplitudes (-45 to 0 dB echo level, step size 5 dB). Pairs of pulses and echoes were presented diotically. The resulting neuronal activity was measured within a time window of 20-50 ms, starting directly after the echo presentation. Only units classified as “facilitated” (response to pulse/echo pairs at least 30% stronger than the sum of the responses to isolated pulses and echoes) were further analyzed with regard to basic echo delay tuning and spatial tuning characteristics. The DRF of each unit was further characterized by measuring the echo delay at the maximum response (best delay, BD) and the echo level at the maximum response (best level, BL), corresponding to Hechavarría et al. (2013b).

Characterization of three-dimensional tuning

We used again a combination of artificial “pulse” and “echo” to test the spatial directionality of cortical delay tuned neurons. The “pulse” was mimicked by using a prerecorded echolocation pulse of *P. discolor* containing no directionality. For the simulated “echo”, this pulse (see Figure 3 A) was convolved with the transfer function of call emission of *P. discolor* (Vanderelst et al., 2010, see example in Figure 3 B) and the left and right ear pair of a standardized, simulated head-related transfer function (Firzlaff and Schuller, 2003; Mey et al., 2008, see example in Figure 3 C) corresponding to the tested spatial directions (from -67.5° to +67.5° in azimuth and elevation, spacing of 15.0°). We did not use individual HRTFs as the differences between the HRTFs of individual bats showed only a minor degree of inter-individual variability (Firzlaff and Schuller, 2003). Geometric and atmospheric attenuation was calculated in MATLAB® with the

same method described for the echo-acoustic flow project. The resulting echoes included all relevant spatial cues, such as ITDs, frequency dependent ILDs and spectral profiles as well as distance-dependent and frequency-dependent sound attenuation (example in Figure 3 D). Note that the presented echo level in this simulation is always a function of the directional call emission level, the outer ear directionality and the traveled physical distance of pulses and echoes (corresponding to the echo delay). The “pulses” were then further attenuated by 26 dB to mimic the typical level of self-stimulation by vocalization (Pietsch and Schuller, 1987). Afterwards, “pulses” and “echoes” were combined including different tested echo delays.

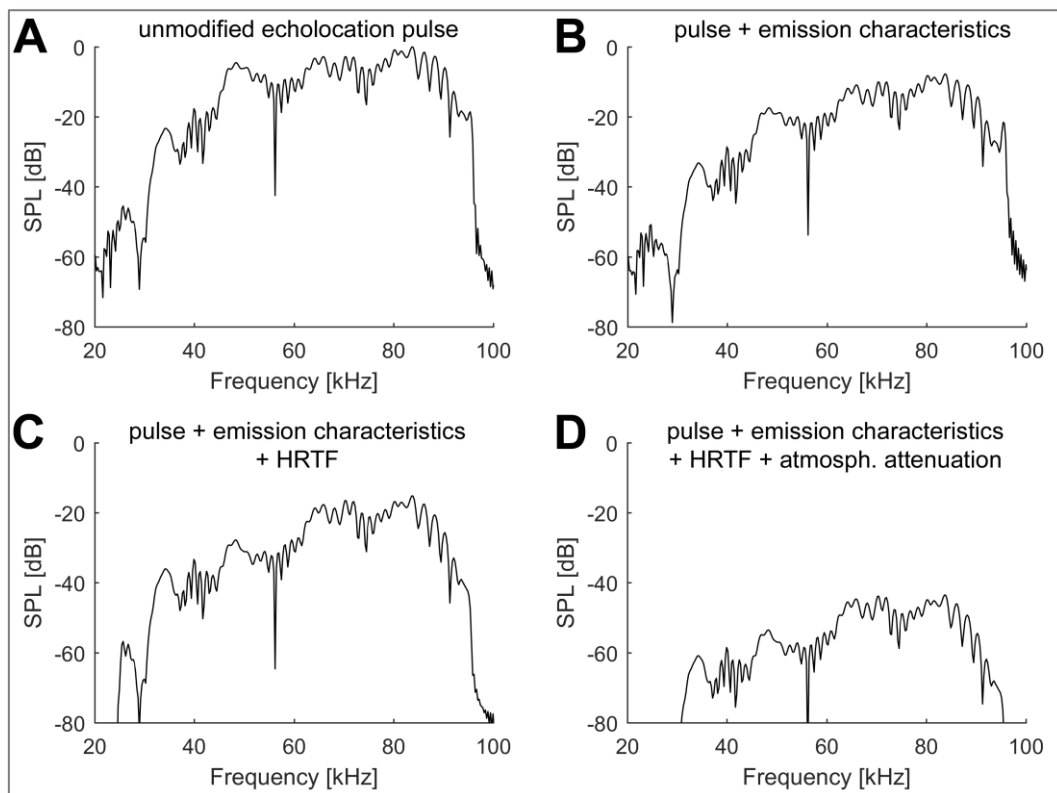


Figure 3: Frequency content of virtual echoes at different steps of generation

(A-D) Spectra of the simulated echoes (ipsilateral ear) derived from the original echolocation pulse at different steps of generation. The final echoes were simulated from a position of $+22.5^\circ$ azimuth and $+7.5^\circ$ elevation. The simulated target distance was 1.54 m, corresponding to an echo delay of 9 ms. For each panel, the x-axis shows the frequency and the y-axis the respective sound pressure level (SPL). (A) Spectrum of the unmodified, original echolocation pulse. (B) Spectrum of the echolocation pulse after simulation of the pulse emission characteristics. (C) Spectrum of the echoes derived from the original pulse and including pulse emission characteristics and HRTF. (D) Spectrum of the final echoes including pulse emission characteristics, HRTF and distance and frequency dependent atmospheric as well as geometric attenuation.

(Figure adapted from Greiter and Firzlaff, 2017b. Adapted with permission.)

Each unit’s spatial directionality was tested at an echo delay and absolute echo level corresponding to the unit’s best delay and best level as measured in the corresponding DRF. Additional records were performed at different shorter and longer echo delays for each unit. As described by Hagemann et al. (2010) and due to our own experience in *P. discolor* in the project

focusing on echo-acoustic flow fields (Greiter and Firzlaff, 2017a), combination-sensitive neurons encoding different delay ranges are not uniformly distributed across the AC but show an overrepresentation of short echo delays. Furthermore, the delay-bandwidth of these neurons increases at longer echo delays (Hagemann et al., 2010). Because of this phenomenon, we did not use linearly spaced but logarithmically spaced echo delay steps to investigate the spatial directionality of the combination sensitive neurons at different echo delays. For this, the following 5 standardized delay steps (X) were used:

$$\text{echo delay} = BD \times 1.25^X$$

$$X = \{-2, -1, 0, +1, +2\}$$

Using this standardized, logarithmically spaced echo delay steps enabled us to directly compare each unit's spatial directionality at different echo delays (corresponding to a physical distance to a virtual object) and calculate a three-dimensional receptive field for each tested unit. The presented pulse level was kept constant at different delay steps, the echo levels changed as a function of echo delay (i.e. distance dependent sound attenuation). Further records were done at the units' BD and echo levels of BL+10 dB and BL-10 dB to test the influence of the presented sound pressure level on the spatial directionality of the cortical delay tuned neurons.

For the analysis of the records, the neuronal activity was measured in the same time window as specified in the corresponding DRF (20-50 ms time window, starting directly after the echo presentation). Delay dependent spatial receptive fields (DSRF) were visualized as filled contour plots for each tested echo delay. The spike count in all records of each unit at different echo delays was normalized on the maximum response elicited in the recordings. In most units, the highest spike count was elicited at the units' BD. Threshold curves were calculated for each record using a threshold of 50% of the normalized maximum response for each unit. The DSRFs were further characterized by measuring the spatial position eliciting the maximum response (best azimuth (BAZ), best elevation (BEL)), the centroid (geometric center in azimuth and elevation, MATLAB® function) and the width of the spatial receptive field (measured at the 50% contour line) for each delay step, corresponding to Suga et al. (1990).

The results were statistically analyzed using a Kruskal-Wallis test for multiple comparisons, followed by a pairwise Bonferroni corrected Wilcoxon-Mann-Whitney test to investigate differences between distributions of different parameters. Correlation analysis was done using a Spearman's rank correlation analysis (MATLAB® Statistics Toolbox). All parameters were considered as not normally distributed.

INFLUENCE OF EAR MOVEMENTS ON SPATIAL RECEPTIVE FIELDS IN THE SUPERIOR COLLICULUS

In the following section, the data on the representation of space and the frequency tuning in the superior colliculus were published as part of the publication:

*“Congruent representation of visual and acoustic space in the superior colliculus of the echolocating bat *Phyllostomus discolor*”
(Hoffmann et al., 2016)*

The data on the influence of ear movements on spatial receptive fields was not published before. The following text and the figures were written and generated exclusively for this thesis and were not part of any publication before.

Results

Spatial tuning in the superior colliculus

In this project, the neuronal responses of 64 units in the SC of *P. discolor* were analyzed. For each unit, the spatial tuning was determined while electrically stimulating a specific ear muscle (“stimulation”) and without such a stimulation (“control”).

Figure 4 A shows an example for a spatial receptive field of a SC unit (control) which responded best to a position contralateral to the recording site at $+22.5^\circ$ azimuth (best azimuth = BAZ) and -7.5° elevation (best elevation = BEL). As the maximum responses of the units can only be measured at discrete positions (step size 15° in azimuth and elevation), I additionally analyzed the geometric center of each receptive field (centroid) to investigate the spatial tuning in more detail. The centroid of the example shown in Figure 4 A was at a position of $+20.5^\circ$ azimuth and -15° elevation.

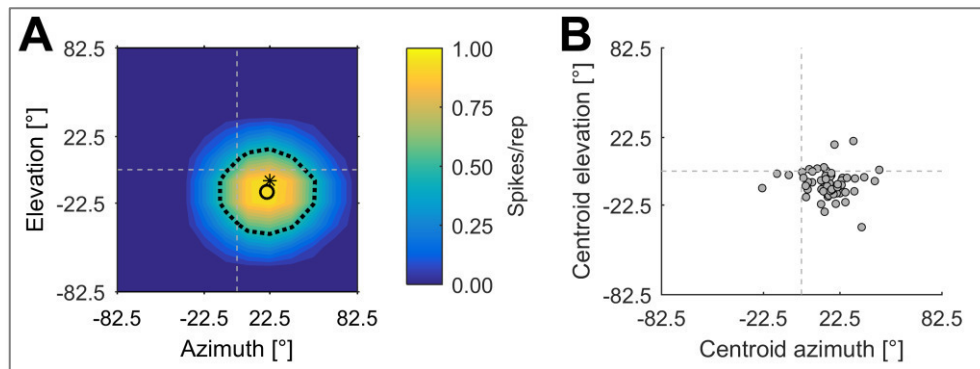


Figure 4: Spatial tuning of units in the superior colliculus

(A) Example of a neuron's spatial receptive field in the SC. The spike count per repetition is color-coded. The spatial receptive field is represented by the black dotted line corresponding to the response threshold at 50% of the unit's maximal spike count. The geometric center of the unit's spatial receptive field (centroid) is marked by a black circle (at +20.5° azimuth and -15.0° elevation). The spatial position eliciting the maximal response is marked by a black asterisk (at +22.5° azimuth and -7.5° elevation). (B) Distribution of the centroids of all analyzed units in the control recordings. Recordings from neurons in the left and right hemisphere were normalized to one side. Azimuth positions $>0^\circ$ correspond to positions contralateral to the recording site.

To gather first insights in the spatial response properties of the SC neurons, I analyzed the spatial tuning of all recorded units in the control recordings (without ear stimulation). In total, most units responded to positions contralateral (azimuth $>0^\circ$) to the recording site and slightly below the horizon (elevation $<0^\circ$). The centroid positions in azimuth ranged from -23.2° to $+45.8^\circ$ (median: 15.9°). The centroid positions in elevation ranged from -37.5° to $+20.2^\circ$ (median: -9.9°). Figure 4 B shows the centroid positions from all analyzed units (control).

I further analyzed, if a unit's spatial directionality depended on its location in the superior colliculus. For this, I tested for correlation between each unit's SRF centroid position (control) in azimuth or elevation against the unit's physical coordinates in the SC. Note that the stereotaxic coordinates of each cell were measured as medio-lateral position, rostro-caudal position and depth under the brain surface (i.e. under the brain penetration point of the electrode). The actual depth in the SC or the position of a recorded cell in a specific layer of the SC can be estimated from these coordinates. However, for the statistical analysis only the depth under the surface was used. The results can be seen in the following Table 1:

| Centroid position | Medio-lateral position | | Rostro-caudal position | | Depth under surface | |
|-------------------|------------------------|------|------------------------|--------|---------------------|------|
| | ρ (rho) | p | ρ (rho) | p | ρ (rho) | p |
| Azimuth | 0.01 | 0.92 | 0.36 | 0.004* | 0.23 | 0.07 |
| Elevation | -0.16 | 0.20 | -0.07 | 0.60 | 0.03 | 0.78 |

Table 1: Correlation analysis between SRF centroids during control and the units' coordinates in the SC

The table shows the results from the correlation analysis between each units SRF centroid (during control) in either azimuth or elevation (rows) and their medio-lateral, rostro-caudal position or depth under the brain surface (pairs of columns). For each combination, the correlation coefficient ρ (rho, first column) and the p-value (second column) for a Spearman rank correlation analysis are given. The data were not normally distributed. A red font color and an asterisk indicate a significant correlation (significance level 0.05).

The statistical analysis reveals a significant correlation ($p = 0.004$) between each unit's position along the rostro-caudal axis and its azimuth coding. Units tend to respond to more frontal positions in the frontal part of the SC while units in the caudal part respond to more lateral positions (Figure 5). No correlation could be found between the centroid position in azimuth and medio-lateral position or depth. Furthermore, no significant correlation could be found for each unit's centroid position in elevation and its position in the SC.

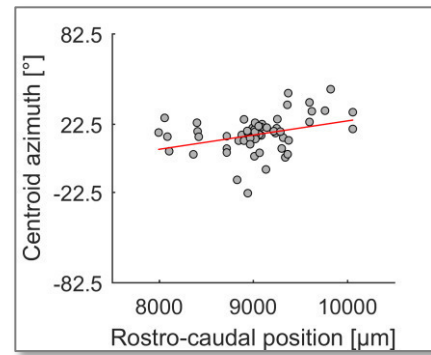


Figure 5: Correlation between rostro-caudal position and azimuth coding.

The x-axis shows the positions of all recorded units along the rostro-caudal axis, the y-axis their SRF centroid (control) in azimuth. The red line indicates a possible linear correlation.

Influence of ear movements on spatial receptive fields

I hypothesized that the spatial tuning of the SC neurons is shifted or at least modified by a simulated ear movement through electrical stimulation of the ear muscles. To check this hypothesis, I compared the spatial receptive fields for each unit between the control and the stimulation recording. An example for the two measurements is shown in Figure 6. In this example, the unit responds to exactly the same direction in the control measurement and during the stimulation of the adductor muscle. Both the SRF outlines and the centroids (at $+20^\circ$ azimuth, -15° elevation) are at the same position in the control and the stimulation condition. Only the BEL moves from -7.5° during control to -22.5° during stimulation (BAZ constant at 22°).

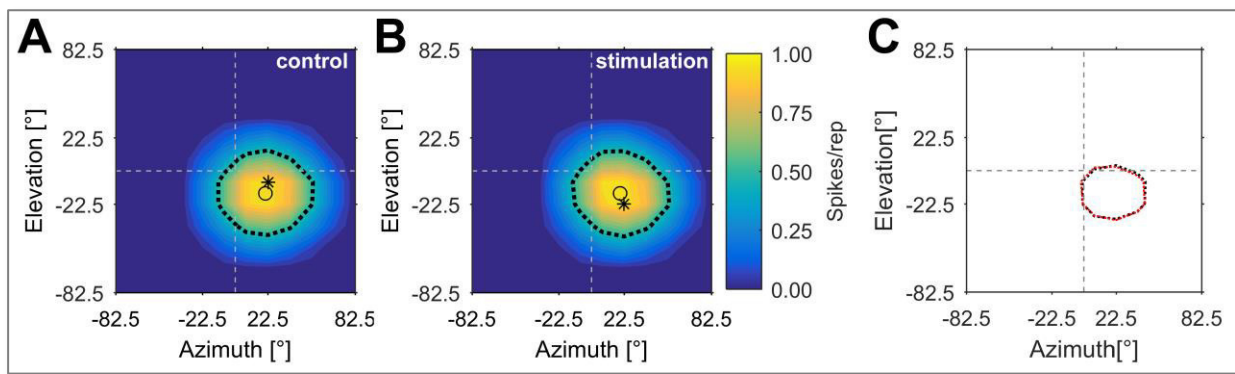


Figure 6: Comparison between spatial receptive fields of a unit during electrical ear stimulation and control

(A,B) Spatial receptive fields of a SC unit during the control recording (A) and the recording with electrical stimulation of the adductor ear muscle (B). The spike count per repetition is color-coded. The spatial receptive field is represented by the black dotted line corresponding to the response threshold at 50% of the unit's maximal spike count. The geometric center of the unit's spatial receptive field (centroid) is marked by a black circle; the spatial position eliciting the maximal response is marked by a black asterisk. (C) Comparison between the outlines of the SRFs during the control recording (black dotted line) and the stimulation (red dotted line).

In total, the neuronal responses of 42 units were analyzed while stimulating the adductor muscle and 22 units were analyzed while stimulating the elevator muscle. I checked for each stimulated muscle group for differences in spatial tuning between the stimulation and the control recording by analyzing the centroid position in azimuth and elevation as well as the general size (area) of the receptive fields.

In records where the adductor muscle was stimulated ($n = 42$), the median centroid in azimuth was at 15.9° (STD: $\pm 13.0^\circ$, control) and 16.8° (STD: $\pm 12.9^\circ$, stimulation), respectively. The median centroid in elevation was at -11.5° (STD: $\pm 7.4^\circ$, control) and -10.8° (STD: $\pm 8.9^\circ$, stimulation). The median area of the receptive fields, measured in steradians (sr), was 0.30 sr (STD: ± 0.23 sr, control) and 0.31 sr (STD: ± 0.22 sr, stimulation). Note that the 50% threshold (border) of the receptive fields is always relative to the maximum spike response occurring in either the stimulation or the control measurement. Due to this, an increase or decrease in the spike rate during stimulation consequently leads to an increased or decreased size of the receptive fields. However, no significant differences could be found between adductor stimulation and control records for any parameter (centroid azimuth: $p = 0.90$, centroid elevation: $p = 0.89$, SRF area: $p = 0.90$). In the following Figure 7, the results of the adductor stimulation recordings and their controls are shown as boxplots:

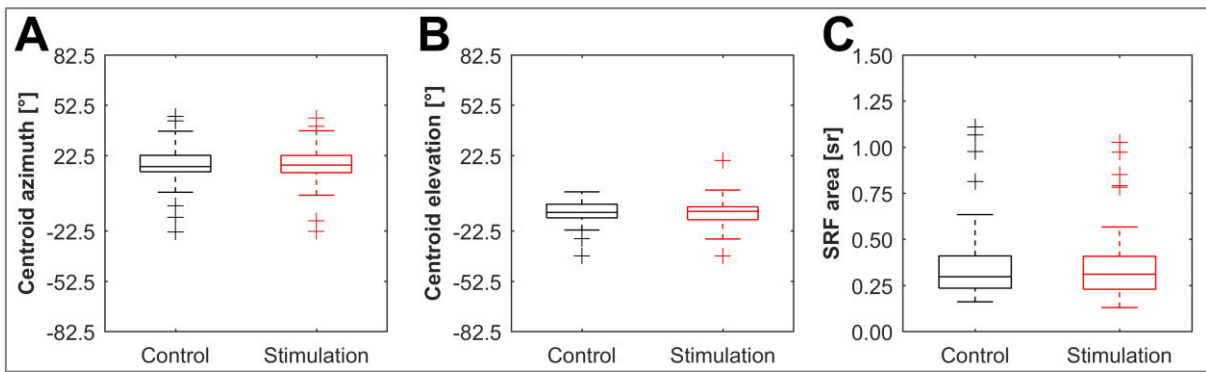


Figure 7: Spatial tuning during stimulation of the adductor muscle

The boxplots show the SRF centroid positions in azimuth (A) and in elevation (B) as well as the SRF area (C) during the control recording (black) and the stimulation of the adductor muscle (red). The boxes represent the median (center line) and the interquartile range (IQR) of the values. Whiskers indicate values within 1.5 x IQR. Crosses mark outliers (outside 1.5 IQR)

In records where the elevator muscle was stimulated ($n = 22$), the median centroid in azimuth was at 15.7° (STD: $\pm 9.1^\circ$, control) and 14.9° (STD: $\pm 9.5^\circ$, stimulation), respectively. The median centroid in elevation was at -4.7° (STD: $\pm 9.5^\circ$, control) and -4.5° (STD: $\pm 12.6^\circ$, stimulation). The median area of the receptive fields was 0.26 sr (STD: ± 0.32 sr, control) and 0.25 sr (STD: ± 0.21 sr, stimulation). No significant differences could be found between elevator muscle stimulation and control (centroid azimuth: $p = 0.95$, centroid elevation: $p = 0.94$, SRF area: $p = 0.73$). In the following Figure 8, the results of the elevator muscle stimulation and their controls are shown as boxplots:

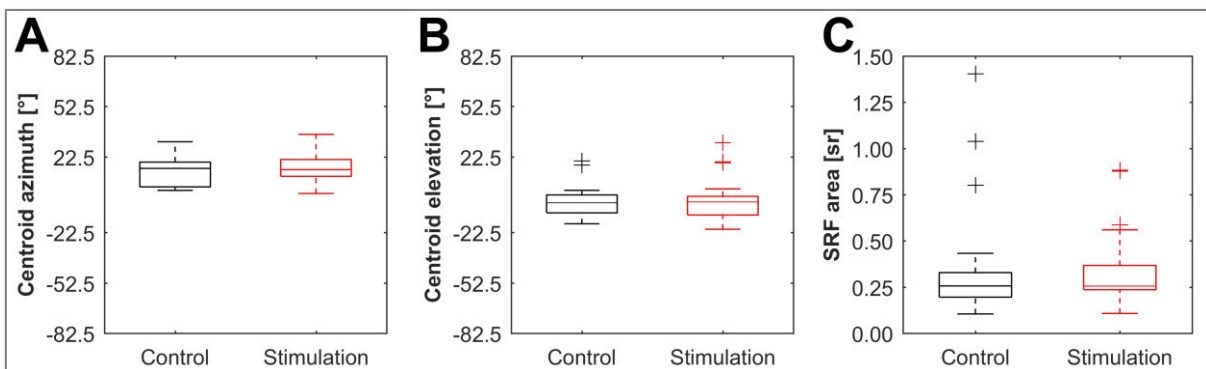


Figure 8: Spatial tuning during stimulation of the elevator muscle

The boxplots show the SRF centroid positions in azimuth (A) and in elevation (B) as well as the SRF area (C) during the control recording (black) and the stimulation of the elevator muscle (red). The boxes represent the median (center line) and the interquartile range (IQR) of the values. Whiskers indicate values within 1.5 x IQR. Crosses mark outliers (outside 1.5 IQR)

I further tested, if any relationship between the units spatial tuning and their location in the SC existed during the stimulation of the different muscle groups. For this, I again tested for correlations between the units' SRF centroid positions (stimulation) in azimuth or elevation

against their physical coordinates in the SC. The results for the stimulation of the adductor muscle are shown in the following Table 2:

| Centroid position | Medio-lateral position | | Rostro-caudal position | | Depth under surface | |
|-------------------|------------------------|-------|------------------------|---------|---------------------|------|
| | ρ (rho) | p | ρ (rho) | p | ρ (rho) | p |
| Azimuth | -0.34 | 0.03* | 0.50 | 0.0007* | 0.19 | 0.22 |
| Elevation | 0.02 | 0.88 | 0.02 | 0.91 | 0.08 | 0.60 |

Table 2: Correlation analysis between SRF centroids during adductor stimulation and the units' coordinates in the SC

The table shows the results from the correlation analysis between each units SRF centroid (during stimulation of the adductor muscle, $n = 42$) in either azimuth or elevation (rows) and their medio-lateral, rostro-caudal position or depth under the brain surface (pairs of columns). For each combination, the correlation coefficient ρ (rho, first column) and the p-value (second column) for a Spearman rank correlation analysis are given. The data were not normally distributed. A red font color and an asterisk indicate a significant correlation (significance level 0.05).

The correlation analysis reveals a significant correlation between each unit's medio-lateral position and its centroid in azimuth during the stimulation of the adductor muscle (see Figure 9 A). Furthermore, a highly significant correlation between each unit's rostro-caudal position in the SC and its azimuth coding could be found. The correlation during the stimulation of the adductor muscle seems to be even more pronounced than in the control measurements, but as we found not differences in the direct comparison of control and stimulation measurements, this might be coincidence. However, units in the rostral SC respond preferably to frontal positions while units in the caudal SC respond to more lateral positions (Figure 9 B).

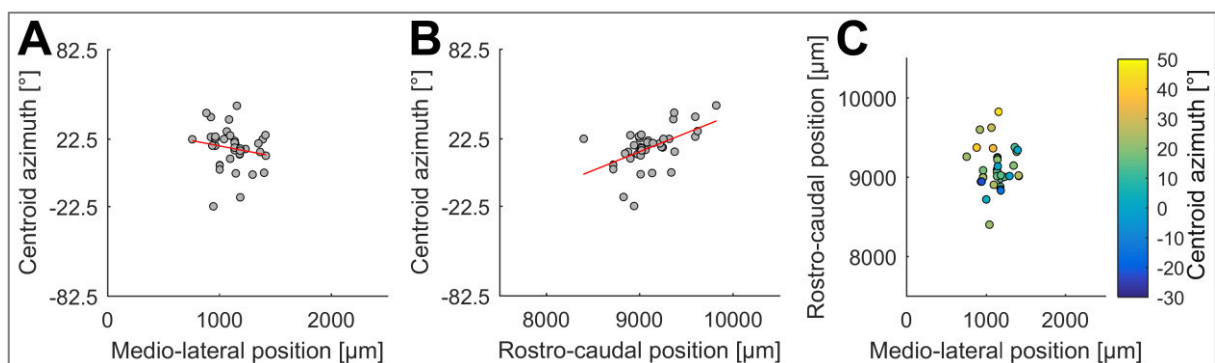


Figure 9: Correlation between azimuth coding and position in SC during adductor stimulation

(A,B) The x-axis shows the positions of all recorded units along the medio-lateral (A) and rostro-caudal (B) axis, the y-axis their SRF centroid in azimuth during stimulation of the adductor muscle. The red line indicates a possible linear correlation.

(C) The figure shows the units' medio-lateral (x-axis) and rostro-caudal (y-axis) position in the SC. The centroid in azimuth is color-coded. Units responding to frontal positions are mainly in the rostral and lateral SC while units responding to contralateral positions are rather in the caudal and medial SC.

In the analysis of the centroid positions during stimulation of the elevator muscle and each unit's location in the SC, again a significant correlation between the medio-lateral position and centroid in azimuth could be found (see Table 3 and Figure 10 A). However, there was no obvious relation between the rostro-caudal position and the centroid in azimuth anymore, which could of course be caused by the lower number of records in the statistical tests:

| Centroid position | Medio-lateral position | | Rostro-caudal position | | Depth under surface | |
|-------------------|------------------------|-------|------------------------|------|---------------------|------|
| | ρ (rho) | p | ρ (rho) | p | ρ (rho) | p |
| Azimuth | 0.46 | 0.03* | 0.20 | 0.37 | 0.27 | 0.22 |
| Elevation | -0.29 | 0.19 | -0.02 | 0.93 | 0.02 | 0.94 |

Table 3: Correlation analysis between SRF centroids during elevator stimulation and the units' coordinates in the SC

The table shows the results from the correlation analysis between each units SRF centroid (during stimulation of the elevator muscle, $n = 22$) in either azimuth or elevation (rows) and their medio-lateral, rostro-caudal position or depth under the brain surface (pairs of columns). For each combination, the correlation coefficient ρ (rho, first column) and the p-value (second column) for a Spearman rank correlation analysis are given. The data were not normally distributed. A red font color and an asterisk indicate a significant correlation (significance level 0.05).

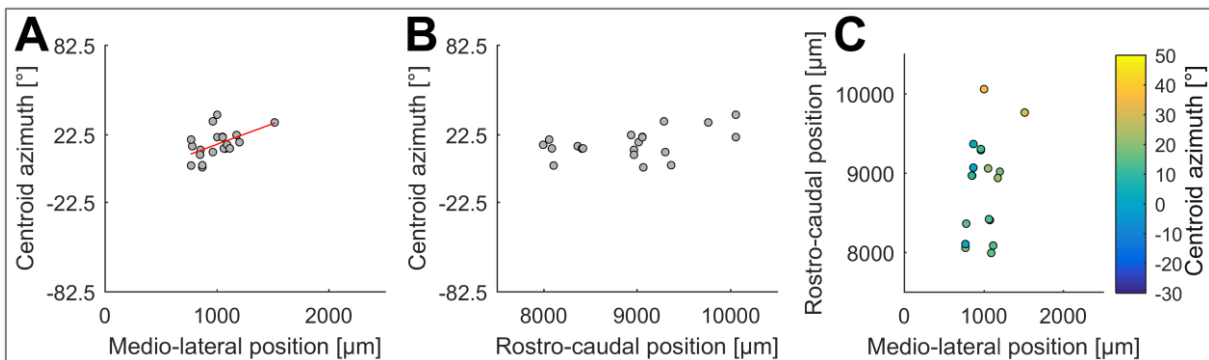


Figure 10: Correlation between azimuth coding and position in SC during elevator stimulation

(A,B) The x-axis shows the positions of all recorded units along the medio-lateral (A) and rostro-caudal (B) axis, the y-axis their SRF centroid in azimuth during stimulation of the elevator muscle. The red line indicates a possible linear correlation.

(C) The figure shows the units' medio-lateral (x-axis) and rostro-caudal (y-axis) position in the SC. The centroid in azimuth is color-coded. Although no significant correlation between rostro-caudal position and azimuth coding could be found, units tend to respond to more lateral positions in the caudal SC.

Frequency tuning in the superior colliculus

Besides analyzing the influence of ear stimulation on the spatial tuning of the SC neurons, I additionally investigated the frequency tuning of a subset of neurons to gather further insights into basic response properties of these cells.

Figure 11 shows an example of a tuning curve for a SC unit. This unit had a characteristic frequency (CF) of 77 kHz.

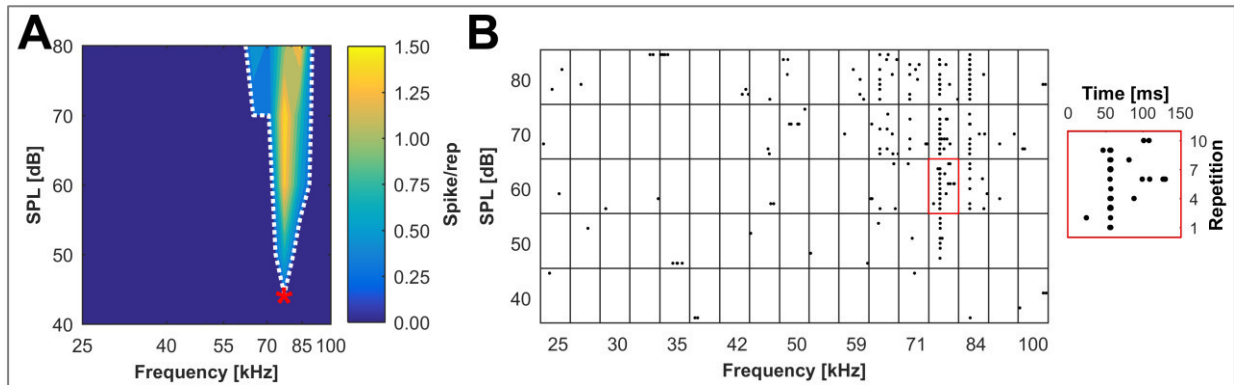


Figure 11: Frequency tuning of a unit in the superior colliculus

(A) Tuning curve of a SC unit. The acoustic stimuli consisted of pure tones with 20 ms duration, changing frequencies between 25 – 100 kHz (center frequency 50 kHz, range 2 octaves, 8 steps/octave) and changing sound pressure levels between 40 – 80 dB SPL. The neuronal responses to these stimuli are color-coded. The white dotted line marks the threshold of 20% of the unit's maximum response. The characteristic frequency (CF, 77 kHz) at the unit's threshold is marked by a red asterisk. (B) Rasterplots showing neuronal responses elicited by the different presented acoustic stimuli. The cutout (red box in the rasterplot and right panel) shows the response to a pure tone with 77 kHz at 60 dB SPL. The x-axis shows the recording time from 0 – 150 ms. The presentation of the pure tone started at 50 ms and had a duration of 20 ms. The y-axis shows different repetitions.

In total, 152 units were analyzed with respect to frequency tuning throughout the SC. CFs of these units ranged from 22 – 92 kHz (median: 66 kHz). Interestingly, the CFs of these units were not uniformly distributed but showed an obvious decrease along the rostral-caudal axis. A statistical analysis revealed a highly significant correlation between each unit's CF and its rostral-caudal position in the SC ($\rho = -0.58$, $p = 6.7 \cdot 10^{-15}$). Furthermore, CF was significantly correlated with the medio-lateral position in the SC ($\rho = -0.21$, $p = 0.027$) as well as with the depth under the brain surface ($\rho = -0.35$, $p = 1.9 \cdot 10^{-6}$). However, it is important to note that the frontal part of the SC is located deeper under the overlying cortical structures than the more caudal part of the SC. Thereby, there is a covariation of the depth of the SC under the brain surface and its rostral-caudal position. In consequence, as CF changes significantly along the rostral-caudal axis, a significant correlation between CF and the depth under the brain surface can be expected as well. Figure 12 shows the distribution of CF along different dimensions of the SC.

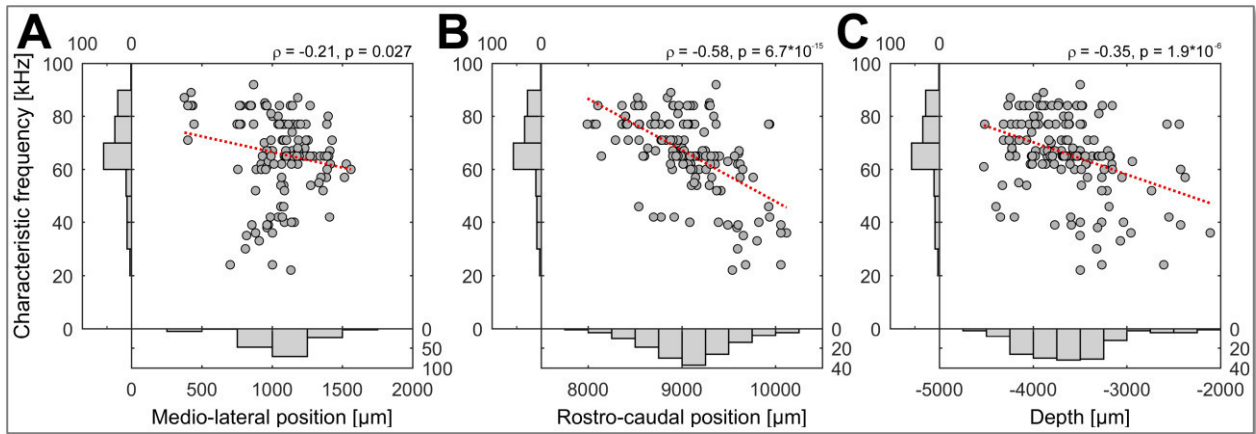


Figure 12: Frequency tuning in the superior colliculus

Distribution of characteristic frequencies of 152 units in the SC. The figures show the frequency tuning along the medio-lateral axis (A), the rostro-caudal axis (B) and in different depths under the brain surface (C). For each panel, the x-axis shows the physical coordinate of each unit in the brain and the y-axis each unit's CF. The histogram below each scatter plot indicates the distribution of the measured units at different coordinates and the histogram left of each scatter plot indicates the distribution of CF. A correlation analysis revealed a significant relation between each unit's CF and its medio-lateral (A), rostro-caudal (B) position as well as its depth under the brain surface (C). The dotted red line (linear regression) indicates the trend.

Discussion

Our results in this project demonstrate a topographic-like distribution of azimuth coding along the rostro-caudal axis in the SC. This topography seemed to be more pronounced during the stimulation of the adductor ear muscle than during the controls. No correlation between the rostro-caudal positions of the units and their azimuth coding could be found during elevator stimulation. A rather weak but still significant correlation was further found during the adductor and elevator muscle stimulation between the units' medio-lateral positions in the SC and their azimuth coding, while no such correlation was found during the control measurements. The higher correlation during the stimulation records might indicate that the spatial tuning of the SC units is influenced by a movement of the ears and that a possible topography might depend on or at least be modified by ear movements. However, the fact that I found no indication of any differences in the units' centroid positions or their receptive field size (and coupled neuronal response rate) between stimulation and control measurements stands in contrast to the results from the topographic analysis and indicates a coincidence.

A reason for this might be the method of our ear stimulation. I decided to stimulate only single, specific ear muscles (e.g. elevator muscle, adductor muscle) to enable a clear and straightforward statistical analysis of the results. However, electrical stimulation of single, specific ear muscles does not correspond well to the natural, complex proprioceptive

information caused by a movement or turning of the ear where multiple muscles are involved. Furthermore, the complex movements of a bat's ears during passive hearing and active echolocation are only partly understood and could not be realistically simulated with a simple electrical stimulation of one muscle. Recent research suggests a more or less stereotypic movement of the ears during echolocation: During call emission, the ears seem to be mainly pointed forward and upwards to a kind of standard position, while they are moved down and sideways during the following 50 ms (the time period between calls where echoes can be expected, see Kugler and Wiegrebe, 2017). It remains unclear if these scanning movements of the ears are compensated in the neuronal system or if the bat only starts to take the ear position into account when specific objects (e.g. prey, objects in flight path) are identified, become more relevant for the bat and need to be accurately localized.

Another restriction in our study was that one cannot rule out the possibility that the electrical stimulation was not strong enough or suited to cause a proprioceptive sensory input to the midbrain. It is known that a stimulation of pinna muscle receptors evokes responses in the dorsal cochlear nucleus in cats (Kanold and Young, 2001) and that there are somatosensory fibers to the inferior as well as to the superior colliculus (Aitkin et al., 1978; Meredith and Stein, 1986). In our study, I found in rare cases a direct neuronal response of neurons in the SC to electric stimulation or touch of the skin (not shown in the results). However, as these responses were also evoked by stimulation near to but not directly at the ear muscles, this can also be a somatosensory input from the skin and not from the proprioceptive fibers of the muscle. It remains unclear to which extent afferent proprioceptive fibers from the ear muscles, apart from the known somatosensory connections from the skin, reach the SC. Tracing studies using neuronal tracers to investigate the connections from the ear muscles to the brain might help to unravel this question but were not successful in this study. Furthermore, I cannot completely rule out a possible influence of the anesthesia on the proprioception and the afferent connections to the midbrain. Even if the auditory sensation is not significantly influenced by anesthesia (Firzlaff et al., 2006) and the neuronal responses of cells in the dorsal cochlear nucleus to ear stimulation in cats were found under general anesthesia (Kanold and Young, 2001), the anesthesia might have a significant influence on the afferent proprioceptive connections to the midbrain.

Topography and frequency tuning in the superior colliculus

The general topography I found in this study corroborates findings in other mammals. For example, in cats and guinea-pigs a topographic representation of space in the acoustic layers of the SC and a close relation to the topography of the visual layers was found (King and Palmer, 1983; Middlebrooks and Knudsen, 1984). The evidence for a topographic map of acoustic space in bats was up to now very limited. Some studies indicated an orderly map of azimuthal space in the SC (Valentine and Moss, 1997; Wong, 1984) while other studies found no such distribution (Jen et al., 1984). Our data now provides further evidence for a topographic map of acoustic space.

In this study, I further found a clear decrease of the characteristic frequencies along the rostro-caudal axis. The data on a tonotopy in the SC is also controversial. Studies in bats (*Eptesicus fuscus*) found no tonotopic distribution (Jen et al., 1984). Furthermore, in guinea pigs no tonotopy of the SC neurons was found, but the patterns of frequency selectivity roughly correlated with the frequency transfer characteristics of the auditory periphery (i.e. sensitivity to mid frequencies at the rostral pole, broad frequency range including highest frequencies in the middle part of the SC, mid and high frequencies in caudal part; Carlile and Pettigrew, 1987). However, as this data was derived from local field potentials and not from single units, the comparison to the above mentioned study on the topography in guinea pigs is difficult. My data points to a relation between CF and azimuth coding. Neurons in the frontal parts of the SC show a preference for high frequencies and frontal spatial positions while neurons in the caudal SC respond preferably to lower frequencies and more lateral positions. This pattern correlates well with the HRTF for our bats (Firzlaff and Schuller, 2003). The relation between frequency tuning and spatial coding is further supported by the weak but still significant correlation of CF along the medio-lateral axis and the at least in some tests significant correlation between azimuth coding and medio-lateral position.

Conclusion

This study could not show a direct influence of simulated ear movement on the spatial receptive fields of SC neurons. However, the data provides convincing evidence of a topographic representation of space along the rostro-caudal axis in the superior colliculus of *P. discolor*.

ECHO-ACOUSTIC FLOW SHAPES OBJECT REPRESENTATION IN SPATIALLY COMPLEX ACOUSTIC SCENES

The text and the figures of following section correspond to the publication:

*“Echo-acoustic flow shapes object representation in spatially complex acoustic scenes”
(Greiter and Firzlaff, 2017a)*

The article is published in the Journal of Neurophysiology which permits authors the reproduction of published articles for dissertations without charge or further license.

Results

Delay Response Fields

We used Delay Response Fields (DRFs) to gather an initial insight into the basic echo delay tuning properties of the AC neurons and to enable a direct comparison with the response characteristics of dynamic flight sequences as well as data obtained from other bats.

Within this project, a total of 156 units were recorded in the posterior dorsal field (PDF) of the auditory cortex in 3 bats. 110 units (71%) exhibited a facilitated response to the presented pulse/echo pairs. Echo delays ranged from 1 to 29 ms. For all 110 delay-sensitive units, best delays (BD) and characteristic delays (CD) were determined.

Figure 13 shows the DRFs of two exemplary delay-sensitive neurons. The unit in the frontal part of the PDF (Figure 13 A) was selective for shorter echo delays, with a BD of 8.0 ms at -30 dB echo level and a CD with 9.5 ms at -38 dB echo level. The unit in the caudal part of the PDF (Figure 13 B) responded to longer echo delays at a BD of 20.0 ms at -30 dB and a CD of 20.0 ms at -39 dB echo level.

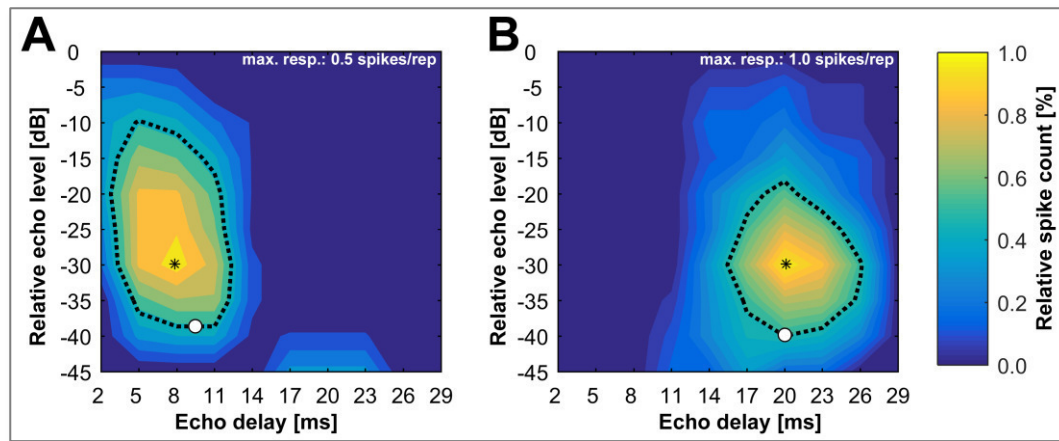


Figure 13: DRFs for two delay-sensitive units

Responses of two delay-sensitive units from the rostral (A) and caudal (B) part of the posterior dorsal field in the AC. The spike count in both DRFs is normalized and color-coded. The black dotted contour line represents the response threshold at 50% of the units maximal spike rate. The echo delay/echo level combination eliciting the maximal response is marked by a black asterisk (best delay = BD). The echo delay with the lowest threshold (characteristic delay = CD) is marked by a circle. The best delays were 8.0 ms (A) and 20.0 ms (B) and the characteristic delays were 9.5 ms (A) and 20.0 ms (B), respectively.

(Figure adapted from Greiter and Firzlaff, 2017a. Adapted with permission.)

The BDs of all 110 delay-sensitive units ranged from 3.0 to 26.0 ms (median: 9.2 ms), and the CD from 2.0 to 29.0 ms (median: 9.5 ms). For both the BD and CD, short delays were overrepresented. Units in the frontal part of the PDF were mainly tuned to short echo delays and both BD and CD increased along the rostro-caudal axis.

We calculated a cortical echo delay tuning map for the PDF of the AC using the BDs and the stereotaxic coordinates of all delay-sensitive units (Figure 14). The echo delay tuning map clearly shows an increase of BD along the rostro-caudal axis as well as slightly increasing delays along the medio-lateral axis. A correlation analysis (Spearman's rank correlation) revealed a highly significant correlation between the BDs and the units' rostro-caudal positions (correlation coefficient $\rho = 0.66$, $p = 8.14 \cdot 10^{-14}$) as well as a significant but weak correlation between the BDs and the units' medio-lateral positions ($\rho = 0.34$, $p = 7.60 \cdot 10^{-4}$).

The units' CDs showed a similar distribution to that of the BDs along the rostro-caudal axis ($\rho = 0.65$, $p = 2.77 \cdot 10^{-14}$) with only slightly increasing delays along the medio-lateral axis ($\rho = 0.33$, $p = 1.00 \cdot 10^{-3}$).

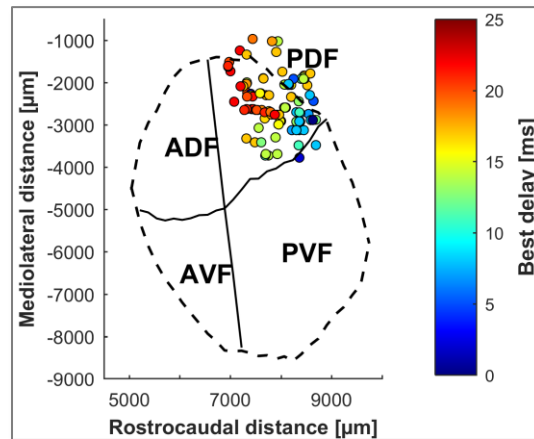


Figure 14: Cortical distribution of BD

(C) Best delays of all recorded delay-sensitive units projected on the flattened surface of the AC. The position of each unit is marked by circles; the BD is color-coded. The outlines of the AC are indicated by dashed lines and the borders of the four subfields by solid lines. AC outlines and subfields are according to Hoffmann et al., 2008. ADF: anterior dorsal field; AVF: anterior ventral field; PVF: posterior ventral field; PDF: posterior dorsal field.

(Figure adapted from Greiter and Firzlaff, 2017a. Adapted with permission.)

Object focusing in naturalistic flight sequences

In the simulations of naturalistic flight sequences, data were recorded from a total of 107 units. For every presented sequence, the sum of spikes following each presented pulse/echo pair within the sequence was analyzed. Spike responses were determined for sequences presenting both targets individually and in combination. To determine the specific response of a unit to each target, the pulse/echo pair evoking the maximum response within sequences presenting only target 1 or target 2, respectively, was identified. 86 of 107 units (80%) showed a facilitated (see Methods) and specific response to both individually presented targets for at least one of the simulated echolocation pulse rates. In detail, 83/107 (78%) units showed specific responses for both individually presented objects in sequences with a constant pulse rate, 58/107 (54%) responded to the sequences with a linearly increasing pulse rate and 58/107 (54%) to the sequences with simulated strobe groups, respectively.

Figure 15 shows two examples of units responding in the presented pulse/echo sequences. The PSTHs (Figure 15 A left column) show clear responses of a unit to the individual presentations

of target 1 and target 2, respectively (middle and bottom panels). The PSTH of the combined presentation of both targets (top panel), however, clearly resembles the individual presentation of target 1, whereas the response to target 2 is missing. The analysis of the sum of spikes for each pulse/echo pair within the sequence (second column) in the combined presentation of both targets shows that the unit responded equally to target 1 (>50 % of the response in the individual presentation), but that the response to target 2 was strongly reduced (<50% of the response in the individual presentation). This means that the unit focused to target 1 in the complex flight sequence. Figure 15 B illustrates an example of a unit focusing on the second target while the response to target 1 is significantly (less than 50% of the response in the individual presentation) reduced.

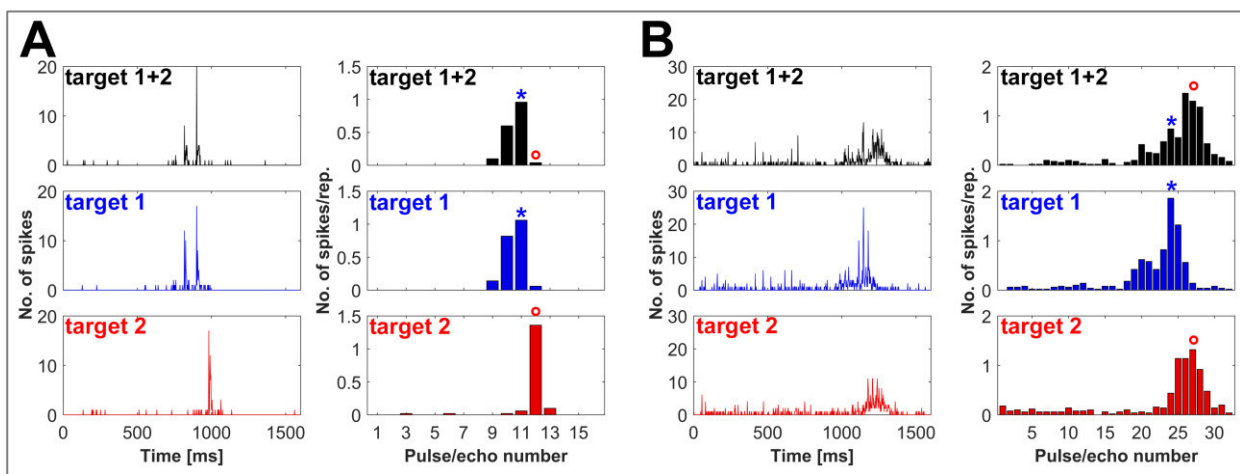


Figure 15: Examples of units focusing on different targets in naturalistic pulse/echo sequences

Neuronal responses of two different units (A,B) in naturalistic flight sequences. For each, the left column shows the PSTH (bin width = 2ms) and the right column shows the mean number of spikes / repetition (50 repetitions) for every pulse/echo pair within the sequence. The first row shows the response to the sequence where both targets were presented together. The second and third row shows the responses of the sequences, where only **target 1** or **target 2** were presented. The **blue asterisk** marks the pulse/echo pair evoking the highest spike rate for target 1, and the **red circle** indicates the response to target 2 in each individual presentation. The acoustic stimulation in each sequence is preceded by a 50 ms silent period to determine the level of spontaneous activity and it is followed by another 200 ms silent period. (A) Unit showing a clear response to both targets in the individual presentations while focusing on target 1 in the complex flight sequence. The sequence was simulated with a constant pulse rate. (B) Unit focusing on target 2 in a sequence with a linearly increasing pulse rate.

(Figure adapted from Greiter and Firzlaff, 2017a. Adapted with permission.)

In total, in the simulations of flight sequences with a constant pulse rate, 32/83 units (39%) responded equally to both targets in the complex sequence, 29/83 (35%) focused their response on target 1, and 9/83 (11%) focused on target 2. In the records of 10/83 (12%) units, the response decreased for both targets. In 3/83 records (4%) the responses for both targets overlapped and could not be further analyzed.

Since we were interested in determining whether increasing pulse rates simulating a target approach phase had any impact on the cortical object representation, we also tested sequences with linearly increasing pulse rates and strobe groups for the same units whenever possible. As not all neurons exhibited a facilitated and specific response for all simulated pulse rates with respect to our strict criteria (see Methods), fewer neurons could be analyzed in sequences with increasing pulse rates.

In flight sequences with linearly increasing pulse rates, 26/58 (45%) units responded equally to both targets, 18/58 (31%) focused on target 1, and 11/58 (19%) focused on target 2. Only 3 units (5%) showed a decrease in their spike rates for both presented objects. An example of a unit responding to a sequence with a linearly increasing pulse rate is shown in Figure 15 B. Note that, as the interval between the pulses decrease from 83 ms to 27 ms within the sequence, the differences between successive pulse/echo pairs with respect to echo delay and echo level decline. Thus, units usually responded in the last part of those sequences to more successive pulse/echo pairs compared to sequences with a constant pulse rate.

In the sequences simulating strobe groups, units responded similarly as in the sequences with linearly increasing pulse rates. 29/58 (50%) responded equally to both targets, 16/58 (28%) focused on target 1 and 9/58 (16%) focused on target 2. In the records of 4 units (7%), the responses decreased for both targets.

The presentation of the sequences at different pulse rates revealed no substantial differences in object selection. The overall tendency of neurons locking onto either target 1 or 2 is similar for all pulse rates. In total $\approx 46\%$ of the recorded neurons focused on one of the two targets in a complex flight sequence, and from these about two-thirds responded only to target 1 and about one-third focused on target 2.

In general, neurons tended to focus mainly on target 1 if they responded during the first and middle part of the flight sequence (i.e. neurons tuned to long or medium echo delays). If they responded in the last section of the sequence (i.e. heading distance > 3.0 m, short echo delays), where the angle to target 1 increased rapidly, they mainly focused on target 2 (Figure 16). This indicates that the targets are processed sequentially in the auditory cortex of *P. discolor*.

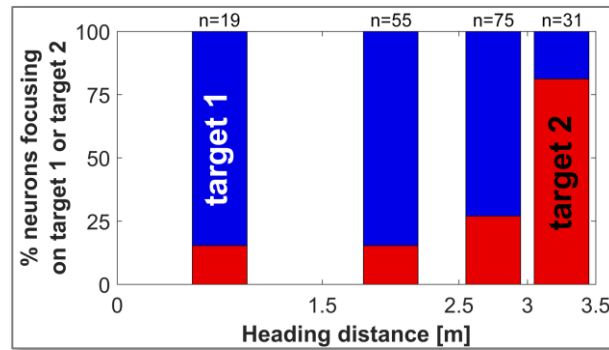


Figure 16: Units focus depending on heading distance

Percentage of records where units focus was either on **target 1** or **target 2**. Neurons in the first part of the flight sequence tend to focus on target 1. In the final part of the sequence (heading distance > 3.0 m) neurons exhibit a preference for focusing on target 2. At a heading distance of 3.5 m, the bat passes target 1.

(Figure adapted from Greiter and Firzlaff, 2017a. Adapted with permission.)

We investigated whether the selective responses to specific objects within the sequence depended on single parameters, such as echo delay or echo level, alone, or are a result of a complex interaction of multiple dynamically changing parameters. For this, we further analyzed the echo levels and echo delays at the maximum response positions for all the units that focused either on target 1 or target 2. Since we had found no differences between different pulse rates in respect to object focusing, we combined the results from all of the simulated temporal pulse patterns for this analysis.

At first glance it seems most likely that in a complex pattern of incoming echoes units might specifically respond to the loudest or earliest object echoes. However, our data point in the opposite direction: Figure 17 shows an example of a unit specifically responding to target 1 in the combined sequence. The unit showed its maximum response to target 1 at an echo delay of 6.8 ms and at an echo level of -14.8 dB. The unit's maximum response to target 2 was at an echo delay of 5.9 ms at an echo level of -11.0 dB. This means that by locking onto target 1, the neuron selectively responded to the object that had the longer echo delay but the fainter echo level. It did not select the target with the loudest echoes within the sequence.

To analyze the temporal relationship of pulse and echoes of the two objects in detail, one can look at two independent measures:

- a) relative timing of echoes after each pulse
- b) absolute echo delay (representing the physical distance to the target) at maximum response

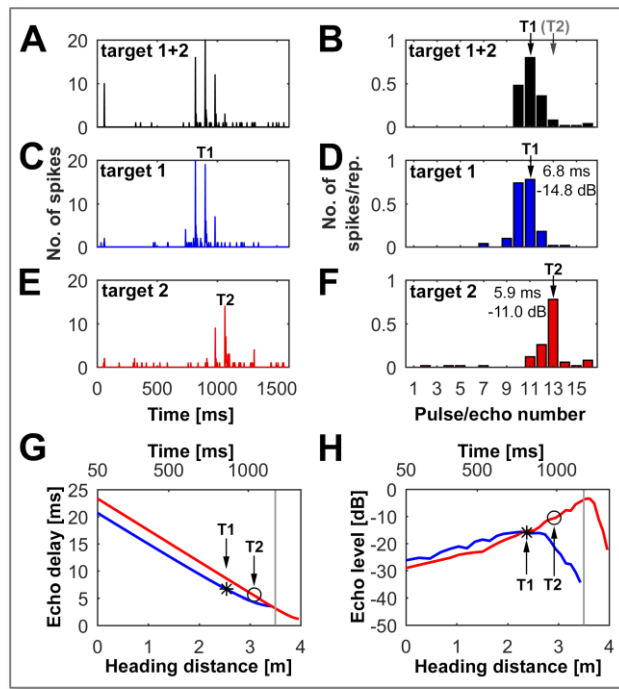


Figure 17: Echo delay and echo level of unit responding in naturalistic pulse/echo sequence

(A-F) Neuronal responses of cortical units in naturalistic flight sequences focusing on target 1. The first row shows a simulation with both targets (A,B), the second row a sequence presenting only target 1 (C,D) and the third row a sequence with only target 2 (E,F). For each sequence, the left column (A,C,E) shows the PSTH (bin width = 2ms), and the right column (B,D,F) the mean number of spikes / repetition for every pulse/echo pair within the sequence. For each target (target 1 = T1, target 2 = T2), the maximum response within the sequence is indicated by an arrow. The echo delay and echo level at each maximum response position is indicated in the PSTHs in D and F. The acoustic stimulation in each sequence is preceded by a 50 ms silent period to determine the level of spontaneous activity and it is followed by another 200 ms silent period.

(G,H) Progression of echo delay (G) and echo level (H) for target 1 (blue line) and target 2 (red line). The delay and level at the maximum response of target 1 (black asterisk, T1) and target 2 (black circle, T2) are indicated.

(Figure adapted from Greiter and Firzlafl, 2017a. Adapted with permission.)

a): Relative timing of echoes:

In all presented virtual pulse/echo sequences, the bat receives after each pulse first the echo from target 1 and after that the echo from target 2 (Figure 2 E) until it begins to pass target 1 at 3.50 m heading distance. When the bat reaches a heading distance of 3.43 m, the temporal order of the echoes is reversed. After 3.43 m heading distance, the bat receives the echo from target 2 before the echo from target 1 (see Figure 2 F). However, note that only in sequences with linear increasing pulse rate, a single pulse/echo pair was simulated between 3.43 m and 3.50 m heading distance. Our data clearly show that about 1/3 of the recorded neurons already focus on target 2 before the bat passes target 1 at 3.5 m heading distance (see Figure 16). This means most of these neurons selectively responded not to the first but to the second echo after the pulse. Because of this, we can exclude forward suppression or synaptic depression as underlying mechanisms for target preference at least for units that lock onto target 2.

b): Absolute echo delay:

In the analysis of all recorded units in respect to echo delay at each maximum response position (see Figure 17 G,H), about one half of the neurons (48%) selectively responded to the object with the shorter echo delay (i.e. shorter target distance), and the other half (52%) to the object with the longer echo delay (i.e. longer target distance). These results indicate that the focusing on specific objects within the sequences cannot be a direct consequence of the echo delay.

The analysis of the echo levels revealed that in most of the records (92%), the target 2 echo level exceeded that of target 1 at the maximum response positions. As more neurons locked onto target 1 instead of target 2, about 61% of the units selected the object with the lower echo level. Consequently, the response to specific objects cannot result from echo level alone.

These results show that neurons did not focus on the earliest, loudest, or most dominant object echo, but rather that target focusing is caused by a complex interaction consisting of multiple dynamically changing parameters (i.e. echo-acoustic flow).

Cortical delay tuning in naturalistic flight sequences

In addition to the cortical object representation, we analyzed the specific delays of all units that showed facilitated and specific responses to both individually presented targets for each pulse rate.

Figure 18 A shows an example of a unit's response in sequences with a linearly increasing pulse rate. In the sequence where only target 1 was presented, the highest spike rate was evoked at pulse/echo pair #22, which corresponded to an echo delay of 4.4 ms. In the simulation presenting only the second target, the highest response is evoked later in the sequence at pulse/echo pair #26, which corresponded to an echo delay of 3.5 ms. Note that the specific delay for target 2, which is the object closer to the bat's flight path (see Figure 2 A) is shorter than the specific delay for target 1. Figure 18 B shows the DRF from the same unit. In the static delay response field, the unit is selective for significantly longer delays than in the dynamic flight sequence (BD = 7.0 ms, CD = 8.0 ms).

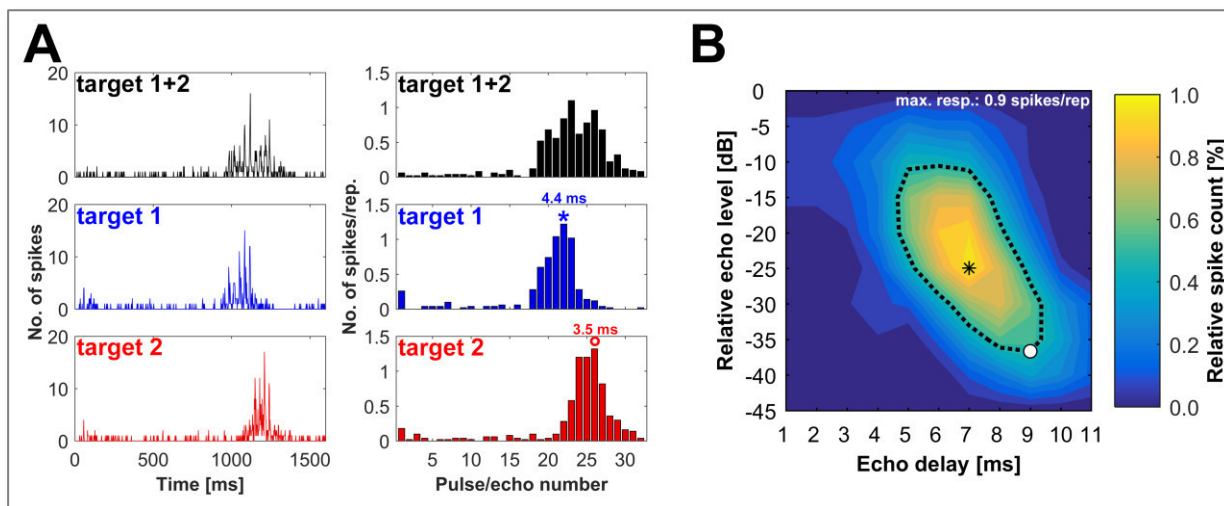


Figure 18: Specific delay in naturalistic flight sequence compared to the static delay response field

(A) Neuronal response of a facilitated unit to naturalistic flight sequences with linearly increasing pulse rates. The left column shows the PSTH (bin width = 2 ms), and the right column shows the mean number of spikes / repetition for each pulse/echo pair. The first row shows the response to the sequence where both targets were presented together. The second and third row show the responses of sequences, where only **target 1** or **target 2** was presented. The acoustic stimulation in each sequence is preceded by a 50 ms silent period to determine the level of spontaneous activity and it is followed by another 200 ms silent period. The **blue asterisk** marks the pulse/echo pair evoking the highest spike rate for the sequence with target 1, the **red circle** marks the best response for target 2. The specific delays are indicated at each maximum response position. (B) The DRF for the same unit as shown in A. The black asterisk marks BD, the circle CD. Note that the BD with 7.0 ms is significantly longer than the specific delays in the naturalistic flight sequence.

(Figure adapted from Greiter and Firzlaff, 2017a. Adapted with permission.)

Cortical echo delay tuning maps were calculated using the specific delays of all units tested for the different targets and pulse rates (Figure 19). All maps for both targets and all simulated pulse rates show units with shorter specific delays in the frontal part of the PDF and increasing specific delays along the rostro-caudal axis. A correlation analysis revealed that there was a significant relationship between the rostro-caudal position and the specific delay for both objects and all simulated pulse rates ($p < 0.001$). The units' medio-lateral positions and specific delays showed no significant correlation. All calculated echo delay maps in Figure 19 are tuned to noticeably shorter echo delays than the maps constructed from the delay response fields (Figure 14), and they show a striking overrepresentation of short delays.

Both calculated delay-tuning maps for simulations with a constant pulse rate (Figure 19 A and D) revealed a tuning to considerably longer specific delays than in sequences with a linearly increasing pulse rate (Figure 19 B and E) or strobe groups (Figure 19 C and F). Furthermore, units, as shown in Figure 18 A, tended to respond to shorter echo delays for target 2 than for target 1.

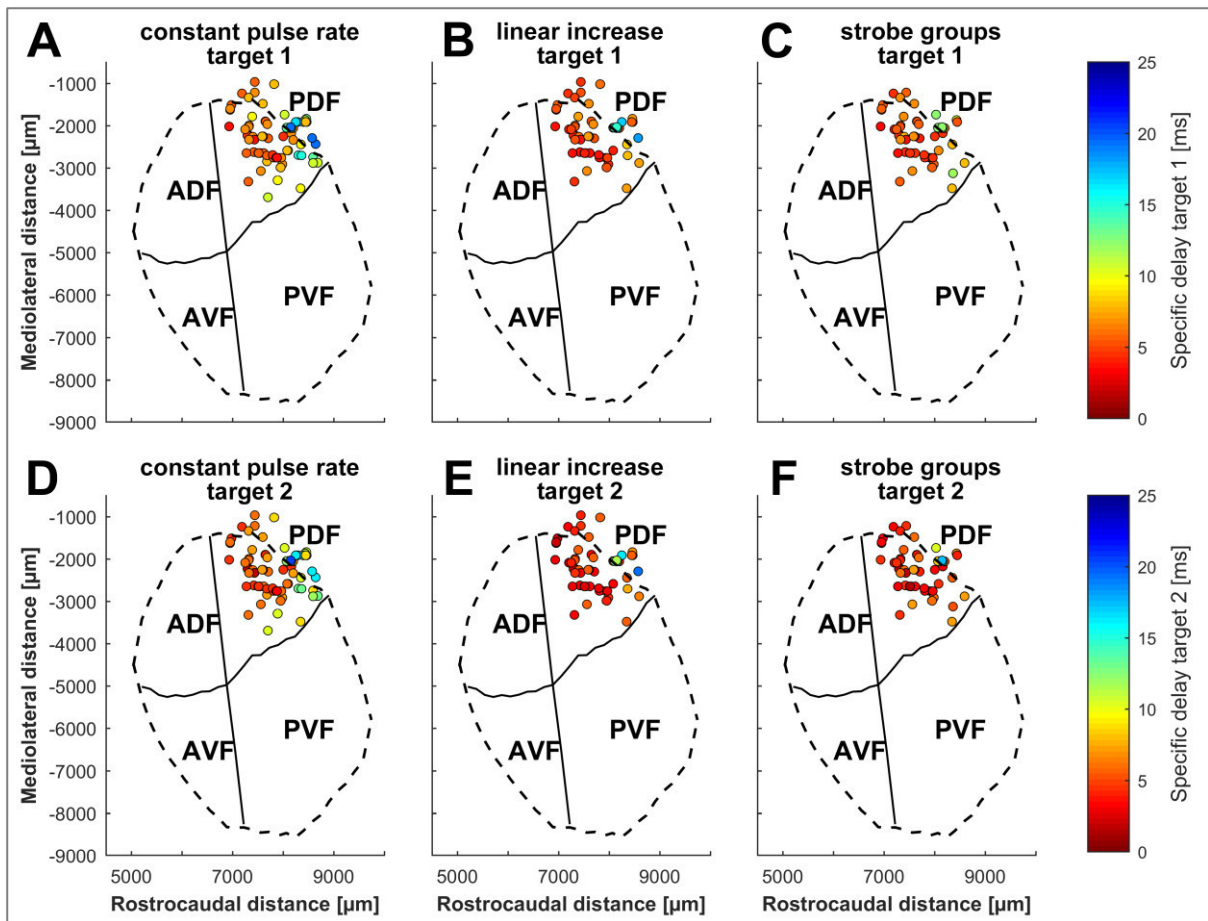


Figure 19: Cortical delay tuning maps showing distribution of specific delays from naturalistic flight sequences

Specific delays of all analyzed units projected onto the flattened surface of the auditory cortex. (A-C) The specific delays of units for sequences where only target 1 was presented; (D-F) the specific delays of units for target 2.

The sequences were presented simulating a constant pulse rate (A,D), a linearly increasing pulse rate (B,E) and strobe groups (C,F). The outlines of the auditory cortex are indicated by dashed lines and the borders of the four subfields by solid lines. ADF: anterior dorsal field; AVF: anterior ventral field; PVF: posterior ventral field; PDF: posterior dorsal field.

(Figure adapted from Greiter and Firzlaff, 2017a. Adapted with permission.)

To study these effects in detail, the distributions of the specific delays for both targets and the different pulse rates were statistically analyzed. The analysis included all units that responded in sequences for at least one of the simulated pulse rates. The tests revealed that there were significantly longer specific delays in simulations with a constant pulse rate than for those with a linearly increasing pulse rate (target 1: $p < 0.001$, target 2: $p < 0.001$) or for the strobe groups (target 1: $p < 0.001$, target 2: $p < 0.001$) for targets 1 and 2 (Figure 20 B). The specific delays in the sequences with a linearly increasing pulse rate were not significantly different from those of the strobe groups. Furthermore, units tended to respond at shorter delays to target 2 (the object nearer to the bats flight path) than for target 1 for all simulated pulse rates. The specific delays for a linearly increasing pulse rate ($p < 0.001$) and for the strobe groups ($p < 0.001$) differed significantly between both targets.

In total, the median specific delays for targets 1 and 2, respectively, were 6.8 ms and 6.0 ms for a constant pulse rate, decreased to 5.2 ms and 4.0 ms (target 1 and target 2) for a linearly increasing pulse rate, and were 5.6 ms and 4.5 ms for the simulated strobe groups. All of the units showed considerable shorter delays in the naturalistic flight sequences than in the static delay response fields (Figure 20 A and B). The distribution of the BDs from the delay response fields differed significantly from those of the specific delays in all flight sequences ($p < 0.001$), except in the simulation of target 1 at a constant pulse rate.

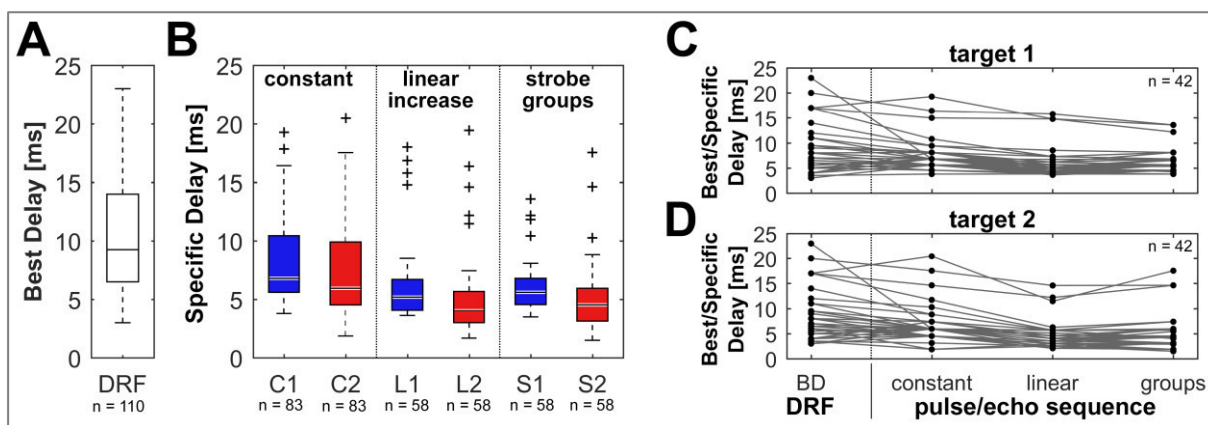


Figure 20: Best delay from static DRFs in relation to specific delays from naturalistic pulse/echo sequences

(A) Boxplot with BDs from all units for which static delay response fields were recorded. The box represents the median (center line) and the interquartile range (IQR) of the BDs. Whiskers indicate values within $1.5 \times$ IQR. (B) Boxplots with specific delays from all units that responded in naturalistic flight sequences for at least one of the simulated pulse rates. The boxes show the specific delays for each target and pulse rate. Whiskers indicate values within $1.5 \times$ IQR, black crosses mark outliers. Blue boxes show specific delays for target 1, red boxes specific delays for target 2. Units in flight sequences with a constant pulse rate (C1,C2) responded at significant longer delays than in flight sequences with linearly increasing pulse rates (L1,L2) or strobe groups (S1,S2). Note the different delay range of specific delays from the dynamic naturalistic flight sequences compared to the BDs from the static DRFs. (C,D) BDs and specific delays for units that responded to static DRFs as well as to all the presented flight sequences at all different pulse rates. (C) BDs and specific delays for target 1. (D) BDs and specific delays for target 2. Note the consistent trend of decreasing echo delays in natural dynamic pulse/echo sequences at increasing pulse rates. (Figure adapted from Greiter and Firzlaff, 2017a. Adapted with permission.)

The trend of decreasing best/specific delays could also be seen on a neuron-by-neuron's basis, when we analyzed only neurons that responded in DRFs as well as in dynamic pulse/echo sequences for all simulated pulse rates (Figure 20 C and D). The BDs from the static DRFs differed significantly from the specific delays in sequences with linearly increasing pulse rates (target 1: $p < 0.01$, target 2: $p < 0.001$) and at least for target 2 in sequences with strobe groups (target 1: not significant, target 2: $p < 0.001$). Furthermore, the specific delays in sequences presented at constant pulse rate differed significantly from those in sequences with linearly increasing pulse rates (target 1: $p < 0.001$, target 2: $p < 0.001$) and strobe groups (target 1: $p < 0.01$, target 2: $p < 0.001$). Due to the limited number of units in this analysis ($n=42$), no

significant differences could be found between BDs from the DRFs and specific delays in sequences with constant pulse rate.

Discussion

In this project, we investigated the cortical representation of echo streams originating from two simultaneously presented objects in simulated naturalistic flight sequences. Our data show that cortical neurons in bats can selectively respond to streams of echoes from specific objects in complex dynamic acoustic scenes. Furthermore, our results show that the dynamic stimulus presentation and changing temporal patterns of sonar emissions can have a substantial influence on the target range representation in the cortical map.

Basic delay tuning properties

We used a standard approach (see Hagemann et al., 2010; Hechavarría et al., 2013a; Suga and O'Neill, 1979) of statically presented pairs of echolocation pulses and echoes with changing echo delays and echo levels to investigate the basic delay tuning characteristics of cortical neurons. Neurons selective to such pairs of pulses and echoes were mainly found in the posterior dorsal field of the AC in *P. discolor*. Recent studies strongly indicate a chronotopic arrangement of delay-tuned neurons in this region (Bartenstein et al., 2014; Hoffmann et al., 2013). However, a standard approach to determine delay tuning was still missing.

Our results from this project clearly show chronotopically arranged delay-tuned neurons in the PDF of the AC in *P. discolor*. BDs ranged from 3 ms in the rostral part and up to 26 ms in the caudal part of the PDF (median: 9.2 ms). This corresponds well to earlier findings on the spatiotemporal response characteristics in *P. discolor* (delay: 2-26 ms, median: 9.0 ms, Hoffmann et al., 2013) and other bats (Dear et al., 1993a; Hagemann et al., 2010; Hechavarría et al., 2013a; O'Neill and Suga, 1982; Schuller et al., 1991; Wong et al., 1992).

Cortical object representation in dynamic flight sequences

It has been proposed that bats perceptually organize acoustic information into echo streams in order to track specific objects during flight in complex environments. Many different acoustic parameters such as echo direction, intensity, timing, duration, and frequency are discussed to contribute to echo stream segregation in bats (Kanwal et al., 2003; Moss and Surlykke, 2010). Although attention-based mechanisms might also play a role, neurophysiological studies on auditory stream segregation often suggest rather basic underlying neural processes such as frequency selectivity and short-term adaptation (e.g. Fishman et al., 2001; Micheyl et al., 2005). Recent studies further showed, that forward suppression induced by naturalistic echo streams lead to a sharper tuning of cortical delay-tuned neurons (Beetz et al., 2016b).

Our study used the simulation of naturalistic flight sequences to investigate the cortical representation of objects in complex, dynamic acoustic scenes and to study a possible neural basis of echo stream segregation in bats using naturalistic stimuli. Therefore, in our dynamic simulation many parameters co-varied during acoustic stimulation (e.g. echo level, echo delay, echo reflection angles and pulse rate). In the following, we will discuss the possible influence of some of these parameters on echo stream segregation and cortical object representation.

While all of the analyzed neurons could respond to both targets when presented individually, about half of them selectively responded to only one of the targets in a complex situation. Neurons tended to lock on the first target in the first and middle part of the pulse/echo sequence, while in the final part of the pulse/echo sequence, shortly before passing target 1, neurons showed a preference in responding only to target 2.

This suggests that different acoustic targets are processed sequentially in a fly-by situation and that target preference is not directly influenced by any single parameter such as echo delay or level, but rather by a complex interaction of multiple dynamically changing parameters. To test this hypothesis, we analyzed echo amplitudes and timings for the neurons responding selectively to only one of the targets. At a first glance, it seems likely that due to forward suppression, neurons might always respond only to the first echo in a series of arriving echoes from multiple objects (Luan et al., 2003; Wehr and Zador, 2005). In our virtual flight sequences, after each pulse, the bats first receive the echo from target 1 and then the echo from target 2, until it passed target 1 at 3.5 m heading distance. However, our data revealed that, even before the bat in the simulated flight sequence actually passed target 1 (at 3.5 m heading distance),

increasing numbers of neurons started to lock on target 2 (Figure 16). This excludes a simple forward suppression mechanism due to the timing of the echoes.

In addition, echo level might have an influence on object focusing. In a complex stream of incoming echoes, a response of the neurons to the loudest or most dominant echoes seems likely. Our results, however, show that more than half of the focusing neurons specifically responded to the fainter echoes in the sequence. Only in the final part of the simulated flight sequence, shortly before passing target 1, the increasing number of neurons focusing on target 2 might be substantially influenced by the echo level. When the bats started to pass target 1, the echo angle rapidly increased which led to drastically decreasing echo levels for target 1. However, as all of these neurons responded significantly to target 1 in the individual presentation, the echo levels were still above response threshold.

Our data suggest that the focusing onto a specific object in a complex flight sequence depends not merely on a single parameter such as echo delay or level alone, but on complex interactions of many different dynamically changing parameters that, in their sum, make up echo-acoustic flow information.

Classical studies in auditory physiology using pairs or sequences of pure tones or click stimuli investigated the influence of mechanisms like forward suppression, synaptic depression and facilitation or lateral inhibition on auditory processing (Oswald et al., 2006; Scholes et al., 2011; Wehr and Zador, 2005). As mentioned above, we can exclude forward suppression as underlying mechanism at least for all cells that specifically responded to target 2 while the response to target 1 was reduced. However, intracellular recordings would be required to provide more insights about mechanistic details.

It would be interesting to see if responses during the pulse/echo sequence could be predicted from the static DRFs. However, delay tuning characteristics of neurons in the AC also critically depend on the pulse repetition rate (Wong et al., 1992). Therefore, such a prediction would most probably fail.

As shown above, increasing numbers of neurons started to lock on target 2 even before the bat in the simulated flight sequences actually passed target 1. In a recent study, Fujioka et al. (2016) showed in flight room experiments that bats also attended future target information to optimize their flight paths. Our findings may be interpreted in a similar way: when the bat has almost reached the position of the closer located target 1, target 2 becomes more important

for the bat and the neural representation of target 2 consequently starts to increase. Therefore, our findings may describe some kind of non-attention driven neural mechanism that is important for bats for planning flight paths in complex environments.

Dear et al. (1993b) suggested a concurrent cortical representation of multiple objects at different distances. Our data, however, indicates a sequential processing of targets at the level of single neurons. It needs to be shown in future experiments if the population of delay tuned neurons can process multiple objects at different positions in the auditory cortex simultaneously. Therefore, simultaneous recordings from multiple positions in the cortical target distance map by using multielectrode arrays might help to clarify this question. Beetz et al. (2016a) showed that neurons respond best to echoes from the nearest target in sequences containing echoes from multiple objects positioned behind each other and that the representation of the other objects is suppressed in larger parts of cortical target range map.

Impact of pulse emission pattern on object representation and delay tuning

We simulated different pulse rates to investigate the influence of different temporal pulse patterning on object representation. Other studies reported a greater prevalence of sonar sound groups for bats hunting close to a cluttered background than in open space. It was suggested that these sonar sound groups have immediate consequences for the bat's perception of space and enhance spatio-temporal accuracy in tracking and figure ground segregation (Kothari et al., 2014; Moss et al., 2006; Moss and Surlykke, 2001). In our study, the different simulated pulse rates had no direct influence on target focusing but they did have a significant impact on the target range distribution, thereby restricting the cortical object representation at high pulse rates to close range objects.

The distribution of specific delays and thereby the target range map is shifted in a shorter range at increasing pulse rates compared to a constant pulse rate and especially to the statically presented pulse/echo pairs (see Figure 20). These findings corroborate earlier studies on the influence of pulse repetition rate on delay-tuned neurons (O'Neill and Suga, 1982; Tanaka and Wong, 1993; Wong et al., 1992) and further emphasize the functional significance of this delay shift: the bat focuses its target range map to the most relevant objects and suppresses irrelevant background clutter while increasing the pulse rate during target approach.

Auditory scene analysis in complex natural environment

Over the past 20 years, auditory scene analysis and stream segregation has been intensively studied in behavioral and neurophysiological studies in humans and different vertebrates, in most cases by using a classical pattern of alternating pure tones (Bregman, 1990; Fay, 1998; MacDougall-Shackleton et al., 1998; Noorden, 1975). Neurophysiological studies suggest that, in addition to an influence of attention on the organization of sounds, basic neural processes such as short-term adaptation and frequency selectivity play a major role in stream segregation (Scholes et al., 2015). In the present study, we show that selective focusing on one object in two streams of bio-sonar information cannot simply be related to short-term adaptation during processing of echo delay or echo amplitude alone: neither the object reflection with the shortest delay nor the object reflecting the echo with the largest amplitude was the one the neurons were focusing to in their response. Focusing rather depended on the complex dynamic changes of echo parameters occurring during flight, i.e. echo-acoustic flow information.

Conclusion

This project provides insights into the neural processing underlying auditory scene analysis in bats. Neurons in the auditory cortex of anesthetized bats can separate different echo streams and selectively lock onto echoes from specific objects in a complex dynamic environment while the representation of other objects is suppressed. Furthermore, our data show a crucial influence of dynamic naturalistic stimulations on the cortical target range representation. Our results demonstrate that the selective representation of streams of acoustic signals in mammals depends on the integration of multiple dynamically changing acoustic parameters.

THREE-DIMENSIONAL RECEPTIVE FIELDS IN THE AUDITORY CORTEX

The text and the figures of following section correspond to the publication:

*“Representation of three-dimensional space in the auditory cortex of the echolocating bat *P. discolor*” (Greiter and Firzlaff, 2017b)*

The article is published in PLOS one under the terms of the Creative Commons Attribution license which permits free reproduction of published articles.

Results

Basic delay tuning properties

A total of 95 units were recorded in the posterior dorsal field (PDF) of the auditory cortex in 3 bats. 67/95 units (71%) showed a facilitated response to pairs of pulses and echoes. For all these units ($n=67$), DRFs were obtained. An example is shown in Figure 21 A. This unit responds best at an echo delay of 7 ms (best delay = BD) at an echo level of -20 dB (best level = BL). The BDs for all 67 analyzed units ranged from 2.6 ms to 17.0 ms (median: 7.0 ms), the units' BL ranged from -45 dB to 0 dB (median: -20 dB) relative to the presented pulse level (absolute echo level 40 - 85 dB SPL, median: 60 dB SPL). The BDs of the recorded units increased along the rostro-caudal axis (Figure 21 B). Units with short BDs were significantly more rostral than those with longer BDs ($RHO = 0.78$, $P < 0.001$). No correlation could be found between the units' BDs and the medio-lateral positions in the cortex ($p > 0.05$). BLs did not significantly correlate with the neurons' positions in the auditory cortex.

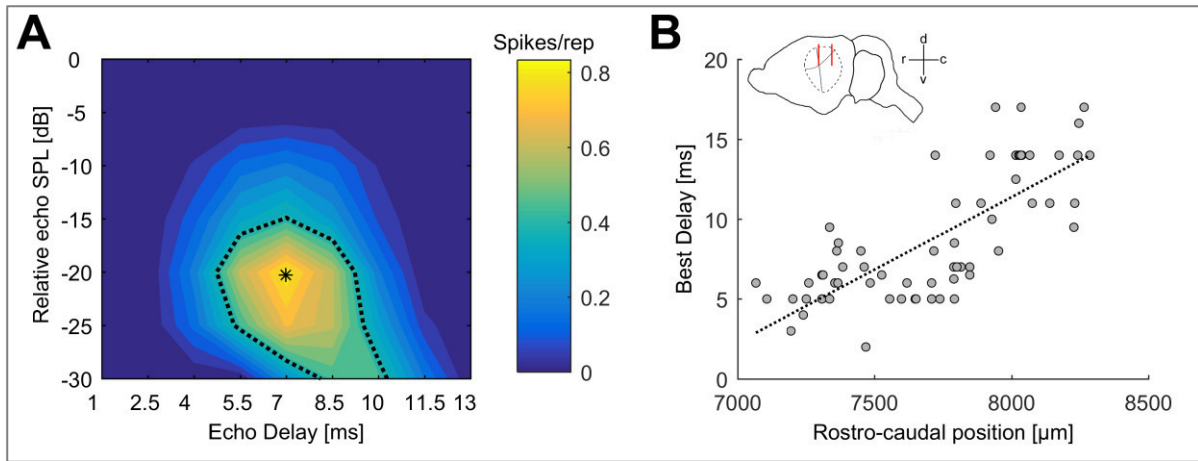


Figure 21: Delay tuning in the auditory cortex

(A) DRF of a cortical unit. The spike count per repetition is color-coded; the black dotted contour line represents the response threshold at 50% of the units maximal spike count. The echo delay/echo level combination eliciting the maximal response is marked by a black asterisk (BD = 7 ms, BL = -20 dB). (B) Distribution of BDs along the rostro-caudal axis in the PDF of the AC. Units encoding short echo delays are located in the frontal part of the PDF, units with long best delays in the caudal part of the PDF. The dotted line indicates a linear regression. The position of the analyzed units in the cortex is sketched above the data points. Black lines indicate the bat's brain, dashed lines indicate the position of the auditory cortex and red lines mark the rostro-caudal range from 7000 – 8500 μm as shown below. d: dorsal, v: ventral, r: rostral, c: caudal. (Figure adapted from Greiter and Firzlaff, 2017b. Adapted with permission.)

Spatial selectivity of neurons at best delay

For all units that showed a facilitated response to pairs of pulses and echoes ($n=67$ in this project), spatial response characteristics were determined using pulse/echo pairs with an echo delay corresponding to each unit's best delay and an absolute echo level corresponding to the each unit's BL as measured in the DRF. The spatial receptive field of a unit at a specific echo delay is called delay dependent spatial receptive field (DSRF) in the following section. An example is shown in Figure 22. (This unit's DRF is shown in Figure 21 A.) The unit responds best at a spatial position of 7.5° azimuth (best azimuth = BAZ) and -7.5° elevation (best elevation = BEL). The geometric center of the receptive field (centroid) is near the BAZ/BEL position at 12.9° azimuth and -6.9° elevation. The 50% contour line (dashed line in Figure 22 A) can be further used to measure the spatial tuning of the recorded neuron by determining the width of the receptive field in azimuth and elevation. The unit shown in Figure 22 has a DSRF width in azimuth of 52° and a width in elevation of 48° .

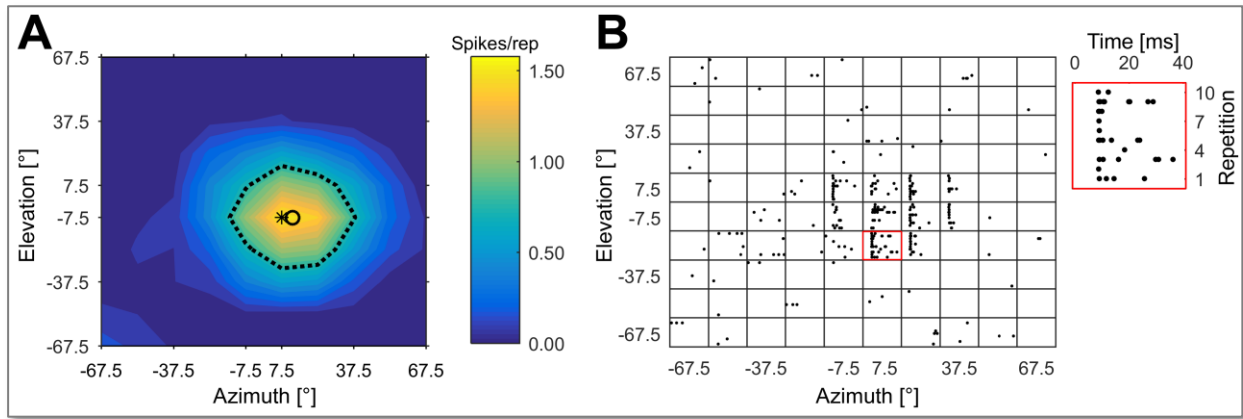


Figure 22: Delay dependent spatial receptive field

(A) DSRF of a cortical unit. Pulses and echoes were separated by an echo delay of 7 ms, corresponding to the unit's BD. The spike count per repetition is color-coded. The spatial receptive field is represented by the black dotted contour line corresponding to the response threshold at 50% of the unit's maximal spike count. The spatial position eliciting the maximal response is marked by a black asterisk (at 7.5° azimuth and -7.5° elevation). The geometric center of the unit's spatial receptive field (centroid) is marked by a black circle (at 12.9° azimuth and -6.9° elevation). (B) Rasterplots showing neuronal responses elicited by pulse echo pairs at different spatial positions. The time window corresponds to the chosen response window for this unit. The echo was presented at 0 ms, the pulse at -7 ms (7ms before the echo = 7 ms echo delay). The cutout shows the response from a spatial position of 7.5° azimuth and -22.5° elevation (red box).

(Figure adapted from Greiter and Firzlaff, 2017b. Adapted with permission.)

The BAZ/BEL positions for all analyzed units are shown in Figure 23 A. The units' BDs are color-coded. Most units responded best to echoes directly in front of the bat or in the lower contralateral quadrant. Note that due to the discrete positions recorded in azimuth and elevation, multiple units responded at the same spatial positions and are therefore grouped together in the figure. The BAZ ranged from -22.5° (ipsilateral) to +67.5° (contralateral), with a median at +7.5°. The BEL ranged from -67.5° (below the bat) to +22.5° (above the bat), with a median at -7.5°. As the BAZ/BEL were restricted to discrete positions in azimuth and elevation, we further analyzed the centroid positions of the spatial receptive fields to get a more detailed impression of the spatial directionality of these cells. The distribution of the centroids of all analyzed units is shown in Figure 23 B and corresponds roughly to the BAZ/BEL positions. Most spatial receptive fields were targeted to frontal positions or to the lower contralateral quadrant. The centroid positions ranged from -27.6° to +47.9° (median: +8.5°) in azimuth and from -45.5° to +39.5° (median: -7.6°) in elevation.

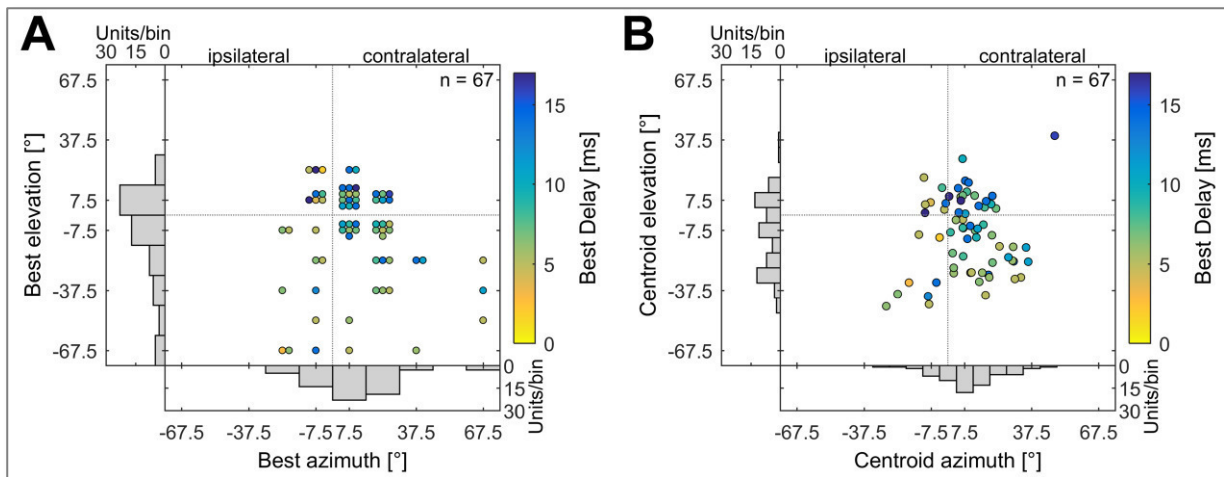


Figure 23: BAZ/BEL and centroid positions of all analyzed units

(A) Distribution of BAZ and BEL. The best responses were measured at discrete spatial positions (15° binning). Multiple units responding at the same position are grouped together in the figure. Each unit's BD is color-coded. The lower histogram shows the distribution of BAZ and the left histogram the distribution of BEL. (B) Distribution of centroids of the spatial receptive fields. The lower histogram shows the distribution of the centroid positions in azimuth, the left histogram the distribution of the centroid positions in elevation (bin width 7.5°). All azimuth positions are normalized to one hemisphere. Azimuth positions $> 0^\circ$ correspond to positions contralateral to the recording site.

(Figure adapted from Greiter and Firzlaff, 2017b. Adapted with permission.)

We further tested, if units with different best delays showed different spatial directionality. For this, units were separated in two equal sized groups according to their BDs. Units with short BDs ($BD \leq 7\text{ms}$) tended to respond best to positions below the bat (median: -7.5° , $n = 34$) while units with long BDs ($BD > 7\text{ms}$) responded mainly to positions in the horizontal plane or slightly above (median: $+7.5^\circ$, $n = 33$). The differences of BEL between these two groups were significant (Wilcoxon: $p < 0.01$) and each unit's BD and BEL were significantly correlated (Spearman: $p < 0.01$, $\rho = 0.33$). However, the distribution of BAZ showed no differences between units tuned to shorter or longer echo delays (Figure 24 A,B).

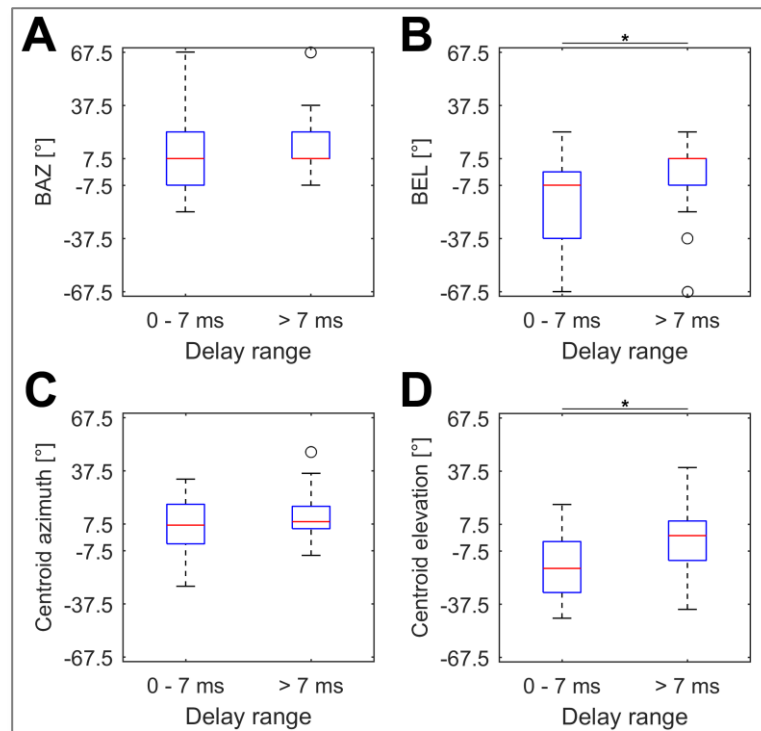


Figure 24: Azimuth and elevation at different best delays

Boxplots of BAZ (A), BEL (B), centroid positions in azimuth (C) and in elevation (D) for all analyzed units with best delays ≤ 7 ms (left box, $n = 34$) and > 7 ms (right box, $n = 33$). All boxes represent the median (red center line) and the interquartile range (IQR); whiskers indicate values within $1.5 \times$ IQR, black circles mark outliers. Significant differences between different groups are indicated by a black asterisk.

(Figure adapted from Greiter and Firzlaff, 2017b. Adapted with permission.)

Corresponding to BAZ/BEL, the centroids from units with short BDs ($BD \leq 7$ ms, median elevation: -17.4° , $n = 34$) were located at lower elevations than centroids from units with long BDs ($BD > 7$ ms, median elevation: $+1.1^\circ$, $n = 33$). The differences between these two groups were significant ($p < 0.01$) and BD and centroid positions in elevation were again significantly correlated (Spearman: $p < 0.01$, $\rho = 0.37$). No differences could be found for the centroid positions in azimuth with respect to different ranges of BD (Figure 24 C,B).

We checked a possible influence of BD and BL of all units on the size of their spatial receptive fields. We found a significant correlation between each unit's BD and the width of the DSRF in azimuth ($p = 0.01$), but not between BD and the width in elevation ($p > 0.05$). DSRFs were significantly smaller in azimuth but not in elevation at longer BDs compared to short BDs. We found no correlation between each unit's BL and the width of the spatial receptive fields in azimuth ($p > 0.05$) and elevation ($p > 0.05$).

We further investigated if the neurons spatial directionality depended on their location in the auditory cortex, or in other words, if delay tuned neurons form a topographic representation of space in the PDF of the auditory cortex. Our results show no correlation between each unit's medio-lateral position in the cortex and the centroid position in azimuth ($p = 0.14$) or elevation ($p = 0.35$) and no correlation between each unit's rostral-caudal position and centroid position in azimuth ($p = 0.90$). We found, however, a topographic arrangement of elevation along the rostral-caudal axis. Each unit's centroid position in elevation and its rostral-caudal position were significantly correlated ($p < 0.01$). This means, neurons responding at short echo delays are positioned in the rostral part of the PDF and respond to lower elevations while neurons responding at longer echo delays are located in the caudal part of the PDF and respond preferably to positions in the horizontal plane or above.

We were wondering, if this correlation between BD and best elevation could be explained by the change of simple acoustic parameters due to our simulation and thus be just a simple epiphenomenon. Because of this, we investigated the influence of distance and frequency depended sound damping at different echo delays on the echo levels and echo frequency content. As the FM-sweeps of *P. discolor* contain most energy at around 60 kHz, we specifically analyzed echo levels at this frequency.

As shown in Figure 25, at an echo delay of 15 ms (\triangleq 2.6 m target distance), echo levels drop about 18 dB (at 60 kHz) compared to an echo delay of 3 ms (\triangleq 0.5 m). While the region of highest echo level remains quite stable at the same spatial position, the overall intensity increases at shorter delays. Thus spatial positions with low echo level in the 15 ms delay condition show higher echo levels in the 3 ms delay condition. If the maximum echo level in the 15 ms condition is near the neurons' response threshold, the SRF should systematically increase in size and become more unspecific when echo delay decreases. However, this is clearly not the case in our data. As we will later on show (compare Figure 28), SRFs remain spatially focused even at short echo delays and SRFs of neurons with longer best delays shift to significantly higher positions in elevation but show no change in azimuth (compare Figure 24). Therefore, more complex neural processing must underlie the shape and size of SRFs (e.g. additional neuronal computation of interaural level differences and/or monaural inhibitory interactions).

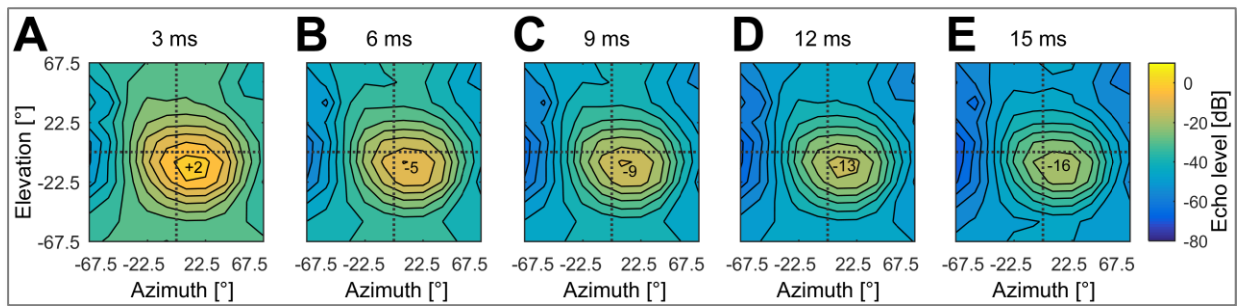


Figure 25: Simulated echo levels at different echo delays

Echo levels at 60 kHz relative to the presented pulse level at echo delays of 3 ms (A), 6 ms (B), 9 ms (C), 12 ms (D) and 15 ms (E). Relative echo levels are color-coded. The black lines correspond to differences of 5 dB. Echo levels at different spatial positions are calculated using the pulse emission characteristics of *P. discolor*, distance and frequency dependent sound damping (corresponding to the echo delay or physical distance in air) and the HRTF. For each echo delay, the maximum echo levels [dB] are indicated at the loudest position.

(Figure adapted from Greiter and Firzlaff, 2017b. Adapted with permission.)

It would have been interesting to investigate the influence of the frequency content of the echoes on the spatial selectivity of the combination sensitive neurons in more detail. However, these neurons did not respond to presented pure tones. Because of this, it was not possible to gather basic data on frequency tuning characteristics. We further tried to use bandpass-filtered pairs of pulses and echoes, but found that again most units did not respond to these bandpass-filtered stimuli but only to broadband pairs of pulses and echoes.

We further analyzed the spatial tuning of the delay-tuned neurons by measuring the width of the spatial receptive fields of all units in azimuth and elevation at each unit's BD and BL. The spatial receptive fields stretched across an angle of 45.7° up to 129.4° (median: 67.2°) in azimuth and 45.0° up to 118.9° (median: 64.8°) in elevation. As most units respond to frontal positions or positions in the lower contralateral space and span usually more than 45°, the receptive fields of these units show a high degree of overlap. Only the receptive fields of 9/67 (13%) recorded units did not overlap with at least one other unit.

Influence of call/echo level on spatial tuning

We further tested the influence of the presented pulse and echo level on the spatial directionality in a subset of the recorded neurons ($n = 40$). Note that, in our simulation, the echo level is always a function of the presented pulse level, echo delay and spatial position. Increasing pulse levels and consequently increasing echo levels led to considerably higher spike response rates in all units. At the spatial position eliciting the maximum response, the median spike count per repetition of all analyzed units was 0.6 at BL -10 dB, 1.0 at BL +0 dB and 1.5 at BL +10 dB (Figure 26 A). Due to this increase of the spike count at increasing sound pressure levels, the width of each spatial receptive field was measured at the contour line corresponding to 50% of the unit's maximum response at each presented echo level (BL -10 dB, BL +0 dB, BL +10 dB). An example of a unit responding at different presented call/echo levels is shown in Figure 26 B-D.

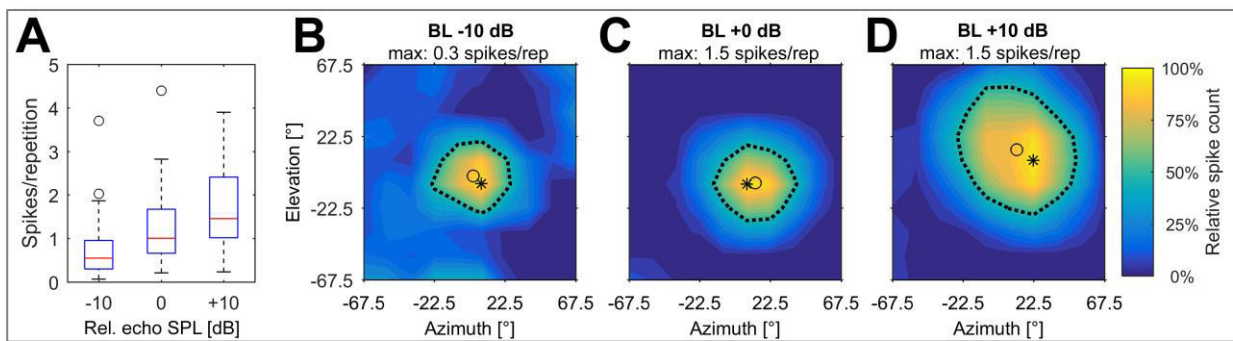


Figure 26: Influence of call/echo level on spatial tuning

(A) Boxplots of maximum spike count for all analyzed units ($n = 40$) and for each presented pulse/echo level. The boxes represent the median (red center line) and the interquartile range (IQR); whiskers indicate values within 1.5x IQR, black circles mark outliers. (B-D) Spatial receptive fields of a unit at the unit's BD and echo levels of BL -10 dB (B), BL +0 dB (C) and BL +10 dB (D). The relative spike count in relation to the maximum response at each echo level is color-coded. The maximum spike count per repetition at each presented echo level is given on top of each figure. In each figure, the black asterisk marks the position of the maximum response and the black circle marks the centroid of the receptive field.

(Figure adapted from Greiter and Firzlauff, 2017b. Adapted with permission.)

The spatial receptive fields tended to broaden in azimuth and elevation at increasing sound pressure levels. The median width in azimuth was 60.5° (-10 dB), 69.9° (+0 dB) and 77.3° (+10 dB), respectively (Figure 27 A). Differences in SRF azimuthal width were significant between relative echo levels of -10 dB and +10 dB ($p = 0.003$), but not between the other groups. The median width in elevation was 49.7° (-10 dB), 62.9° (+0 dB) and 81.1° (+10 dB), respectively (Figure 27 B). SRF width was significantly different between an echo level of -10 dB and 0 dB ($p = 0.015$), 0 dB and +10 dB ($p = 0.014$) and -10 dB and +10 dB ($p = 0.001$). The Bonferroni corrected significance level (p value) for multiple testing was 0.017.

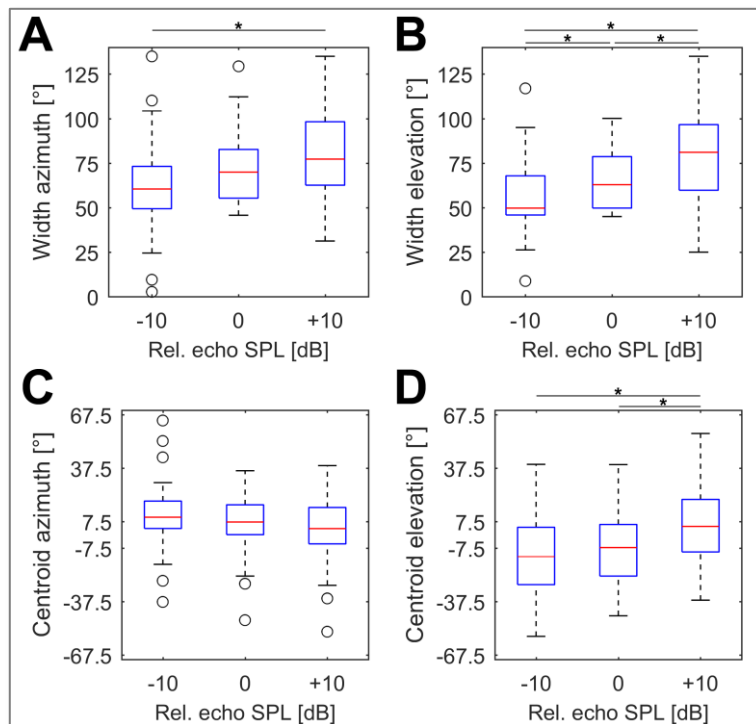


Figure 27: SRF width and centroid position of receptive fields at different echo levels

(A,B) Boxplots showing the widths of the spatial receptive fields of all analyzed units in azimuth (A) and elevation (B) at an echo level of BD -10 dB, BD +0 dB and BD +10 dB, respectively. (C,D) Boxplots showing centroid positions of the spatial receptive fields in azimuth (C) and elevation (D). Significant differences between different groups are indicated by a black asterisk (significance level after Bonferroni: 0.017).

(Figure adapted from Greiter and Firzlaff, 2017b. Adapted with permission.)

Furthermore, units tended to respond to more frontal positions at higher sound pressure levels. The median azimuth centroid positions were 9.9° at -10 dB, 7.2° at +0 dB and 3.5° at +10 dB. However, the azimuth centroid positions were not significantly different between different pulse/echo levels (Figure 27 C). The trend of responses to more frontal positions at higher pulse/echo levels was more pronounced for the centroid positions in elevation: the median elevation centroid positions were -12.3° at -10 dB, -1.2° at +0 dB and 4.8° at +10 dB (Figure 27 D). Centroid positions in elevation differed significantly between a call/echo level of BD +0 dB and +10 dB ($p = 0.016$) as well as BD -10 dB and +10 dB ($p = 0.006$), but not between -10 dB and +0 dB ($p = 0.67$).

Three dimensional response properties

In a subset of units ($n = 27$), we performed additional recordings at different standardized, logarithmically spaced echo delay steps (see methods section), including each unit's BD, to investigate the three dimensional response properties of the delay tuned neurons. An example for the response of a cortical unit to these five delay steps is shown in Figure 28. This unit shows its highest response rate at its Best Delay of 6.0 ms. The response to the presented stimuli decreases at shorter or longer echo delays. The spatial direction eliciting the maximum response, however, is in all recorded echo delay steps at approximate 22.5° in azimuth and -7.5° in elevation.

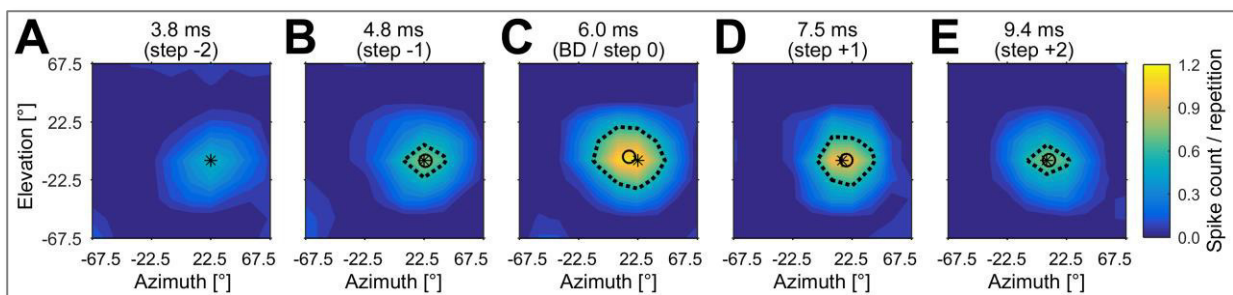


Figure 28: Spatial receptive fields at different echo delay steps

Example of a unit's spatial receptive field at echo delay steps of 3.8 ms (A), 4.8 ms (B), BD = 6.0 ms (C), 7.5 ms (D) and 9.4 ms (E). The spike count per repetition is color-coded. All receptive fields at different echo delay steps are normalized on the maximum spike count evoked within these five delay steps. This unit responded best with 1.2 spikes per repetition at the unit's BD of 6 ms. The maximum response position at each echo delay step is marked by a black asterisk; the receptive fields are indicated by a black dashed line (corresponding to 50% of the maximum response), and the centroid of each spatial receptive field is marked by a black circle. Note that, as the unit's response drops below 50% of the maximum response rate at an echo delay of 3.8 ms, no spatial receptive field is shown.

(Figure adapted from Greiter and Firzlaff, 2017b. Adapted with permission.)

We analyzed the spike count and the spatial directionality of all 27 units at the different delay steps. Due to the DRFs of each unit, the highest spike count would be expected at each unit's BD. In our data, however, the median maximum spike count was elicited at delay step “-1” (one delay step shorter than each unit's BD, see Figure 29 A). The median spike count per repetition was 0.87 (step -2), 1.16 (-1), 0.99 (0 = BD), 0.80 (+1) and 0.60 (+2). Significant differences between the spike counts were found only between steps -1 and +2 ($p = 0.0007$) as well as between 0=BD and +2 ($p = 0.0099$). The Bonferroni corrected significance level was 0.01. These results show that most units responded at shorter echo delays when naturalistic “spatial” stimuli were presented in contrast to the measurements in the DRFs without any spatial information.

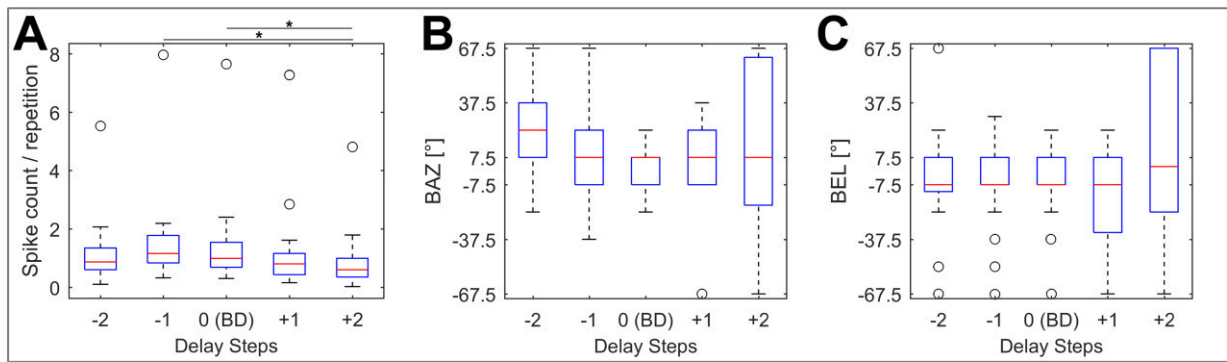


Figure 29: Maximum response and spatial directionality at different echo delay steps

(A) Boxplots of maximum spike counts per repetition for different, logarithmically spaced echo delay steps. The maximum number of spikes is elicited at delay step “-1” (one delay step shorter than each unit’s BD). Significant differences are indicated by a black asterisk. (B,C) Boxplots of BAZ (B) and of BEL (C) at different echo delay steps. No significant differences were found between different echo delay steps with respect to BAZ or BEL.

(Figure adapted from Greiter and Firzlaff, 2017b. Adapted with permission.)

In some units, the neuronal response decreased below the threshold of 50% of the maximum response at the delay steps -2 or +2. Because of this, we could not analyze the centroid position for these neurons at these delay steps, but used BAZ and BEL as a measurement of spatial directionality at the different echo delays steps.

The analysis of BAZ and BEL for all 27 units clearly shows that the neurons respond to the same spatial direction at different echo delays (Figure 29 B,C), independent of the changing echo levels due to distance dependent sound attenuation (see Figure 25). In contrast to the spatial directionality of units with different BDs, no significant differences were found between BAZ or BEL at different delay steps of the 3D fields. The median BAZ was 22.5° (step -2), 7.5° (-1), 7.5° (0 = BD), 7.5° (+1) and 7.5° (+2), respectively. The median BEL was -7.5° (step -2), -7.5° (-1), -7.5° (0 = BD), -7.5° (+1) and +2.5° (+2), respectively. In general, the variability of BAZ and BEL increases with increasing echo delays. An analysis of the centroid positions basically yields the same results (not shown here).

Figure 30 shows an example of a three-dimensional receptive field. Due to the different spike counts at different echo delay steps, the unit exhibits an ellipsoid shaped, three-dimensional receptive field. The axis of the receptive field, through the BAZ/BEL positions at each echo delay step, gives an estimate of the unit’s directionality. The unit’s directionality is spatially constant across different echo delay steps.

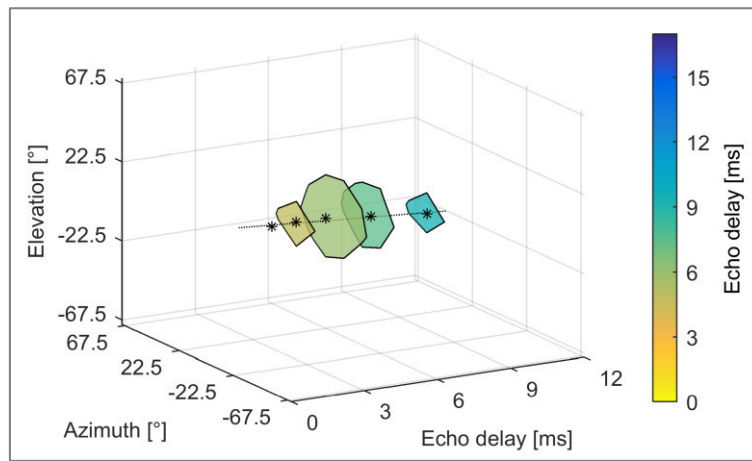


Figure 30: Three-dimensional receptive field of cortical combination-sensitive neuron

Spatial receptive fields of the same unit as shown in Figure 28 in three-dimensional space. The receptive fields (50% contour line) at each echo delay step (3.8 ms, 4.8 ms, 6.0 ms = BD, 7.5 ms, 9.4 ms) are indicated by a black solid line, the colored area indicates the respective echo delay and the black asterisks mark BAZ/BEL. The response rate and consequently the size of the receptive fields normalized on the maximum response at BD decrease at shorter or longer echo delays than the unit's BD. Because of this, the black outlines of the receptive fields at different delay steps indicate a three-dimensional response volume in space where the neurons respond with at least 50% of their maximum response. The dotted black line shows the linear regression through BAZ/BEL at the different echo delay steps and indicates the unit's spatial directionality. (Figure adapted from Greiter and Firzlaff, 2017b. Adapted with permission.)

The width of the receptive fields (measured as 50% contour line corresponding to each unit's maximum response) at the different echo delay steps changed according to the spike count (Figure 31). The units exhibited the broadest receptive field at each unit's delay step -1. At shorter or longer delays, the receptive field size decreased. In part of the cells, the response rate decreased below the threshold of 50% at some of the delay steps.

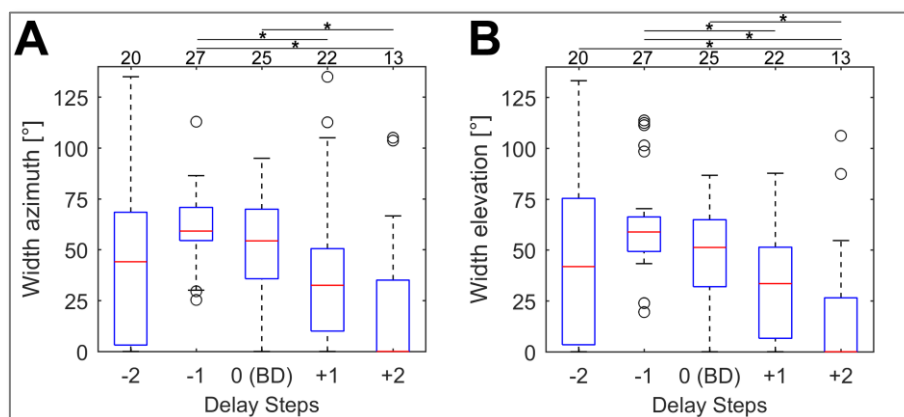


Figure 31: Sizes of the receptive fields at different echo delay steps

Boxplots showing width of the receptive fields in azimuth (A) and elevation (B) of all analyzed units ($n=27$) at the logarithmically spaced echo delay steps. The units show the broadest receptive fields at step -1. In part of the cells, the response drops below the threshold of 50% of the maximum response at some echo delay steps (no receptive field, width = 0°). The number of units exhibiting a receptive field width $> 0^\circ$ is noted above each figure. Significant differences between different delay steps in respect to field width in azimuth or elevation are indicated by a black asterisk. (Figure adapted from Greiter and Firzlaff, 2017b. Adapted with permission.)

Discussion

In this project, we investigated the cortical representation of three-dimensional space in the echolocating bat *P. discolor*. We hypothesized that combination-sensitive neurons encoding target distance can also process directional information. Our data reveal that neurons tuned to specific echo delays responded selectively to specific spatial directions, thereby mainly encoding positions in the horizontal plane and lower, contralateral space. We found a covariance of best elevation, best delay and rostro-caudal position of the combination-sensitive neurons in the AC. Neurons exhibited a higher spatial selectivity at lower sound pressure levels.

Delay tuning and spatial selectivity

Our data on the delay tuning properties and the chronotopic distribution of the combination-sensitive neurons in the PDF of the AC corresponds to the project on echo-acoustic flow fields (Greiter and Firzlaff, 2017a) as well as to other recent studies in *Phyllostomus discolor* and closely related species (Hagemann et al., 2010; Hoffmann et al., 2013). Furthermore, this study clearly shows a selectivity of these combination-sensitive neurons to specific spatial directions. The mean size of the spatial receptive fields in azimuth ($\approx 70^\circ$) and elevation ($\approx 63^\circ$) was well inside the range reported for cortical neurons in other bat species (about 60° in azimuth and 100° in elevation in pallid bats (Razak et al., 2015)) and considerably smaller than reported for other mammals (up to about 160° in humans (Derey et al., 2015), $\leq 140^\circ$ in rhesus monkeys (Tian et al., 2001), $\leq 180^\circ$ in cats (Lee and Middlebrooks, 2011; Mickey and Middlebrooks, 2003; Middlebrooks et al., 1998)).

Interestingly, most neurons in our study encoded the frontal and lower contralateral space, while only few neurons encoded positions slightly above the horizon or on the ipsilateral side. When we combine the results from neurons in both hemispheres, these neurons encode a large spatial area to the front, below and to a lesser extend above the horizon. This region corresponds roughly to the biosonar receptive field shown for neurons in the superior colliculi of the midbrain in *P. discolor* (Hoffmann et al., 2016). Thus, the spatial selectivity of these neurons is focused on locations which might be most relevant for the echolocating bat: positions along the bats flight path and on the ground where prey can be expected. A

comparable spatial selectivity of FM neurons for spatial positions along the flight path has already been described for pallid bats (Razak et al., 2015).

In contrast to Suga et al. (1990) who proposed that directional information is not processed by the combination-sensitive neurons, but is processed in parallel by a separate population of neurons, our data demonstrate that these neurons have well confined spatial receptive fields and are suited process directional information.

However, it is notable that the spatial selectivity depended on the presented sound pressure level. Neurons became less specific at higher sound pressure levels. Razak et al. (2015) proposed, that the expansion of the spatial receptive fields with increasing sound levels might simply reflect ear directionality. The systematic enlargement of the receptive fields at increasing levels in our data fits well to this hypothesis.

The bats, however, might in some situations actually benefit from a lower spatial selectivity of these neurons as this facilitates target detection at specific distances. After target detection, an active control of sonar emission level, directionality and timing might help to optimize echo perception and target-clutter separation (Brinklőv et al., 2011; Kothari et al., 2014). The targeting of ears and head might then enable more precise target localization by increasing spectral and intensity differences between the ears (Wohlgemuth et al., 2016a). Furthermore, our results from the simulation of echo-acoustic flow fields as well as other recent studies in *P. discolor* showed that dynamic stimulation leads to spatially more focused receptive fields and that echo-acoustic flow facilitates target segregation (Greiter and Firzlaff, 2017a; Hoffmann et al., 2010).

Systematic representation of target elevation

Our data show a covariance of best elevation, best delay and rostro-caudal position of the combination-sensitive units in the PDF of the AC. This means, the representation of elevation is topographically aligned in the PDF. Interestingly, units tuned to long echo delays or distant targets responded to positions in the horizontal plane while units tuned to shorter echo delays or closer targets preferentially responded to positions below the horizon (Figure 32). This might be especially useful in a typical overfly situation encountered during foraging. During the approach to foraging grounds, the bats perception is targeted on distant objects along the flight path. At close range, however, when the bat is flying or hovering near a foraging tree, the

perception is targeted more downwards towards possible food. Such an arrangement of best elevation might be further influenced by the bats typical foraging behavior: *P. discolor* is not an aerial hunter of insects, but forages around flowering trees and feeds on a mixture of nectar, pollen, fruits and insects among the trees (Kwiecinski, 2006). Thus positions below the bat might be most relevant during foraging. On longer distances (e.g. during commuting flights) positions along a possible flight path might be more relevant.

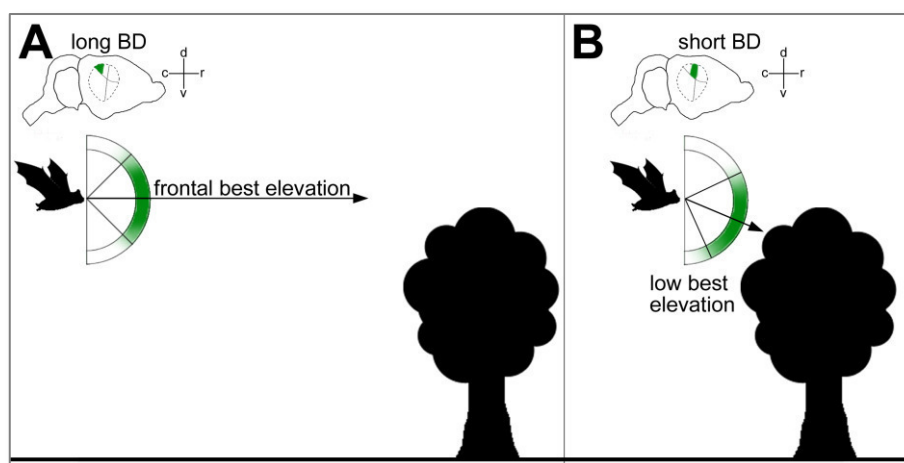


Figure 32: Systematic representation of target elevation and echo delay

Schematic drawing illustrating the possible implication of the covariation of BD and elevation for target representation in the cortical target-range map. (A) At long distances to the target, neurons with long BDs in the caudal region of the PDF respond preferably to echoes from frontal positions. (B) At short distances to the target, neurons with short BDs in the rostral region of the PDF respond preferably to positions below the bat. Arrows represent the direction of best elevation. d: dorsal, v: ventral, r: rostral, c: caudal.

(Figure adapted from Greiter and Firzlaff, 2017b. Adapted with permission.)

We can further show, that this arrangement of best elevation cannot be explained by the change of single acoustic parameters like echo level as a function of echo delay. If the spatial directionality of these neurons would be mainly determined by the echo level and HRTF, one would expect more unspecific responses to the loud echoes at short echo delays. At longer echo delays and thereby more distance dependent sound attenuation, responses would become more specific to the most intense positions of the HRTF: near to the horizontal plane and slightly contralateral. Our data, however, shows a high specificity of the neurons at all echo delays and a clear and consistent shift to lower elevations at short echo delays.

It seems most likely that, besides absolute echo levels, interaural level differences shape spatial directionality of the combination-sensitive neurons, at least in azimuth. The influence of interaural level differences on azimuth selectivity in the auditory cortex was shown for different species, including bats (Razak and Fuzessery, 2002; Rutkowski et al., 2000; Samson et al., 1994). However, a systematic investigation of the influence of interaural level differences on the

spatial directionality of the combination-sensitive neurons was beyond the scope of this study, but might be targeted in the future.

Hoffman et al., who investigated the spatiotemporal response characteristics of cortical neurons by using a reverse-correlation technique (Hoffmann et al., 2013; Hoffmann et al., 2015), already found a spatial selectivity of combination-sensitive cortical neurons in *P. discolor*. However, as they used no classical pulse/echo paradigm and did not simulate pulse emission characteristics as well as a change of echo levels due to the distance or echo delay, a direct comparison to the current results is difficult. To our knowledge, no other study systematically investigated the topography of azimuth and elevation coding in the AC of *P. discolor* or closely related species so far. Unlike the topographic representations found in the visual cortex (Alonso, 2016; Kremkow et al., 2016), the representation of acoustic spatial information in the auditory cortex in mammals remains a matter of debate (Brewer and Barton, 2016; Ortiz-Rios et al., 2017). While maps of auditory space are well established already on the level of the midbrain (King, 1999; Knudsen and Konishi, 1978), a similar map has not been found in the auditory cortex of various mammals so far (Middlebrooks and Pettigrew, 1981; Rajan et al., 1990). Neurons with similar binaural properties rather form local clusters than an orderly map (Rutkowski et al., 2000). This is surprising as numerous ablation studies have shown the importance of the auditory cortex (and different subfields within) for behaviorally measured sound localization (Jenkins and Masterton, 1982; Lomber and Malhotra, 2008). A remedy for this might come from studies showing that spike timing and spike pattern might be more important than changes in firing rate (e.g. Brugge et al., 1996; Nelken et al., 2005). However, localization accuracy based on spike-timing of single neurons still proved to be insufficiently broad, putting forward the view that spatial position of sound sources are encoded via population codes based on either spike timing or firing rates (Miller and Recanzone, 2009; Stecker and Middlebrooks, 2003).

The sound localization in bats, however, benefits from the high directionality of the sound emitting and sound receiving structures (i.e. nose leaf and pinnae) for frequencies in the ultrasonic range. This directionality might be reflected in the neural representation of space relatively i.e., in sharp spatial tuning of cortical SRFs of *P. discolor* measured in our experiments. Evidence for a special representation of auditory space in AC comes also from other bats. Razak (2011) showed that in the primary tonotopic areas of the AC in pallid bats (*Anthrozous pallidus*), a systematic representation of sound azimuth exists. Importantly, this is not a point-by-point

space map, but space is encoded in form of a systematic change in the extent of activated cortex as azimuth changes from ipsilateral to contralateral locations. However, space representation in the auditory cortex of bats might differ between regions involved in passive hearing (e.g. when a bat listens to prey generated sounds) or regions involved in active echolocation. Razak et al. (2015) showed that neurons in regions of the AC selective for echolocation specific frequency-modulated sweeps were more focused towards the midline while neurons in the noise-selective region were broadly tuned to contralateral azimuth. SRF size and target elevation were correlated with the characteristic frequency for neurons in the noise selective region but not in the frequency-modulated sweep-selective region in these bats. Our results reveal now for the first time a topographic-like representation of elevation of the combination-sensitive neurons in the PDF of the AC in *P. discolor*.

Three-dimensional representation of space

The systematic recordings at different echo delay steps revealed a clear tuning of the combination-sensitive neurons to three-dimensional space. Interestingly, most units responded best at an echo delay shorter than each unit's best delay (derived from the DRF). This might be influenced by the higher echo levels at shorter echo delay steps in our simulation or simply by the limited precision we used to determine the basic delay tuning properties of each unit in the corresponding DRF. However, there might also be a difference between the echo delay tuning of cells when measured with pulse/echo combinations containing spatial information (e.g. interaural level differences and spectral differences) in contrast to the measurements without any spatial cues as in the DRFs. Our studies as well as other studies using naturalistic pulse/echo sequences to determine the response characteristics of combination-sensitive neurons already presented evidence, that a dynamic change of spatial and temporal information has a significant impact on the delay tuning properties of these neurons (Bartenstein et al., 2014; Beetz et al., 2016b; Greiter and Firzlaff, 2017a).

However, our data clearly show that each unit has a "specific" delay, corresponding to a physical distance to the target, and a "specific" spatial direction in azimuth and elevation where it responds best. Interestingly, neurons exhibited the same spatial directionality at all presented echo delay steps. Despite the fact that the echo levels and echo frequency content change according to the different echo delay steps (as a function of distance and frequency depended sound damping), neurons spatial directionality remained constant for each neuron at different

delay steps. This means that each neuron specifically encodes a direction and a specific delay range, or in other words, a specific volume in three-dimensional space (see Figure 30).

At a non-optimal echo delay, the spike response and consequently the size of the spatial receptive fields decrease. Because of this, the neurons responses become more “selective” to specific spatial directions. This indicates that neurons near to, but not exactly at their best delay might be better suited for target localization. The same effect of a higher spatial selectivity could be shown at lower pulse/echo levels when tested at each unit’s best delay. This means that by actively adjusting the pulse/echo level during target approach, the bat can increase its target localization abilities. It is important to note that the bat can not only increase or decrease its vocalization level, but can of course adjust multiple biosonar parameters like sonar beam width, direction and frequency content as well as temporal parameters to optimize sensory acquisition (Jakobsen et al., 2015; Kounitsky et al., 2015).

Moreover, it is most likely that an active orienting behavior including targeting of head and ears at specific targets enables a more flexible and on the same time precise localization. As mentioned above, these combination-sensitive neurons most probably do not form a static representation of three-dimensional space. According to the dynamic nature of the target distance map (Bartenstein et al., 2014; Greiter and Firzlaff, 2017a) and the reported sharpening of spatial receptive fields evoked by dynamic stimulation (Hoffmann et al., 2010), it seems most likely that the three-dimensional response properties of these cortical combination-sensitive neurons are further modified by echo-acoustic flow information and active orienting behaviors like sonar vocalization pattern or head and pinna movements as well as top-down attentional effects (Wohlgemuth et al., 2016a; Wohlgemuth et al., 2016b).

Conclusion

We found, that combination-sensitive neurons in the AC of *Phyllostomus discolor* can process target distance information as well as directional information and are thereby suited to encode a three-dimensional representation of space. Our data further reveal a topographic distribution of best elevation i.e., neurons in the rostral part of the target distance map representing short delays prefer elevations below the horizon. Top-down attentional effects and echo-acoustic flow information in natural scenes might further help to increase spatial selectivity and allow more precise target discrimination.

GENERAL DISCUSSION

This work focused on the representation of dynamic echo-acoustic scenes in bats. For the last decades, research on auditory perception in bats as well as in other mammals focused either on the neuronal representation of single, mostly static acoustic parameters (e.g. frequency, sound pressure level, repetition rate) or on normally behaving animals in a more or less natural environment. In freely behaving animals, the investigation of the neuronal basis of auditory perception is still not easy and only recently the use of multi-electrode arrays and wireless systems allow a better neurophysiological investigation in moving or flying animals. In contrast to this, neurophysiology in anesthetized animals allows a tightly controlled experiment with a straightforward analysis. But the presentation of single, often static acoustic parameters is far from a natural complex and dynamic acoustic environment. In the last years, more and more studies revealed the dynamic character of computational maps of space in the brain and showed that they often form not just a topographic representation of a single parameter but that they strongly depend on and are influenced by a multitude of related parameters (Bartenstein et al., 2014; Hechavarría et al., 2013b; Schreiner and Winer, 2007).

In my thesis, I investigated the neuronal representations of acoustic space by using more naturalistic, complex acoustic stimulations. The use of a species-specific echolocation call is the essential basis to study neuronal responses to naturalistic and not artificial stimuli. However, such a call alone is of course not enough to study neuronal processing of complex, echo-acoustic scenes. In my experiments, I could use the species specific HRTF to generate naturalistic virtual echoes from any position in the frontal hemisphere. It is, of course, important to assure that the differences of the HRTFs between individual bats are negligible (Firzlaff and Schuller, 2003) before using the same HRTF for every bat. The method of generating complete sets of call/echo stimuli or sequences of calls and echoes from more than one object before they were actually presented to the bat allowed for a high flexibility in my experiments but gave also the possibility to tightly control these acoustic stimuli. Furthermore, the presentation of these computer generated sounds *via* ear-phones provides advantages compared to the restrictions one has to face with a stationary loudspeaker (e.g. unwanted echoes from equipment, possible background noise). These methods gave me the prerequisites for the use of naturalistic call/echo sequences to investigate the object representation in the cortical target range map in a complex, dynamic situation.

My results as well as the previous data from Bartenstein et al. (2014) and Beetz et al. (2016a) demonstrate the strong impact of dynamic stimulations on the cortical object representation and target distance map. The older data on cortical delay tuning, derived from mostly static presentations of isolated pairs of calls and echoes, were of course an absolute essential basis for the current experiments. But with the use of more naturalistic stimuli (e.g. call/echo sequences simulating a flight passing specific object) we can now see the highly dynamical and adaptable character of cortical computational maps and the neuronal processing in general. My data demonstrate that the selective representation of objects, even in an anesthetized, unconscious bat, depends on the integration of multiple dynamically changing acoustic parameters. And I could show that, even if a static presentation of acoustic stimuli (i.e. static delay response fields, static spatial receptive fields) gives an essential basis for the understanding of cortical and midbrain processing, the neuronal processing is significantly different when studied under more natural, realistic conditions. Because of this, it would be most interesting to further investigate the described 3-D representation of space in the AC with a more dynamic approach (e.g. pulse/echo sequences simulating a flight). It seems most likely that a naturalistic series of calls and echoes (i.e. with dynamically changing echo levels, echo delay, etc.) might not only influence the cortical echo delay tuning but also modify, maybe sharpen the spatial tuning of AC neurons in azimuth and elevation.

However, a further investigation of object representation and three-dimensional representation of space in awake bats, probably using multi-electrode arrays and wireless systems, might be helpful to study cortical as well as midbrain processing of complex acoustic scenes without the influence of anesthesia. The use of multi-electrode arrays further provides the possibility to study the complete computational maps of space and not just the responses from single neurons in these maps.

My experiments might help to bridge the huge gap between the classical neurophysiological studies on single cells in a static, controlled environment and the behavioral studies of free flying bats in nature. This project answered some specific open questions about neuronal processing, provides new information about the dynamic character of computational maps of space in general and brought up new fascinating scientific questions for future projects.

ABBREVIATIONS

| | |
|------|--|
| AC | Auditory cortex |
| ADF | Anterior dorsal field of the auditory cortex |
| AVF | Anterior ventral field of the auditory cortex |
| BAZ | Best azimuth |
| BD | Best delay |
| BEL | Best elevation |
| BF | Best frequency |
| CD | Characteristic delay |
| CF | Characteristic frequency |
| DRF | Delay response field |
| DSRF | Delay dependent spatial receptive field |
| HRTF | Head related transfer function |
| IC | Inferior colliculus |
| ILD | Interaural level differences |
| ITD | Interaural time differences |
| MGB | Medial geniculate body |
| PDF | Posterior dorsal field of the auditory cortex |
| PSTH | Peristimulus time histogram |
| PVF | Posterior ventral field of the auditory cortex |
| SC | Superior colliculus |
| SRF | Spatial receptive field |
| STD | Standard deviation |
| TDT | Tucker-Davis Technologies |

REFERENCES

- Aitkin LM, Dickhaus H, Schult W, Zimmermann M.** External nucleus of inferior colliculus: auditory and spinal somatosensory afferents and their interactions. *Journal of Neurophysiology* 41, 1978.
- Alonso JM.** The Geometry of Visual Cortical Maps. *Neuron* 91: 716–718, 2016.
- Barquez R, Perez S, Miller B, Diaz M.** The IUCN Red List of Threatened Species. *Phyllostomus discolor* [Online]. <http://dx.doi.org/10.2305/IUCN.UK.2015-4.RLTS.T17216A22136476.en> [20 Apr. 2017].
- Bartenstein S, Gerstenberg N, Vanderelst D, Peremans H, Firzlaff U.** Echo-acoustic flow dynamically modifies the cortical map of target range in bats. *Nat Comms* 5, 2014.
- Beetz MJ, Hechavarría JC, Kössl M.** Cortical neurons of bats respond best to echoes from nearest targets when listening to natural biosonar multi-echo streams. *Scientific reports* 6: 35991, 2016a.
- Beetz MJ, Hechavarría JC, Kössl M.** Temporal tuning in the bat auditory cortex is sharper when studied with natural echolocation sequences. *Scientific reports* 6: 29102, 2016b.
- Bregman AS.** *Auditory scene analysis. The perceptual organization of sound.* Cambridge, Mass.: MIT Press, 1990.
- Brewer AA, Barton B.** Maps of the Auditory Cortex. *Annual review of neuroscience*, 2016.
- Brinkløv S, Jakobsen L, Ratcliffe JM, Kalko, Elisabeth K. V., Surlykke A.** Echolocation call intensity and directionality in flying short-tailed fruit bats, *Carollia perspicillata* (Phyllostomidae). *J. Acoust. Soc. Am.* 129: 427, 2011.
- Brugge JF, Reale RA, Hind JE.** The Structure of Spatial Receptive Fields of Neurons in Primary Auditory Cortex of the Cat. *Journal of Neuroscience* 16: 4420–4437, 1996. <http://www.jneurosci.org/content/16/14/4420>.
- Bruns V, Burda H, Ryan MJ.** Ear morphology of the frog-eating bat (*Trachops cirrhosus*, family. Phyllostomidae): Apparent specializations for low-frequency hearing. *Journal of Morphology* 199: 103–118, 1989. <http://onlinelibrary.wiley.com/doi/10.1002/jmor.1051990109/pdf>.
- Carlile S, Pettigrew AG.** Distribution of frequency sensitivity in the superior colliculus of the guinea pig. *Hearing Research* 31: 123–136, 1987.
- Dear SP, Fritz JB, Haresign T, Ferragamo M, Simmons JA.** Tonotopic and functional organization in the auditory cortex of the big brown bat, *Eptesicus fuscus*. *Journal of Neurophysiology* 70: 1988–2009, 1993a. <http://jn.physiology.org/content/70/5/1988>.
- Dear SP, Simmons JA, Fritz JB.** A possible neuronal basis for representation of acoustic scenes in auditory cortex of the big brown bat. *Nature* 364: 620–623, 1993b.
- Derey K, Valente G, Gelder B de, Formisano E.** Opponent Coding of Sound Location (Azimuth) in Planum Temporale is Robust to Sound-Level Variations. *Cerebral cortex (New York, N.Y. : 1991)*, 2015.
- Esser K-H, Eiermann A.** Tonotopic organization and parcellation of auditory cortex in the FM-bat *Carollia perspicillata*. *Eur J Neurosci* 11: 3669–3682, 1999.
- Fay RR.** Auditory stream segregation in goldfish (*Carassius auratus*). *Hearing Research* 120: 69–76, 1998.
- Fenton MB, Grinnell AD, Popper AN, Fay RR, eds.** *Bat bioacoustics.* New York, New York: Springer Science+Business Media, 2016.
- Firzlaff U, Schornich S, Hoffmann S, Schuller G, Wiegrebe L.** A neural correlate of stochastic echo imaging. *The Journal of Neuroscience* 26: 785–791, 2006.

- Firzlaff U, Schuller G.** Spectral directionality of the external ear of the lesser spear-nosed bat, *Phyllostomus discolor*. *Hearing Research* 181: 27–39, 2003.
- Firzlaff U, Schuller G.** Directionality of hearing in two CF/FM bats, *Pteronotus parnellii* and *Rhinolophus rouxi*. *Hearing Research* 197: 74–86, 2004.
- Fishman YI, Reser DH, Arezzo JC, Steinschneider M.** Neural correlates of auditory stream segregation in primary auditory cortex of the awake monkey. *Hearing Research* 151: 167–187, 2001.
- Fujioka E, Aihara I, Sumiya M, Aihara K, Hiryu S.** Echolocating bats use future-target information for optimal foraging. *Proceedings of the National Academy of Sciences*: 201515091, 2016.
- Gibson JJ.** The visual perception of objective motion and subjective movement. *Psychological Review* 61: 304–314, 1954.
- Goerlitz HR, Geberl C, Wiegrebe L.** Sonar detection of jittering real targets in a free-flying bat. *J. Acoust. Soc. Am.* 128: 1467–1475, 2010.
- Greiter W, Firzlaff U.** Echo-acoustic flow shapes object representation in spatially complex acoustic scenes. *Journal of Neurophysiology*: jn.00860.2016, 2017a.
- Greiter W, Firzlaff U.** Representation of three-dimensional space in the auditory cortex of the echolocating bat *P. discolor*. *PLoS ONE* 12: e0182461, 2017b.
<http://journals.plos.org/plosone/article/file?id=10.1371/journal.pone.0182461&type=printable>.
- Grothe B, Park TJ.** Sensitivity to Interaural Time Differences in the Medial Superior Olive of a Small Mammal, the Mexican Free-Tailed Bat. *J. Neurosci.* 18: 6608–6622, 1998.
<http://www.jneurosci.org/content/jneuro/18/16/6608.full.pdf>.
- Hagemann C, Esser K-H, Kössl M.** Chronotopically Organized Target-Distance Map in the Auditory Cortex of the Short-Tailed Fruit Bat. *Journal of Neurophysiology* 103: 322–333, 2010.
- Hechavarría JC, Macías S, Vater M, Mora EC, Kössl M.** Evolution of neuronal mechanisms for echolocation: specializations for target-range computation in bats of the genus *Pteronotus*. *The Journal of the Acoustical Society of America* 133: 570–578, 2013a.
- Hechavarría JC, Macías S, Vater M, Voss C, Mora EC, Kössl M.** Blurry topography for precise target-distance computations in the auditory cortex of echolocating bats. *Nat Comms* 4, 2013b.
- Hoffmann S, Firzlaff U, Radtke-Schuller S, Schwellnus B, Schuller G.** The auditory cortex of the bat *Phyllostomus discolor*: Localization and organization of basic response properties. *BMC Neurosci* 9: 65, 2008.
- Hoffmann S, Genzel D, Prosch S, Baier L, Weser S, Wiegrebe L, Firzlaff U.** Biosonar navigation above water I: estimating flight height. *Journal of Neurophysiology* 113: 1135–1145, 2015.
- Hoffmann S, Schuller G, Firzlaff U.** Dynamic stimulation evokes spatially focused receptive fields in bat auditory cortex. *European Journal of Neuroscience* 31: 371–385, 2010.
- Hoffmann S, Vega-Zuniga T, Greiter W, Krabichler Q, Bley A, Matthes M, Zimmer C, Firzlaff U, Luksch H.** Congruent representation of visual and acoustic space in the superior colliculus of the echolocating bat *Phyllostomus discolor*. *European Journal of Neuroscience*, 2016.
<http://onlinelibrary.wiley.com/doi/10.1111/ejn.13394/pdf>.
- Hoffmann S, Warmbold A, Wiegrebe L, Firzlaff U.** Spatiotemporal contrast enhancement and feature extraction in the bat auditory midbrain and cortex. *Journal of Neurophysiology* 110: 1257–1268, 2013.

- Holland RA, Waters DA.** Echolocation signals and pinnae movement in the fruitbat *Rousettus aegyptiacus*. *Acta Chiropterologica* 7: 83–90, 2005.
- Izumi A.** Auditory stream segregation in Japanese monkeys. *Cognition* 82: B113–B122, 2002.
- Jakobsen L, Olsen MN, Surlykke A.** Dynamics of the echolocation beam during prey pursuit in aerial hawking bats. *Proceedings of the National Academy of Sciences*: 201419943, 2015.
- Jay MF, Sparks DL.** Auditory receptive fields in primate superior colliculus shift with changes in eye position. *Nature* 309: 345–347, 1984.
- Jen PH, Sun X, Kamada T, Zhang S, Shimozawa T.** Auditory response properties and spatial response areas of superior collicular neurons of the FM bat, *Eptesicus fuscus*. *Journal of Comparative Physiology A* 154: 407–413, 1984.
- Jenkins W, Masterton RB.** Sound localization. Effects of unilateral lesions in the central auditory system. *Journal of Neurophysiology* 47: 987–1016, 1982.
- Jenkins WM, Merzenich MM.** Role of cat primary auditory cortex for sound-localization behavior. *Journal of Neurophysiology* 52: 819–847, 1984. <http://jn.physiology.org/content/jn/52/5/819.full.pdf>.
- Johnson M, Madsen PT, Zimmer WMX, Soto NAd, Tyack PL.** Beaked whales echolocate on prey. *Proc. R. Soc. Lond. B* 271: S383–S386, 2004. http://rspb.royalsocietypublishing.org/content/royprsb/271/Suppl_6/S383.full.pdf.
- Jones G, Holderied MW.** Bat echolocation calls: adaptation and convergent evolution. *Proceedings of the Royal Society B: Biological Sciences* 274: 905–912, 2007.
- Kanold PO, Young ED.** Proprioceptive Information from the Pinna Provides Somatosensory Input to Cat Dorsal Cochlear Nucleus. *The Journal of Neuroscience* 21: 7848–7858, 2001.
- Kanwal J, Medvedev A, Micheyl C.** Neurodynamics for auditory stream segregation: tracking sounds in the mustached bat's natural environment. *Network: Computation in Neural Systems* 14: 413–435, 2003.
- King AJ.** Sensory experience and the formation of a computational map of auditory space in the brain. *Bioessays* 21: 900–911, 1999.
- King AJ, Hutchings ME.** Spatial response properties of acoustically responsive neurons in the superior colliculus of the ferret: a map of auditory space. *Journal of Neurophysiology* 57: 596–624, 1987.
- King AJ, Palmer AR.** Cells responsive to free-field auditory stimuli in guinea-pig superior colliculus: distribution and response properties. *The Journal of Physiology* 342: 361–381, 1983.
- King AJ, Palmer AR.** Integration of visual and auditory information in bimodal neurones in the guinea-pig superior colliculus. *Experimental Brain Research* 60: 492–500, 1985.
- Knudsen EI.** Auditory and visual maps of space in the optic tectum of the owl. *The Journal of Neuroscience* 2: 1177–1194, 1982.
- Knudsen EI, Konishi M.** Space and frequency are represented separately in auditory midbrain of the owl. *Journal of Neurophysiology* 41: 870–884, 1978.
- Kothari NB, Wohlgemuth MJ, Hulgard K, Surlykke A, Moss CF.** Timing matters: sonar call groups facilitate target localization in bats. *Front. Physiol.* 5, 2014.
- Kothari NB, Wohlgemuth MJ, Moss CF.** Midbrain neurons of the free-flying echolocating bat represent three-dimensional space. *J. Acoust. Soc. Am.* 140: 2973, 2016.
- Kounitsky P, Rydell J, Amichai E, Boonman A, Eitan O, Weiss AJ, Yovel Y.** Bats adjust their mouth gape to zoom their biosonar field of view. *Proceedings of the National Academy of Sciences* 112: 6724–6729, 2015.

- Kremkow J, Jin J, Wang Y, Alonso JM.** Principles underlying sensory map topography in primary visual cortex. *Nature* 533: 52–57, 2016.
- Kugler K, Greiter W, Luksch H, Firzlaff U, Wiegrebe L.** Echo-acoustic flow affects flight in bats. *Journal of Experimental Biology*, 2016.
- Kugler K, Wiegrebe L.** Echo-acoustic scanning with noseleaf and ears in phyllostomid bats. *The Journal of experimental biology* 220: 2816–2824, 2017.
- Kwieceński GG.** *Phyllostomus discolor*. *Mammalian Species* 801: 1–11, 2006.
- Lamme VA.** The neurophysiology of figure-ground segregation in primary visual cortex. *J. Neurosci.* 15: 1605–1615, 1995. <http://www.jneurosci.org/content/15/2/1605.full.pdf>.
- Lappe M, Bremmer F, van den Berg AV.** Perception of self-motion from visual flow. *Trends in Cognitive Sciences* 3: 329–336, 1999.
- Lee C, Rohrer WH, Sparks DL.** Population coding of saccadic eye movements by neurons in the superior colliculus. *Nature* 332: 357–360, 1988.
- Lee C-C, Middlebrooks JC.** Auditory cortex spatial sensitivity sharpens during task performance. *Nature neuroscience* 14: 108–114, 2011.
- Linnenschmidt M, Wiegrebe L.** Sonar beam dynamics in leaf-nosed bats. *Scientific reports* 6: 29222, 2016.
- Lomber SG, Malhotra S.** Double dissociation of 'what' and 'where' processing in auditory cortex. *Nature neuroscience* 11: 609–616, 2008.
- Luan R, Wu F, Jen PHS, Sun X.** Effects of forward masking on the responses of the inferior collicular neurons in the big brown bats, *Eptesicus fuscus*. *Chinese Science Bulletin* 48: 1748–1752, 2003. <http://dx.doi.org/10.1360/02wc0570>.
- MacDougall-Shackleton SA, Hulse SH, Gentner TQ, White W.** Auditory scene analysis by European starlings (*Sturnus vulgaris*). Perceptual segregation of tone sequences. *The Journal of the Acoustical Society of America* 103: 3581–3587, 1998.
- McKerrow PJ.** Acoustic flow. In: *IEEE/RSJ International Conference on Intelligent Robots and Systems*, 2008, p. 1365–1370.
- Meredith MA, Stein BE.** Visual, auditory, and somatosensory convergence on cells in superior colliculus results in multisensory integration. *Journal of Neurophysiology* 56: 640–662, 1986.
- Meredith MA, Wallace MT, Stein BE.** Visual, auditory and somatosensory convergence in output neurons of the cat superior colliculus: multisensory properties of the tecto-reticulo-spinal projection. *Exp Brain Res* 88: 181–186, 1992. <http://dx.doi.org/10.1007/BF02259139>.
- Mey F de, Reijniers J, Peremans H, Otani M, Firzlaff U.** Simulated head related transfer function of the phyllostomid bat *Phyllostomus discolor*. *J. Acoust. Soc. Am.* 124: 2123, 2008.
- Micheyl C, Tian B, Carlyon RP, Rauschecker JP.** Perceptual Organization of Tone Sequences in the Auditory Cortex of Awake Macaques. *Neuron* 48: 139–148, 2005.
- Mickey BJ, Middlebrooks JC.** Representation of Auditory Space by Cortical Neurons in Awake Cats. *J. Neurosci.* 23: 8649–8663, 2003. <http://www.jneurosci.org/content/jneuro/23/25/8649.full.pdf>.
- Middlebrooks JC, Knudsen EI.** A neural code for auditory space in the cat's superior colliculus. *The Journal of Neuroscience* 4: 2621–2634, 1984.

- Middlebrooks JC, Knudsen EI.** Changes in external ear position modify the spatial tuning of auditory units in the cat's superior colliculus. *Journal of Neurophysiology* 57: 672–687, 1987.
<http://jn.physiology.org/content/jn/57/3/672.full.pdf>.
- Middlebrooks JC, Pettigrew JD.** Functional classes of neurons in primary auditory cortex of the cat distinguished by sensitivity to sound location. *J Neurosci* 1: 107–120, 1981.
- Middlebrooks JC, Xu L, Eddins AC, Green DM.** Codes for Sound-Source Location in Nontopographic Auditory Cortex. *Journal of Neurophysiology* 80: 863–881, 1998. <http://jn.physiology.org/content/jn/80/2/863.full.pdf>.
- Miller LM, Recanzone GH.** Populations of auditory cortical neurons can accurately encode acoustic space across stimulus intensity. *PNAS* 106: 5931–5935, 2009. <http://www.pnas.org/content/106/14/5931.full>.
- Mogdans J, Ostwald J, Schnitzler H.** The role of pinna movement for the localization of vertical and horizontal wire obstacles in the greater horseshoe bat, *Rhinolopus ferrumequinum*. *J. Acoust. Soc. Am.* 84: 1676–1679, 1988.
- Morrison DW.** Flight Speeds of Some Tropical Forest Bats. *American Midland Naturalist* 104: 189, 1980.
- Moss CF, Bohn K, Gilkenson H, Surlykke A.** Active listening for spatial orientation in a complex auditory scene. *Plos Biol* 4: e79, 2006.
- Moss CF, Schnitzler H-U.** Behavioral Studies of Auditory Information Processing. In: *Hearing by Bats*, edited by Popper AN, Fay RR. New York, NY: Springer New York, 1995, p. 87–145.
- Moss CF, Surlykke A.** Auditory scene analysis by echolocation in bats. *J. Acoust. Soc. Am.* 110: 2207, 2001.
- Moss CF, Surlykke A.** Probing the natural scene by echolocation in bats. *Front. Behav. Neurosci.*, 2010.
- Munoz DP, Wurtz RH.** Role of the rostral superior colliculus in active visual fixation and execution of express saccades. *Journal of Neurophysiology* 67: 1000–1002, 1992. <http://jn.physiology.org/content/jn/67/4/1000.full.pdf>.
- Nelken I, Chechik G, Msrac-Flogel TD, King AJ, Schnupp JWH.** Encoding Stimulus Information by Spike Numbers and Mean Response Time in Primary Auditory Cortex. *J Comput Neurosci* 19: 199–221, 2005.
<https://link.springer.com/content/pdf/10.1007%2Fs10827-005-1739-3.pdf>.
- Neuweiler G.** *The biology of bats*. New York: Oxford University Press, 2000.
- Noorden L van.** *Temporal coherence in the perception of tone sequences*, 1975.
<https://pure.tue.nl/ws/files/3389175/152538.pdf>.
- O'Neill WE, Suga N.** Encoding of target range and its representation in the auditory cortex of the mustached bat. *The Journal of Neuroscience* 2: 17–31, 1982.
- Olsen JF, Suga N.** Combination-sensitive neurons in the medial geniculate body of the mustached bat: encoding of target range information. *Journal of Neurophysiology* 65: 1275–1296, 1991.
<http://jn.physiology.org/content/65/6/1275>.
- Ortiz-Rios M, Azevedo FA, Kuśmierk P, Balla DZ, Munk MH, Keliris GA, Logothetis NK, Rauschecker JP.** Widespread and Opponent fMRI Signals Represent Sound Location in Macaque Auditory Cortex. *Neuron* 93: 971–983.e4, 2017.
- Oshimozawa T, Sun X, Jen PH-S.** Auditory space representation in the superior colliculus of the big brown bat, *Eptesicus fuscus*. *Brain Research* 311: 289–296, 1984.
- Oswald A-MM, Schiff ML, Reyes AD.** Synaptic mechanisms underlying auditory processing. *Current Opinion in Neurobiology* 16: 371–376, 2006.
- Palmer AR, King AJ.** The representation of auditory space in the mammalian superior colliculus. *Nature* 299: 248–249, 1982.

- Pankratov K.** *centroid function (MATLAB)*. Cambridge, Mass.: Massachusetts Institute of Technology, 1995.
- Pawluk D, Kitada R, Abramowicz A, Hamilton C, Lederman SJ.** Haptic figure-ground differentiation via a haptic glance. In: *2010 IEEE Haptics Symposium*, p. 63–66.
- Pietsch G, Schuller G.** Auditory self-stimulation by vocalization in the CF-FM bat, *Rhinolophus rouxi*. *J Comp Physiol A* 160: 635–644, 1987.
- Populin LC, Yin TCT.** Pinna Movements of the Cat during Sound Localization. *J. Neurosci.* 18: 4233–4243, 1998. <http://www.jneurosci.org/content/jneuro/18/11/4233.full.pdf>.
- Portfors CV, Wenstrup JJ.** Delay-Tuned Neurons in the Inferior Colliculus of the Mustached Bat: Implications for Analyses of Target Distance. *Journal of Neurophysiology* 82: 1326–1338, 1999. <http://jn.physiology.org/content/82/3/1326>.
- Rajan R, Aitkin LM, Irvine DR.** Azimuthal sensitivity of neurons in primary auditory cortex of cats. II. Organization along frequency-band strips. *Journal of Neurophysiology* 64: 888–902, 1990. <http://jn.physiology.org/content/64/3/888>.
- Razak KA.** Systematic Representation of Sound Locations in the Primary Auditory Cortex. *J. Neurosci.* 31: 13848–13859, 2011. <http://www.jneurosci.org/content/jneuro/31/39/13848.full.pdf>.
- Razak KA.** Mechanisms underlying azimuth selectivity in the auditory cortex of the pallid bat. *Hearing Research* 290: 1–12, 2012.
- Razak KA, Fuzessery ZM.** Functional Organization of the Pallid Bat Auditory Cortex. Emphasis on Binaural Organization. *Journal of Neurophysiology* 87: 72–86, 2002. <http://jn.physiology.org/content/87/1/72>.
- Razak KA, Yarrow S, Brewton D.** Mechanisms of Sound Localization in Two Functionally Distinct Regions of the Auditory Cortex. *J. Neurosci.* 35: 16105–16115, 2015. <http://www.jneurosci.org/content/35/49/16105.full>.
- Roelfsema PR, Lamme VA, Spekreijse H.** Object-based attention in the primary visual cortex of the macaque monkey. *Nature* 395: 376–381, 1998.
- Rokni D, Hemmelder V, Kapoor V, Murthy VN.** An olfactory cocktail party: figure-ground segregation of odorants in rodents. *Nat Neurosci* 17: 1225–1232, 2014.
- Rother G, Schmidt U.** The influence of visual information on echolocation in *Phyllostomus discolor* (Chiroptera). *Zeitschrift für Säugetierkunde-International Journal of Mammalian Biology* 47: 324–334, 1982.
- Rutkowski RG, Wallace MN, Shackleton TM, Palmer AR.** Organisation of binaural interactions in the primary and dorsocaudal fields of the guinea pig auditory cortex. *Hearing Research* 145: 177–189, 2000.
- Samson FK, Barone P, Clarey JC, Imig TJ.** Effects of ear plugging on single-unit azimuth sensitivity in cat primary auditory cortex. II. Azimuth tuning dependent upon binaural stimulation. *Journal of Neurophysiology* 71: 2194–2216, 1994. <http://jn.physiology.org/content/71/6/2194>.
- Schneider H, Möhres FP.** Die Ohrbewegungen der Hufeisenfledermäuse (Chiroptera, Rhinolophidae) und der Mechanismus des Bildhörens. *Z. Vergl. Physiol.* 44: 1–40, 1960.
- Schnyder HA, Vanderelst D, Bartenstein S, Firzlaff U, Luksch H.** The Avian Head Induces Cues for Sound Localization in Elevation. *PLoS ONE* 9: e112178, 2014.
- Scholes C, Palmer AR, Sumner CJ.** Forward suppression in the auditory cortex is frequency-specific. *The European journal of neuroscience* 33: 1240–1251, 2011.
- Scholes C, Palmer AR, Sumner CJ.** Stream segregation in the anesthetized auditory cortex. *Hearing Research* 328: 48–58, 2015.

- Schreiner CE, Winer JA.** Auditory cortex mapmaking: principles, projections, and plasticity. *Neuron* 56: 356–365, 2007.
- Schul J, Sheridan RA.** Auditory stream segregation in an insect. *Neuroscience* 138: 1–4, 2006.
- Schuller G.** A cheap earphone for small animals with good frequency response in the ultrasonic frequency range. *Journal of Neuroscience Methods* 71: 187–190, 1997.
- Schuller G, O'Neill WE, Radtke-Schuller S.** Facilitation and Delay Sensitivity of Auditory Cortex Neurons in CF-FM Bats, *Rhinolophus rouxi* and *Pteronotus p. parnellii*. *Eur J Neurosci* 3: 1165–1181, 1991.
- Schuller G, Radtke-Schuller S, Betz M.** A stereotaxic method for small animals using experimentally determined reference profiles. *Journal of Neuroscience Methods* 18: 339–350, 1986.
- Siemers BM, Schauer G, Turni H, Merten Sv.** Why do shrews twitter? Communication or simple echo-based orientation. *Biology Letters* 5: 593–596, 2009.
<http://rsbl.royalsocietypublishing.org/content/roybiolett/5/5/593.full.pdf>.
- Simmons JA, Ferragamo M, Moss CF, Stevenson SB, Altes RA.** Discrimination of jittered sonar echoes by the echolocating bat, *Eptesicus fuscus*. The shape of target images in echolocation. *J Comp Physiol A* 167: 589–616, 1990. <https://link.springer.com/content/pdf/10.1007%2FBF00192654.pdf>.
- Stecker GC, Middlebrooks JC.** Distributed coding of sound locations in the auditory cortex. *Biological cybernetics* 89: 341–349, 2003.
- Stilz W-P, Schnitzler H-U.** Estimation of the acoustic range of bat echolocation for extended targets. *J. Acoust. Soc. Am.* 132: 1765–1775, 2012.
- Suga N, Kawasaki M, Burkard RF.** Delay-tuned neurons in auditory cortex of mustached bat are not suited for processing directional information. *Journal of Neurophysiology* 64: 225–235, 1990.
<http://jn.physiology.org/content/64/1/225>.
- Suga N, O'Neill WE.** Neural axis representing target range in the auditory cortex of the mustache bat. *Science* 206: 351–353, 1979.
- Surlykke A, Pedersen SB, Jakobsen L.** Echolocating bats emit a highly directional sonar sound beam in the field. *Proceedings of the Royal Society B: Biological Sciences* 276: 853–860, 2009.
- Tanaka H, Wong D.** The influence of temporal pattern of stimulation on delay tuning of neurons in the auditory cortex of the FM bat, *Myotis lucifugus*. *Hearing Research* 66: 58–66, 1993.
- Tian B, Reser D, Durham A, Kustov A, Rauschecker JP.** Functional specialization in rhesus monkey auditory cortex. *Science* 292: 290–293, 2001.
- Valentine DE, Moss CF.** Spatially selective auditory responses in the superior colliculus of the echolocating bat. *Journal of Neuroscience* 17: 1720–1733, 1997.
- Vanderelst D, Mey F de, Peremans H, Geipel I, Kalko, Elisabeth K. V., Firzlaff U, Dornhaus A.** What Noseleaves Do for FM Bats Depends on Their Degree of Sensorial Specialization. *PLoS ONE* 5: e11893, 2010.
- Warren PA, Rushton SK.** Optic flow processing for the assessment of object movement during ego movement. *Current biology : CB* 19: 1555–1560, 2009.
- Wehr M, Zador AM.** Synaptic mechanisms of forward suppression in rat auditory cortex. *Neuron* 47: 437–445, 2005.
- Wheeler AR, Fulton KA, Gaudette JE, Simmons RA, Matsuo I, Simmons JA.** Echolocating Big Brown Bats, *Eptesicus fuscus*, Modulate Pulse Intervals to Overcome Range Ambiguity in Cluttered Surroundings. *Front. Behav. Neurosci.* 10: 125, 2016.

- Wilson DE, Reeder D.** *Mammal Species of the World. A Taxonomic and Geographic Reference*: Johns Hopkins University Press, 2005. <https://books.google.de/books?id=JgAMbNSt8ikC>.
- Wohlgemuth MJ, Kothari NB, Moss CF.** Action Enhances Acoustic Cues for 3-D Target Localization by Echolocating Bats. *Plos Biol* 14: e1002544, 2016a.
- Wohlgemuth MJ, Luo J, Moss CF.** Three-dimensional auditory localization in the echolocating bat. *Microcircuit computation and evolution* 41: 78–86, 2016b.
- Wong D.** Spatial tuning of auditory neurons in the superior colliculus of the echolocating bat, *Myotis lucifugus*. *Hearing Research* 16: 261–270, 1984.
- Wong D, Maekawa M, Tanaka H.** The effect of pulse repetition rate on the delay sensitivity of neurons in the auditory cortex of the FM bat, *Myotis lucifugus*. *J Comp Physiol A* 170, 1992.
- Young ED, Rice JJ, Tong SC.** Effects of pinna position on head-related transfer functions in the cat. *J. Acoust. Soc. Am.* 99: 3064, 1996.

LIST OF FIGURES

| | |
|--|----|
| Figure 1: Frequency tuning and spatial tuning in the ascending auditory pathway | 9 |
| Figure 2: Generation of naturalistic pulse/echo sequences | 26 |
| Figure 3: Frequency content of virtual echoes at different steps of generation | 31 |
| Figure 4: Spatial tuning of units in the superior colliculus | 34 |
| Figure 5: Correlation between rostro-caudal position and azimuth coding. | 35 |
| Figure 6: Comparison between spatial receptive fields of a unit during electrical ear stimulation and control.... | 36 |
| Figure 7: Spatial tuning during stimulation of the adductor muscle | 37 |
| Figure 8: Spatial tuning during stimulation of the elevator muscle | 37 |
| Figure 9: Correlation between azimuth coding and position in SC during adductor stimulation | 38 |
| Figure 10: Correlation between azimuth coding and position in SC during elevator stimulation..... | 39 |
| Figure 11: Frequency tuning of a unit in the superior colliculus | 40 |
| Figure 12: Frequency tuning in the superior colliculus | 41 |
| Figure 13: DRFs for two delay-sensitive units | 45 |
| Figure 14: Cortical distribution of BD | 46 |
| Figure 15: Examples of units focusing on different targets in naturalistic pulse/echo sequences | 47 |
| Figure 16: Units focus depending on heading distance | 49 |
| Figure 17: Echo delay and echo level of unit responding in naturalistic pulse/echo sequence | 50 |
| Figure 18: Specific delay in naturalistic flight sequence compared to the static delay response field | 52 |
| Figure 19: Cortical delay tuning maps showing distribution of specific delays from naturalistic flight sequences | 53 |
| Figure 20: Best delay from static DRFs in relation to specific delays from naturalistic pulse/echo sequences | 54 |
| Figure 21: Delay tuning in the auditory cortex | 61 |
| Figure 22: Delay dependent spatial receptive field | 62 |
| Figure 23: BAZ/BEL and centroid positions of all analyzed units | 63 |
| Figure 24: Azimuth and elevation at different best delays | 64 |
| Figure 25: Simulated echo levels at different echo delays | 66 |
| Figure 26: Influence of call/echo level on spatial tuning | 67 |
| Figure 27: SRF width and centroid position of receptive fields at different echo levels..... | 68 |
| Figure 28: Spatial receptive fields at different echo delay steps | 69 |
| Figure 29: Maximum response and spatial directionality at different echo delay steps..... | 70 |
| Figure 30: Three-dimensional receptive field of cortical combination-sensitive neuron | 71 |
| Figure 31: Sizes of the receptive fields at different echo delay steps | 71 |
| Figure 32: Systematic representation of target elevation and echo delay..... | 74 |

CURRICULUM VITAE

Wolfgang Greiter

Academic Education

- | | |
|-------------------|---|
| PhD | Technical University of Munich, Chair of Zoology, |
| 03/2014 - present | Doctoral thesis under the supervision of PD Dr. Uwe Firzlaff Topic: „Neuronal representation of dynamic echo-acoustic scenes in bats“ |
| Biology M.Sc. | Technical University of Munich |
| 10/2011 – 01/2014 | Focal points: human biology, neurobiology, genetics Master’s Thesis: „Nerve-Mast cell interaction in the human intestine“ Accepted for publication: <i>Bühner S, Barki N, Greiter W, Giesbertz P, Demir IE, Ceyhan G, Zeller F, Daniel H, Schemann M.</i> <i>Calcium imaging of nerve-mast cell signaling in the human intestine.</i> <i>Frontiers in Physiology., DOI: 10.3389/fphys.2017.00971</i> |
| Biology B.Sc. | Technical University of Munich |
| 10/2008 – 09/2011 | Bachelor’s Thesis: „Distribution of mast cells in the gastrointestinal wall of patients with mastocytosis compared to healthy control persons“ |

ACKNOWLEDGEMENTS

I especially want to thank my supervisor Uwe Firzlaff, who gave me the possibility to gain immense knowledge about bat hearing and echolocation, its neurobiological basis in bats and in other mammals. Furthermore, I was able to gather quite a lot hands-on experience in MATLAB® programming and sound processing in general.

I want to thank Harald Luksch, who ignited my initial fascination in neurobiology and was always there when I needed scientific or other advice during my time at the university in Weihenstephan. Thanks also to Michael Gebhardt who showed me the basics of electrophysiology in his fascinating work with crickets. I further want to thank all other colleagues at the Zoology in Weihenstephan for a good time, a huge number of tasty cakes or muffins and a lot of fun during work as well as on “field trips” to breweries, high rope courses in the Alps and boat trips on the Altmühl!

And I would like to thank my colleagues from the LMU, especially Lutz Wiegrebe for providing a great deal of technical knowledge about sound processing, microphones, loudspeakers, etc. and Kathi Kugler for a lot of fun building a deluxe bat flight channel.

This work was supported by the German Research Foundation (DFG) Grant FI 1546/4-1 to U. Firzlaff.